T.C.

DOKUZ EYLUL UNIVERSITY

IZMIR INTERNATIONAL BIOMEDICINE AND GENOME INSTITUTE

ANALYSIS OF THE MITOTIC KINASE FUNCTIONS BY CHEMICAL GENETICS APPROACHES

MEHMET ERGÜVEN

MOLECULAR BIOLOGY AND GENETICS MASTER'S PROGRAM

MASTER OF SCIENCE THESIS

İZMİR-2019

T.C.

DOKUZ EYLUL UNIVERSITY

IZMIR INTERNATIONAL BIOMEDICINE AND GENOME INSTITUTE

ANALYSIS OF THE MITOTIC KINASE FUNCTIONS BY CHEMICAL GENETICS APPROACHES

MOLECULAR BIOLOGY AND GENETICS MASTER'S PROGRAM

MASTER OF SCIENCE THESIS

MEHMET ERGÜVEN

Supervising Faculty Member: Assoc. Prof. M. Kasım DİRİL

THESIS CODE: DEU.IBG.MSc-2016850014

Dokuz Eylül University İzmir International Biomedicine and Genome Institute

Department of Genomics and Molecular Biotechnology,

Molecular Biology and Genetics Graduate Program Master of Science student

Mehmet ERGÜVEN has successfully completed his Master of Science thesis

titled "Analysis of the mitotic kinase functions by chemical genetics

approaches" on the date of June 11, 2019.

CHAIR, PI

Assoc. Prof. Dr. M. Kasım DİRİL
İzmir International Biomedicine and Genome Institute
Department of Genomics and Molecular Biotechnology

MEMBER

Asst. Prof. Ezgi KARACA EREK
İzmir International Biomedicine and Genome
Institute
Department of Biomedicine and Health
Technologies

MEMBER

Asst. Prof. Hümeyra TAŞKENT SEZGİN
İzmir University of Economics
Faculty of Engineering
Department of Food Engineering

SUBSTITUTE MEMBER

Assoc. Prof. H. Güneş ÖZHAN BAYKAN
İzmir International Biomedicine
and Genome Institute
Department of Biomedicine and Health
Technologies

SUBSTITUTE MEMBER

Assoc. Prof. Efe SEZGİN
İzmir Institute of Technology
Faculty of Engineering
Department of Food Engineering

Dokuz Eylül Üniversitesi İzmir Uluslararası Biyotıp ve Genom Enstitüsü
Genom Bilimleri ve Moleküler Biyoteknoloji Anabilim Dalı,
Moleküler Biyoloji ve Genetik Yüksek Lisans programı öğrencisi Mehmet
ERGÜVEN "Mitotik Kinaz Fonksiyonlarının Kimyasal Genetik Yaklaşımlarla
İncelenmesi" konulu yüksek lisans tezini 11 Haziran, 2019 tarihinde başarılı
olarak tamamlamıştır.

BAŞKAN, DANIŞMAN

Doç. Dr. M. Kasım DİRİL
İzmir Uluslararası Biyotıp ve Genom Enstitüsü
Genom Bilimleri ve Moleküler Biyoteknoloji Anabilim Dalı

ÜYE

Dr. Öğr. Üyesi Ezgi KARACA EREK
İzmir Uluslararası Biyotıp ve Genom Enstitüsü
Biyotıp Ve Sağlık Teknolojileri Anabilim Dalı

ÜYE

Dr. Öğr. Üyesi Hümeyra TAŞKENT SEZGİN
İzmir Ekonomi Üniversitesi
Mühendislik Fakültesi
Gıda Mühendisliği Bölümü

YEDEK ÜYE

Doç. Dr. H. Güneş ÖZHAN BAYKAN
İzmir Uluslararası Biyotıp ve Genom Enstitüsü
Biyotıp Ve Sağlık Teknolojileri Anabilim
Dalı

YEDEK ÜYE

Doç. Dr. Efe SEZGİN
İzmir Yüksek Teknoloji Enstitüsü
Mühendislik Fakültesi
Gıda Mühendisliği Bölümü

TABLE OF CONTENTS

INDEX OF TABLES

INDEX OF FIGURES

LIST OF ABBREVIATIONS

4-OHT	4-hydroxytamoxifen
Å	Angstrom
APC/C	Anaphase Promoting Complex/Cyclosome
APS	Ammonium Persulfate
AS	Analogue-Sensitive
ATP	Adenosine Triphosphate
BSA	Bovine Serum Albumin
BSA	Buried Surface Area
Cdk1	Cyclin Dependent Kinase 1
cDNA	Complementary DNA
cKO-MEF	Conditional Knockout Mouse Embryonic Fibroblast
CMV	Cytomegalovirus
CRISPR	Clustered Regularly Interspaced Short Palindromic Repeats
DAPI	4′,6-diamidino-2-phenylindole
ddH$_2$O	Distilled Deionized water
EtOH	Ethanol
FACS	Fluorescence-Activated Cell Sorting
Gwl	Greatwall
HA	Human Influenza Hemagglutinin
HADDOCK	High Ambiguity Driven protein-protein DOCKing
KD	Kinase Dead
LTR	Long Terminal Repeat

M109A	Methionine to alanine substitution (109th residue).
M109G	Methionine to glycine substitution (109th residue).
Mastl	Microtubule-Associated Serine/Threonine kinase Like
MCC	Mitotic Checkpoint Complex
MetOH	Methanol
MPF	Maturation Promoting Factor
MSA	Multiple Sequence Alignment
NCMR	Non-conserved Middle Region
NEBD	Nuclear Envelope Breakdown
PBS	Phosphate-buffered Saline
PCR	Polymerase Chain Reaction
PDB	Protein Data Bank
PLIP	Protein-Ligand Interaction Profiler
PMSF	Phenylmethylsulfonyl fluoride
PP2A	Protein Phosphatase 2A
PVDF	Polyvinylidene Difluoride
RMSD	Root Mean Square Deviation
SAC	Spindle Assembly Checkpoint
SDS-PAGE	Sodium Dodecyl Sulfate Polyacrylamide Gel Electrophoresis
TBST	Tris-Buffered Saline-Tween 20
V93A	Valine to alanine substitution (93nd residue).
vdW	van der Waals
WT	Wild Type

ACKNOWLEDGEMENTS

Analysis of the Mitotic Kinase Functions by Chemical Genetics Approaches

Mehmet Ergüven,

İzmir International Biomedicine and Genome Institute
Dokuz Eylül University Sağlık Yerleşkesi
Balçova 35340 İzmir/TURKEY

ABSTRACT

Mitosis is the shortest phase of the cell cycle yet it involves dramatic changes in the cellular architecture and processes. Mitotic entry and progression are tightly regulated by the dynamic actions of signaling pathway networks and autoamplification loops. Mastl kinase is responsible for preservation of the hyperphosphorylated state of the mitotic substrates by indirectly inhibiting the major antagonist protein phosphatase, PP2A. Loss of function studies of Mastl kinase have shown defects of chromosomal segregation and subsequent failure of cytokinesis, and underphosphorylation of the mitotic substrates.

To better understand and further characterize the mitotic functions of Mastl kinase, we aimed to engineer its analogue-sensitive mutant variants. We initially worked on editing the endogenous loci in human cell lines using CRISPR-Cas9 system. After failed attempts of editing the endogenous loci, we decided to use the conditional knockout mouse embryonic fibroblasts. Using retroviral vectors, we ectopically expressed the mutant variants of mouse Mastl and deleted the endogenous loci by inducing knockout in these stable cell lines respectively. Our eventual aim was to create an enzyme that will bind ATP and have normal kinase activity, and yet, be sensitive to an ATP analogue inhibitor.

As a result, we observed that the stable cell lines are not viable when knockout was induced. We suspect the possible negative impacts of the mutations on enzymatic activity and insufficient ectopic expression levels. In order to compensate for this possible partial enzymatic inactivation, we are currently switching to lentiviral expression systems to achieve higher expression levels.

Mitotik Kinaz Fonksiyonlarının Kimyasal Genetik Yaklaşımlarla İncelenmesi

Mehmet Ergüven,

İzmir Uluslararası Biyotıp ve Genom Enstitüsü
Dokuz Eylül Üniversitesi Sağlik Yerleşkesi
Balçova 35340 İzmir/TÜRKİYE

ÖZET

Mitoz, hücre döngüsünün en kısa evresi olmasına rağmen hücresel yapı ve işlevlerde çok büyük değişiklikleri içerir. Mitoza giriş ve ilerleme, sinyal yolaklarından oluşan ağların ve otoamplifikasyon döngülerinin dinamik işleyişleriyle garantilenmektedir. Mastl kinaz, protein fosfataz 2A'yı (PP2A) dolaylı olarak inhibe ederek, mitoz sırasında mitotik substratların hiperfosforile hallerinin korunmasını sağlar. Mastl kinaz için yapılan gen yok etme çalışmaları; hücrelerde kromozomların ayrılmasında kusur ve bunun sonucu olarak sitokinezin gerçekleşememesi ve mitotik substratların fosforilasyon düzeylerinde azalmalar göstermiştir.

Mastl kinazın mitotik fonksiyonlarının daha iyi anlaşılabilmesi ve karakterize edilebilmesi için; enzimin analog duyarlı varyantlarını oluşturmayı amaçladık. Öncelikle insan hücre hatlarında, endojen Mastl lokusuna CRISPR-Cas9 metoduyla ilgili mutasyonların yerleştirilmesi amaçlandı. Başarısız denemelerin ardından çalışmaları koşullu knockout fare embriyonik fibroblast hücrelerinde yapmaya karar verdik. Retroviral vektörler aracılığıyla, analog duyarlı kinaz varyantlarını ekzojen olarak ekspresse ettik ve oluşturulan stabil hücre hatları, endojen Mastl lokusunun delesyonu için indüklendiler. Amacımız, ATP'yi bağlayabilen ve normal kinaz aktivitesi veren ve buna ek olarak bir ATP analoğu inhibitörüne duyarlı olan bir enzim oluşturmaktı.

Çalışmanın son durumunda, knockout indüklenmiş stabil hücre hatlarının sağlıklı olmadığını gözledik. Mutasyonlarının enzim aktivitesine olası olumsuz etkilerinden ve yetersiz seviyede ektopik ekspresyondan şüphelendiğimiz için, azalan enzimatik aktiviteyi daha yüksek ekspresyon düzeyleriyle telafi edebilmek amacıyla, lentiviral ekspresyon sistemlerine geçiş sürecinde ön denemeler yapılmaktadır.

Anahtar Sözcükler: kimyasal genetik, HADDOCK, Mastl, mitoz

1. __INTRODUCTION AND AIM__

Although the Mastl knockout phenotype is well-characterized, currently a mechanistic explanation of this phenotype is not present in the literature. Moreover, a mitotic kinase can take different and independent roles in different phases of the cell cycle. To understand and analyze possible, yet unknown functions of the Mastl kinase, and to capture at which phase before cytokinesis its activity becomes dispensable, we aimed to engineer AS (analogue-sensitive) mutant variants of the kinase. Reversible and instantaneous chemical inhibition of the kinase is very important to obtain reliable data from spatio-temporal analyses. As a precaution, we simultaneously prepared four predetermined mutant constructs bearing M109G, M109A, V93A/M109G, and V93A/M109A amino acid substitutions. Using these mutations, we aimed to accommodate bulky ATP analogues into the ATP binding pocket of Mastl kinase. All mutant residues are located across the ATP binding pocket-ATP interface. We selected three ATP analogue inhibitors, namely 1-NA-PP1, 1-NM-PP1, and 3-MB-PP1. Initially, *in silico* and *in vivo* trials with various mutant-inhibitor combinations were aimed to choose an optimal combination to utilize in phenotypic characterization studies, such as analysis of protein colocalization at the kinetochores with live cell imaging and analysis of several key mitotic phosphorylations with Western blot, in a time-dependent manner.

Obtaining such a cell line-drug combination will allow us to probe the functions of the enzyme deeper via spatio-temporal analyses. Potentially, an ultimate, conclusive research can be done to elucidate yet unknown functions of Mastl kinase, beyond the inhibition of PP2A and preservation of the hyperphosphorylated form of Mps1.

2. GENERAL INFORMATION

2.1. Mitosis

Mitosis is the last phase of the cell cycle wherein duplicated genetic material is distributed equally between the newly generated daughter cells. Upon completion of chromosomal segregation, nuclear membrane is reconstituted and karyokinesis (division of the nucleus) is completed. At the end of the phase, genetically identical two daughter cells are formed (Alberts, 2015). Throughout each subphase of the mitosis, the cell undergoes substantial cellular and biochemical changes (Figure 1). The remarkable morphological changes include condensation of DNA to form chromosomes, fragmentation of the nuclear envelope, and rearrangement of the cytoskeleton to form the spindle (Glover, 2012).
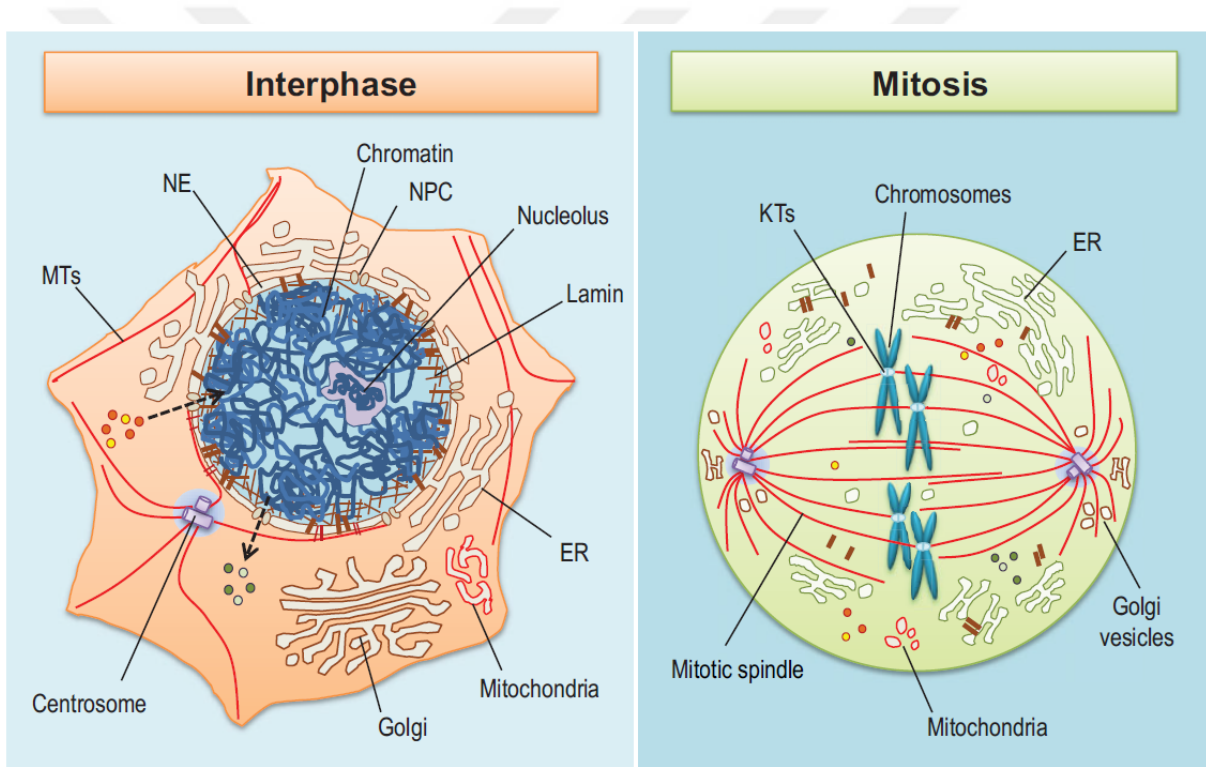
Figure 1. Morphological changes in mitosis. Mitotic cell division requires enormous morphological changes such as condensation of DNA, fragmentation of nuclear envelope, and rearrangement of the cytoskeleton (adapted from Álvarez-Fernández & Malumbres, 2014).

During metaphase, microtubules exert force on the bound kinetochores to coordinate the chromosomes on the metaphase plate. Chromosomes remain on the metaphase plate until all the kinetochore-microtubule attachments are in the correct orientation and the tension is established. This subphase of mitosis is denoted as metaphase. This is followed by anaphase. During anaphase, sister chromatids are separated and they are pulled to the spindle poles by

microtubules. Finally, during telophase, the biochemical and morphological state of the cell is reversed to its interphase state (Figure 2).
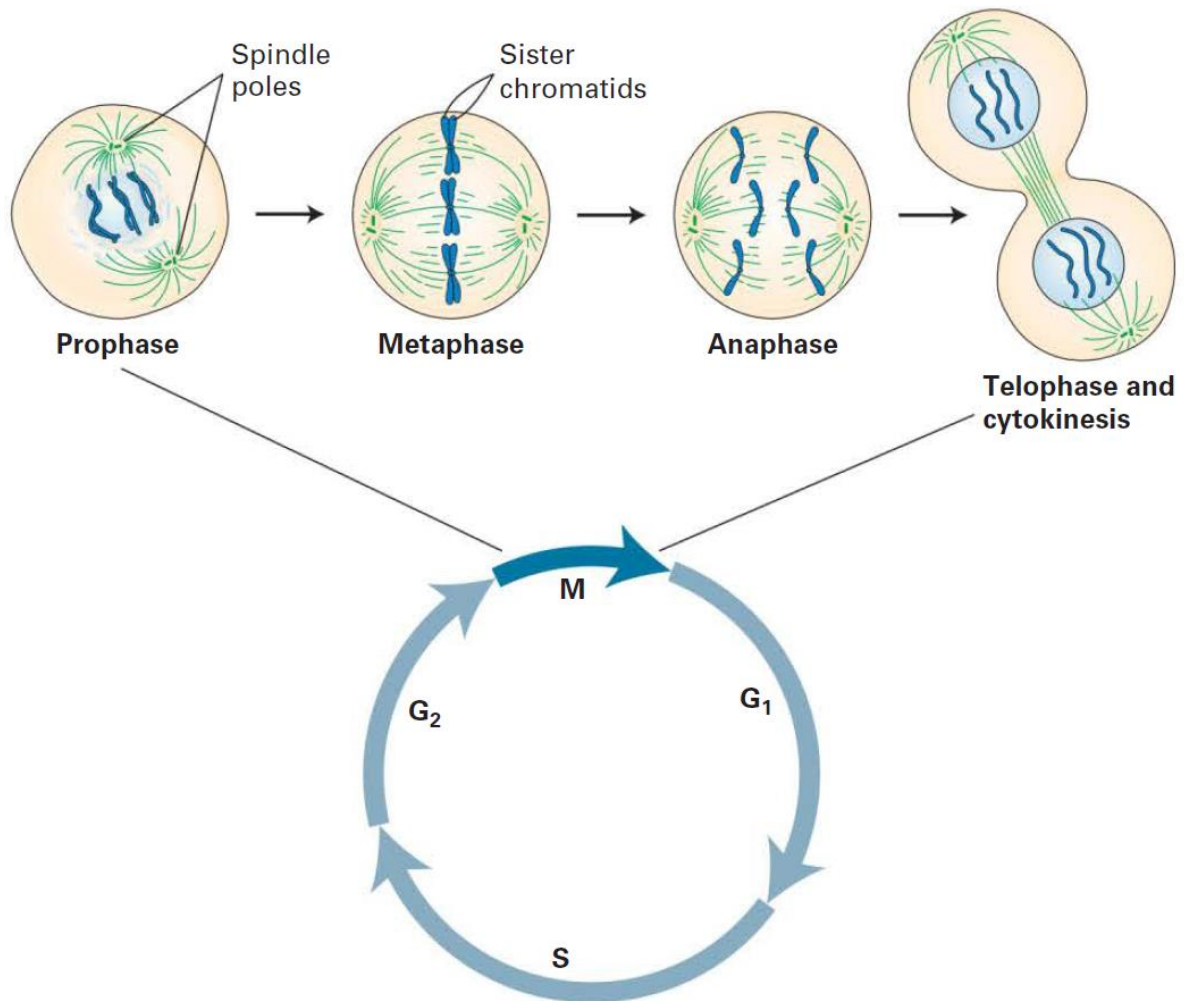
Figure 2. Phases of the cell cycle. Phases of the cell cycle are G1, S, G2, and M, respectively. Mitosis is further classified into 4 sub-phases: Prophase, Metaphase, Anaphase, and Telophase, respectively (adapted from Baxter, Hastings, Law, & Glass, 2008).

As observed for many other cellular processes, mitosis is strictly regulated by post-translational modifications, subcellular localization, and proteolytic degradation of proteins (Baxter et al., 2008). When the short duration of the mitosis and extent of the cellular changes throughout this phase are considered, the regulatory networks that coordinate mitosis have to be robust, efficient, and fast. Post-translational regulation is the type of regulation that can satisfy such a need. Phosphorylation-dephosphorylation dependent post-translational modifications govern the action of many mitotic proteins (H. Kim, Fernandes, & Lee, 2016). Key mitotic kinases work in a network with several layers of positive feedback loops,

constructing a robust signaling cascade which quickly activates the mitotic substrates. Similarly, phosphatases and ubiquitin ligases are responsible for dephosphorylation and proteolytic degradation of the target mitotic proteins, resulting in quick reversal of the mitotic cellular changes at the end of mitosis.

2.2. Phosphorylation-dephosphorylation dependent regulation of mitosis

Active Cdk1/cyclin B complex is the primary kinase that promotes mitosis and it is essential for mitotic entry (Diril et al., 2012). Wee1 and Myt1 kinases inhibit Cdk1 by inhibitory phosphorylations at threonine-14 and tyrosine-15 residues. At the onset of mitosis, phosphorylation of Cdk1 at threonine 161 activates Cdk1/cyclin B complex. Next, Cdk1/cyclin B phosphorylates and activates Cdc25 phosphatase and activated Cdc25 removes the inhibitory phosphorylations on Cdk1 (J. Yu, Zhao, Li, Galas, & Goldberg, 2006). Active Cdk1 phosphorylates many substrates, including Wee1, Myt1, and Cdc25. Phosphorylation of Wee1 and Myt1 by Cdk1 inhibits them, so that these anti-mitotic kinases can no longer block Cdk1 activity. Phosphorylation of Cdc25 by Cdk1 further activates it, which accelerates the activation of the Cdk1 pool of the cell, constructing a positive feedback loop. Most of the phosphorylations on downstream proteins result in activation of factors that promote mitosis and inhibition of factors that promote mitotic exit. To be able to preserve the mitotic state of the cell, mitotic phosphorylations have to be maintained. A strong autoamplification loop has to be coupled with inhibition of the factors promoting mitotic exit (Gharbi-Ayachi et al., 2010). PP2A (protein phosphatase 2A) is the primary antagonist of Cdk1 during mitosis. This phosphatase is indirectly inhibited by Mastl (Microtubule-associated serine/threonine kinase like). Mastl is the human orthologue of Gwl (Greatwall) kinase which was first identified in Drosophila. Mastl kinase phosphorylates two highly homologous, small, thermostable proteins named Arpp19 and Ensa at their Serine 62 and Serine 67 residues, respectively. These two phosphoproteins specifically bind to and inhibit B55∂ bound PP2A isoform. Inhibition of PP2A-B55∂ results in the rapid accumulation of phosphorylations on mitotic substrates. This inhibition also prevents the removal of inhibitory phosphorylations on Wee1 and Myt1, and activating phosphorylation of Cdc25, further supporting the autoamplification loop (Figure 3) and the activity of MPF (maturation promoting factor) (Kim et al., 2012; Mochida, Maslen, Skehel, & Hunt, 2010; Slupe, Merrill, & Strack, 2011).
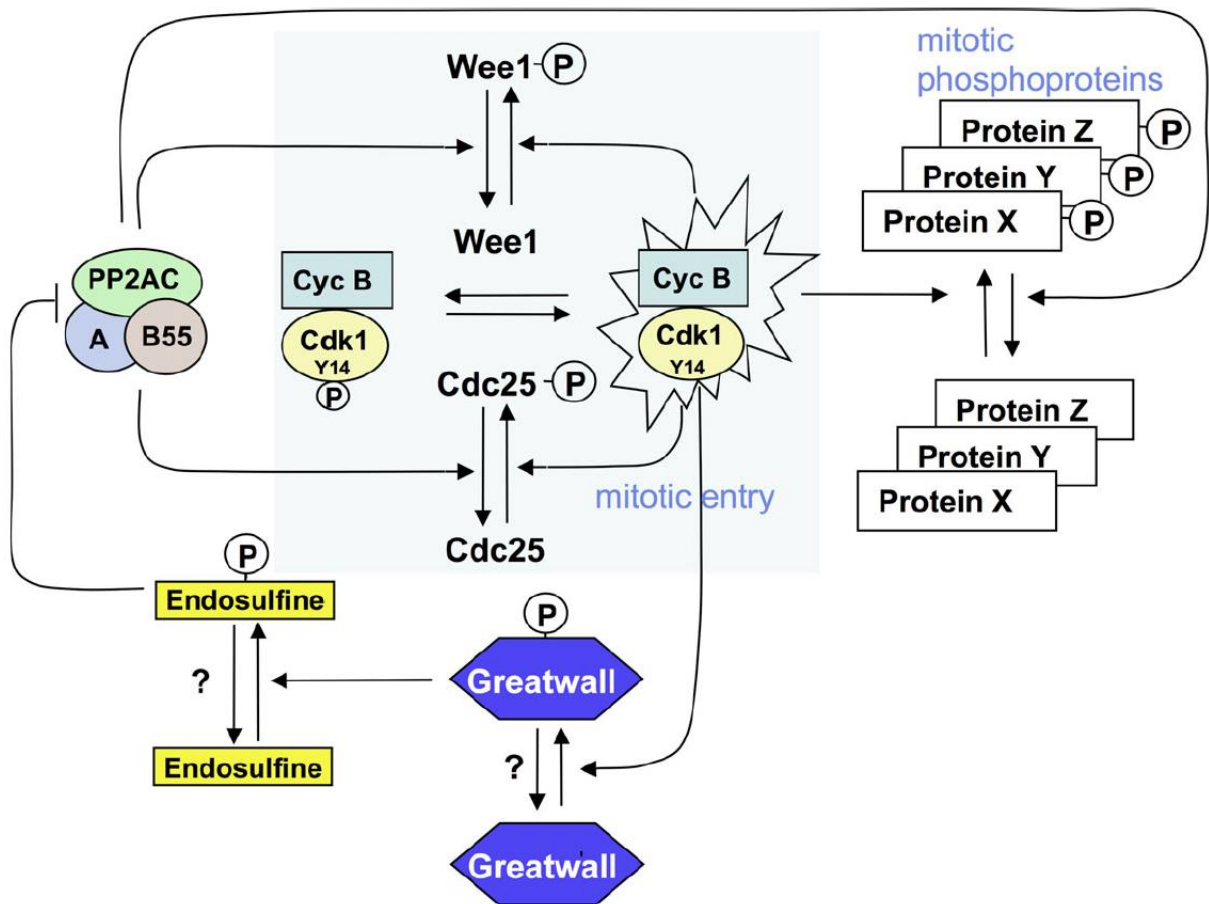
Figure 3. Mastl pathway and MPF autoamplification loop. Contribution of the Mastl (Greatwall)>Arpp19&Ensa>PP2A pathway to the MPF autoamplification loop (adapted from Glover, 2012).

Autoamplification loop activates the activators of MPF and inhibits its inhibitors via interconnected feedback and feedforward loops. As a result, the system is robust and it ensures the preservation of the mitotic alterations in the cell when mitotic entry is triggered. The robustness of the system was demonstrated in Xenopus eggs. Minute amounts of mature oocyte cytoplasm were transferred to an uninduced oocyte and this dilution was serially repeated (Kishimoto, 2015). After each subsequent cytoplasmic transfer, meiotic maturation of the recipient immature oocytes was observed, even in the absence of hormonal induction (Figure 4).
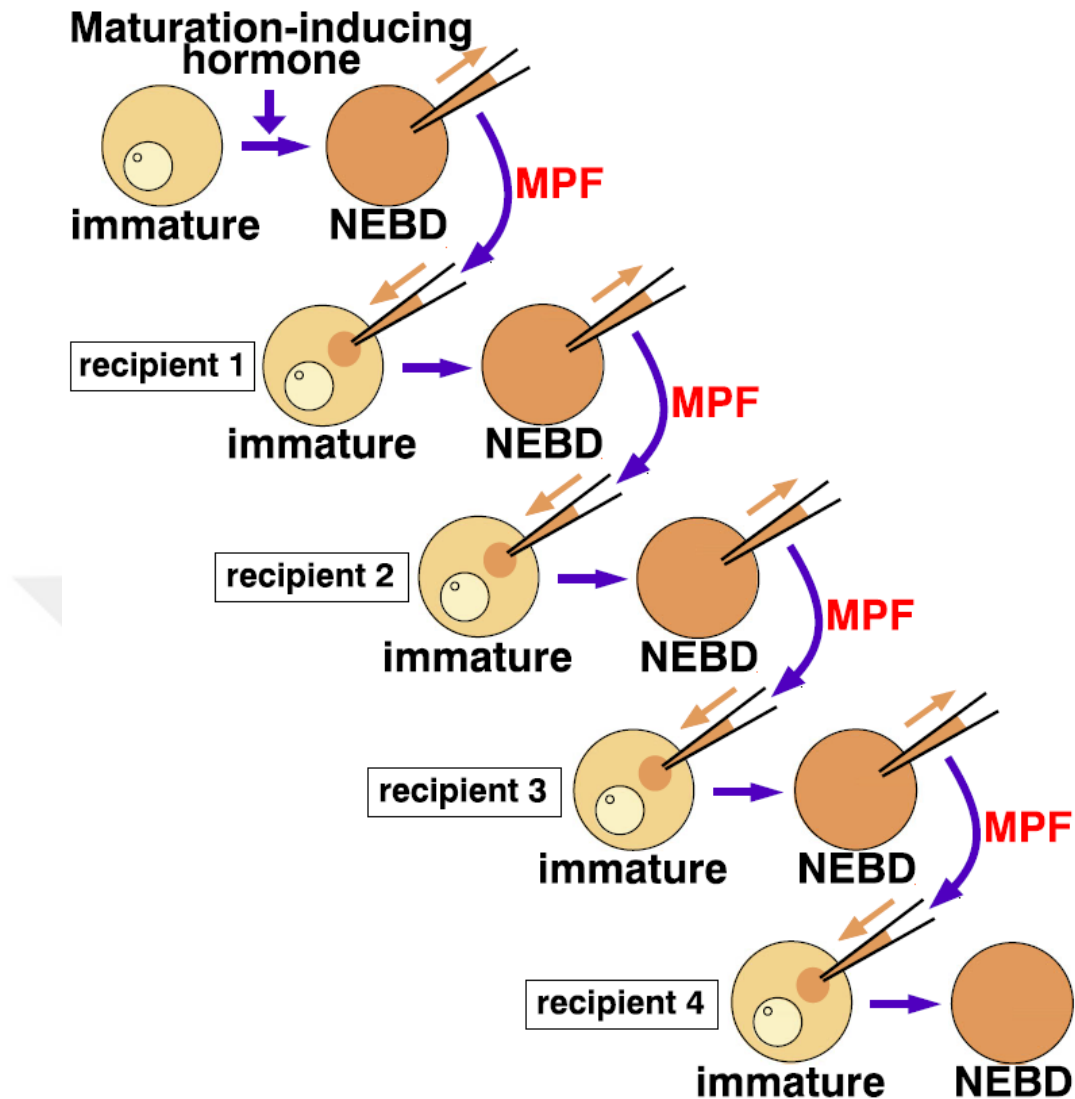
Figure 4. MPF autoamplification loop is a robust system. Cytoplasmic transfer from a meiotic Xenopus egg to immature eggs is sufficient to induce maturation even in the absence of progesterone. Even after four rounds of serial dilutions, the strength of the autoamplification loop was sufficient to induce maturation (adapted from Kishimoto, 2015).

2.3. Spindle assembly checkpoint signaling

It is important for the kinetochores to bind microtubules in the correct orientation for genomic stability. Kinetochores are protein structures located around the centromeres of chromosomes. Under physiologically normal circumstances, transition from metaphase to anaphase is blocked until all the kinetochores are correctly bound bilaterally and tension is established. (Ciliberto & Shah, 2009). Spindle assembly checkpoint (SAC) signaling is a delicate system that senses whether all kinetochore-microtubule bindings are correct or not. If the bindings are complete and correct, then the signal is diminished and the cell is allowed to

proceed to anaphase. Otherwise the signal persists and the cell is arrested at metaphase until the binding requirements are satisfied. Docking of the microtubules to the kinetochores is achieved by the outer kinetochore members KNL1, Ndc80 complex, and Mis12 complex (Kelly & Funabiki, 2009). According to the current model, correct microtubule-kinetochore binding is sensed through a series of conformational changes which ultimately diminish the signal. Briefly, the physical tension exerted upon kinetochores by the pulling action of microtubules from opposite poles, is translated to a chemical output via conformational changes, leading to the silencing of SAC (Kops et al., 2005). Some studies using microtubule poisons have also revealed presence of other unknown contributors to SAC silencing and stood against the accepted notion explained above (Tauchman, Boehm, & DeLuca, 2015). The kinetochore-microtubule binding occurs randomly. Erratic microtubule-kinetochore attachments are unstable and bilateral attachments are stable. As a result, erroneous bindings are easy to dissociate and correct bindings are persistent. Because of this difference, kinetochore-microtubule attachments are dynamically established and broken until correct attachment occurs (Figure 5).

Cohesin is a ring-like protein complex that acts like a cuff and holds the sister chromatids together. Cleavage of this protein at the N-terminal domain of its Scc1 subunit by a cysteine protease called separase, removes the force that holds the sister chromatids together. Now the remaining force on the kinetochores is the pulling effect of the microtubules. As a result, the sister chromatids segregate to the opposite poles. Securin is an inhibitory protein that initially binds to and inhibits separase. At this inhibited state, separase can not free the arms of the sister chromatids from cohesin. When all the kinetochores are correctly bound to the microtubules, SAC signaling is silenced. Anaphase promoting complex-cyclosome (APC/C) is now freed from the inhibitory effect of SAC signaling. APC/C ubiquitinates and marks securin for proteolytic degradation in proteasomes. Only then separase can digest cohesins, freeing the chromosomes to segregate (Shindo, Kumada, & Hirota, 2012).

Inhibition of APC/C by SAC prevents transition from metaphase to anaphase. Kinetochores that are not caught by spindle or attached incorrectly, hence not under tension, form docking sites for members of mitotic checkpoint complex (MCC). The noteworthy members of MCC are Mad1, Mad2, Bub1, and BubR1. There are many other disputed members of MCC, as it is a versatile complex and can be found in many forms, both in terms of the variety of protein constituents and in terms of their stoichiometry. This complex is the source

of the SAC signaling. It is established on unbound kinetochores and emits a diffusing signal to the cytoplasm from there. Active MCC complexes and subcomplexes bind and sequester the essential subunit Cdc20 of APC/C (Ciliberto & Shah, 2009) and directly bind APC/C (Sudakin, Chan, & Yen, 2001) (Figure 5). Both phosphorylation of Cdc20 and direct binding by MCC contribute to the inhibition of APC/C complex (Izawa & Pines, 2015; Jia, Li, & Yu, 2016; Tang, Shu, Oncel, Chen, & Yu, 2004) (Figure 5).
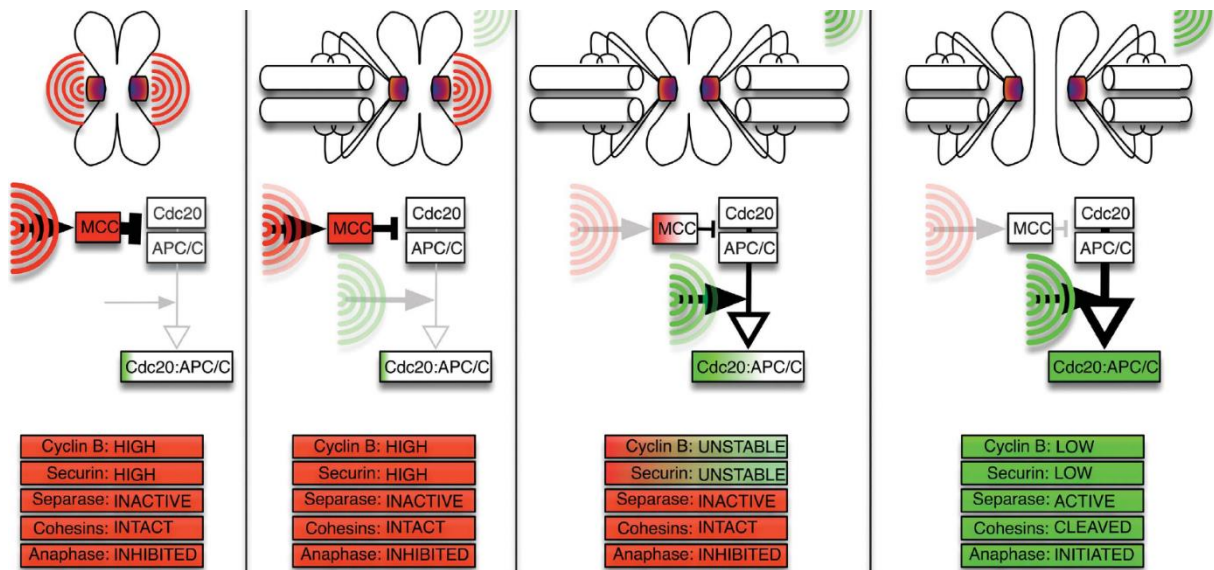
Figure 5. Correlation between the kinetochore tension and SAC signaling. From left to right, gradual silencing of the SAC signaling upon correct kinetochore-microtubule attachment is demonstrated. In the absence of the tension on kinetochores, the SAC signaling is at its peak and the establishment of tension silences the signal (adapted from Ciliberto & Shah, 2009).

The mechanism of SAC signaling explains how even one unattached kinetochore is sufficient to keep SAC signaling active. Even if one unattached kinetochore is present, it will provide docking sites for reprocessing of the inactivated MCC members. Moreover, with respect to the demands of the cell at that moment, unattached kinetochores can expand these docking sites beyond centromeres in order to process more MCC components at a time (Kaisari, Sitry-Shevah, Miniowitz-Shemtov, & Hershko, 2016; Tang, Bharadwaj, Li, & Yu, 2001). Upon establishment of the stable kinetochore-microtubule binding, the MCC complexes are carried towards the spindle poles via dynein motor proteins, thereby diminishing the SAC signaling (Chen & Liu, 2015). But these cargos constantly fall off the microtubules and are ready to diffuse towards any presently unattached kinetochore and APC/C and Cdc20. The rather obligatory aspect of SAC inhibition is dephosphorylation of the Aurora B and Plk1 phosphorylated signaling factors. The major phosphatase that does this job is PP2A-B55∂.

PP2A-B55∂ is recruited to the outer kinetochore by Plk1 phosphorylated BubR1 (Lampson & Kapoor, 2005). There is a dynamic balance between kinase and phosphatase activities at the kinetochore. Upon stable kinetochore-microtubule attachment, the outer kinetochore is pulled away from the inner kinetochore. The Aurora B kinase located in the inner kinetochore can not efficiently phosphorylate the SAC signaling factors located at the outer kinetochore. PP2A-B55∂ located at the outer kinetochore can efficiently inactivate these factors by dephosphorylating them. As a result, the phosphatase activity is no longer rivaled by kinase activity. This summarizes the chemistry of the kinetochore-tension model that terminates the SAC signaling (Alberts, 2015; Baxter et al., 2008). The inactive complex is dispersed and further blocked by binding of p31comet protein (Foley & Kapoor, 2013; Vleugel, Hoogendoorn, Snel, & Kops, 2012; Westhorpe, Tighe, Lara-Gonzalez, & Taylor, 2011). The APC/C and Cdc20 is now freed from the inhibitory effect of the MCC complex. Cdc20 activates APC/C and active APC/C can carry out its previously explained functions to initiate anaphase.

The balance between kinase-phosphatase activity is delicate. Premature exit from mitosis is prevented via Mastl>Arpp19/Ensa>PP2A-B55∂ pathway. During interphase, Mastl and PP2A are speculated to be associated, through which Mastl is maintained in an inhibited state. This interaction prevents phosphorylation of Ensa and Arpp19. During mitosis, Mastl is activated and this pathway starts to work as explained before. PP2A-B55∂ dephosphorylates Arpp19 and Ensa, but at a very slow rate, making these two proteins strong competitive inhibitors of PP2A-B55∂ (Mochida & Hunt, 2012).

2.4. Chemical genetics

In mammalian cells, under normal circumstances, mitosis is completed usually within an hour. Throughout mitosis, DNA is compacted and becomes inaccessible to transcription factors. Due to its very rapid and sequential nature, mitosis can not be regulated at the level of transcription. Rather fast-acting post-translational modifications govern the regulation of mitosis. Protein kinases are enzymes which in general transfer the gamma phosphate group of ATP to the hydroxyl group of the target serine, threonine, or tyrosine residues of the substrate protein. Upon phosphorylation, three negative charges are added per phosphosite, causing a drastic change in the physicochemical state of the protein. This may result in formation or breakage of major intramolecular and intermolecular interactions mainly via docking of phosphoresidues and their neighborhood to basic patches of the same protein or other proteins. This is an important way in which proteins become activated, inactivated, or be able to

communicate to initiate signals. Phosphate groups are eventually removed from these residues by protein phosphatases.

In the past, the use of gene knockout and gene silencing (knockdown) techniques have been utilized for investigation of the functions of mitotic kinases. The disadvantage of these approaches is that both techniques are slow acting at DNA or RNA level and mostly irreversible. Their nature renders these approaches incompatible to use as tools for short term functional analysis and characterization. The ability to make short term and delicate spatio-temporal analysis is especially important in case of mitotic kinases. Mitotic events take very short time and occur in rapid succession when compared to most other processes that cells undergo, such as migration or cell growth.

Loss of several cell cycle regulatory Cyclin-dependent kinases can be compensated by other kinases of the same family in case of gene knockout studies. In gene knockout and silencing, the cell is given enough time to adapt to such a loss of function if the kinase of interest is atonable. A strong example is that in mice, combined knockout of Cdk2, Cdk3, Cdk4, and Cdk6 genes can be compensated by Cdk1 alone, but not vice versa (Santamaría et al., 2007). However, chemical inhibition of Cdk2 showed a strong phenotype in mammalian cell lines, hindering the progression of cell cycle. To do so, they utilized a chemically inhibitable, yet a viable mutant of Cdk2 (Horiuchi et al., 2012).

When the indicated kinase is indispensable and a phenotype is observed in gene knockout or knockdown, the phenotype can not be completely attributed to the loss of catalytic activity, because the protein is abolished (Horiuchi et al., 2012; Lera & Burkard, 2012). Using chemical inhibition, the observed phenotypes can be attributed to the catalytic activity of the kinase. Chemical inhibition allows instantaneous loss of function and similarly instantaneous retrieval of the enzymatic activity upon removal of the inhibitor. In conclusion, permanent loss of a protein kinase at the gene or transcript level and transient blockade of the same protein kinase by chemical inhibition can result in different phenotypic effects.

Spatio-temporal analysis of biological functions of a mitotic protein kinase can be achieved by chemical inhibition of the kinase of interest. However, it can be a challenge to find a commercially available inhibitor or to design a specific inhibitor, because too many protein kinases are present with evolutionarily well-conserved ATP binding pockets. In the case of Mastl kinase, an allegedly specific small compound inhibitor was discovered (Ocasio et al.,

2016), but it is not commercially available and it has not been reported in another research since its discovery. We decided to follow an alternative approach to achieve specific chemical inhibition of Mastl kinase. To bypass the obstacle of drug design, ATP binding pocket of the kinase is engineered with respect to the structural features of ATP analogue small compounds, instead of designing small compounds with respect to the known ATP binding pocket structure. This is the reversed version of the known classical pharmacological approach, and it is named "chemical genetics". Instead of substituting functional groups or rings on a small organic compound scaffold, amino acid residues are substituted within the ATP binding pocket to create an AS (analogue-sensitive), chemically switchable protein kinase. In case of the Cdk2 example explained earlier in this section, the researchers utilized chemical genetics approach to achieve the necessary chemical inhibition. Mps1 dual-specificity protein kinase is indispensable for mitosis. Its chemical genetics analysis revealed a new function of the kinase that could not be addressed with other loss of function techniques published earlier. In addition to the known role of Mps1 in centrosome duplication, it is revealed that it also functions in SAC signaling later during metaphase (Sliedrecht, Zhang, Shokat, & Kops, 2010).

Chemical genetics technique mainly revolves around the use of a bulky ATP analogue as the inhibitor and substitution of the "gatekeeper" residue with a residue that is smaller in size (Figure 6).
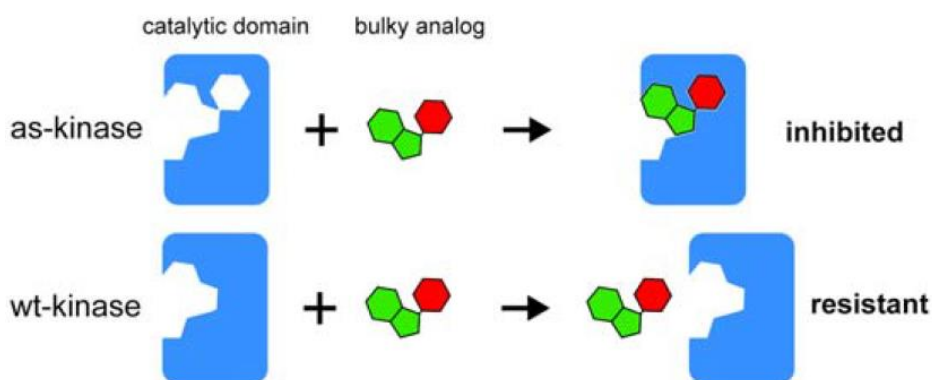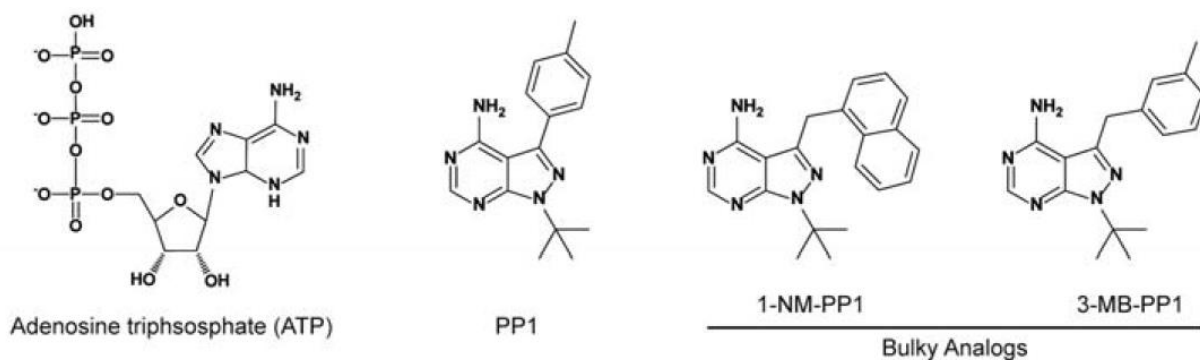
Figure 6. Principle of chemical genetics. In the upper panel, several examples for ATP analogues are given. These molecules contain additional cyclic groups covalently bound to the weak base moiety of each structure. In the lower panel, the inhibition of an AS kinase by an ATP analogue is demonstrated (adapted from Lera & Burkard, 2012).

The "gatekeeper residue" was initially discovered in drug-resistant tumor cells. The residue is located in the ATP binding pocket and its mutation alters the substrate specificity of the protein kinase in natural occurrences, such that a gatekeeper-mutant protein kinase can become drug resistant or constitutively active. A large gatekeeper residue blocks inhibitor compounds by causing steric hindrance, and a small gatekeeper residue allows access of the inhibitor compounds to the hydrophobic core of the ATP binding pocket (Barouch-Bentov & Sauer, 2011; Kissova, Maga, & Crespan, 2016). There are several advantages and limitations of this technique:

Advantages:

- High specificity towards the engineered ATP binding pocket.
- Rapid inhibition of the engineered kinase.
- Rapid reactivation of the kinase upon removal of the inhibitor.

- Less labor intensive when compared to the classical pharmacological approaches involving drug design.

Limitations:

- Mutations in the ATP binding pocket may inactivate the enzyme.
- The drug has to be cell membrane permeable.
- The drug has to be of lowest cytotoxicity.
- Determination of the optimal mutation-drug combination can be tricky.

2.5. Mastl kinase

Protein kinases are transferase class of enzymes that in general transfer the gamma phosphate of ATP to the hydroxyl group of serine, threonine, or tyrosine residues of the substrate protein. Protein kinases are bilobal enzymes and the active site is buried in a cleft between the lobes. Several crucial segments or residues located within the active cleft are the activation loop, DFG motif, glycine-rich loop, gatekeeper residue, and ATP binding pocket. Gatekeeper residue within the ATP binding pocket does not possess a catalytic feature, but its space occupancy is a determinant of whether an inhibitory compound can properly fit in the ATP binding pocket or not. A centrally located loop known as the "activation loop", typically 20-30 residues in length, provides a platform for the peptide substrate binding. Through specific interactions, activation loop sequence of a protein kinase determines the consensus sequence to be phosphorylated in the peptide/protein substrate, thus providing substrate specificity. In inactive state, activation loop is in "DFG-out" conformation that tilts the catalytic aspartate away from the ATP binding pocket and simultaneously blocks the catalytic cleft, thus preventing accession of both ATP and protein substrate. Upon phosphorylation of the activation loop, "DFG-in" conformation occurs and the activation loop is twisted out, as a result, the binding pocket is accessible to the substrates. In "DFG-in" state conformation, side chain of the catalytic aspartate now faces the ATP binding pocket and can interact with the gamma-phosphate of ATP (Huse & Kuriyan, 2002; Zuccotto, Ardini, Casale, & Angiolini, 2010).

The catalytic aspartate is a part of the DFG motif, which is located within the N-terminal segment of the activation loop. The DFG motif chelates the essential cofactor divalent cation, usually a magnesium. Backbone of the glycine rich loop, magnesium cofactor, and a conserved lysine residue located in the ATP binding pocket mainly interact electrostatically with α-phosphate and β-phosphate of the ATP molecule to coordinate the ligand. Catalytic aspartate is

responsible for transfer of the γ-phosphate from ATP to the target residue of a substrate protein. According to the mechanistic hypothesis, the ion-dipole interaction between the negatively charged oxygen of catalytic aspartate carboxylate and hydrogen of the protein substrate hydroxyl group, lowers the pK_a value of the substrate hydroxyl. Hypothetically, this results in conversion of the alcohol group of the target residue into an alkoxide at physiological pH, which is a stronger nucleophile than alcohol. Upon correct positioning of ATP and the substrate protein, nucleophilic attack of the alkoxide to the phosphorus atom of γ-phosphate initiates the enzymatic reaction. On the other hand, pH dependence studies are in conflict with this general acid catalysis model, suggesting a dissociative-like transition state. As in the case of explained catalytic models, kinetic models of protein kinases are also in conflict. The reactions catalyzed by protein kinases require both ATP and a substrate protein, thus, can be viewed as bisubstrate kinetic mechanisms. Bisubstrate reaction kinetics with compulsory ordered ternary complex mechanism was experimentally observed for PI3Kα and p38 MAPKα (LoGrasso et al., 1997; Maheshwari et al., 2017). On the other hand, although the results vary by use of different peptide substrates, steady-state kinetic approaches have revealed that several important protein kinases have shown random bisubstrate kinetic mechanism, again including p38 MAPKα (Adams, 2001; Kornev & Taylor, 2015; Szafranska & Dalby, 2005; Weber, 2010; Weber, Qian, & States, 2018).

Mastl (Microtubule-associated serine/threonine kinase like) is a unique serine/threonine protein kinase among the AGC family kinases. It has an unusually long (~500 residues) linker region between its N-terminal and C-terminal lobes. Studies on Xenopus egg extracts have shown the presence of three critical phosphosites on Mastl kinase. Positions of these residues in mouse Mastl are respectively T193, T206, and S861. T193 and T206 are located in the activation loop within Cdk1 consensus motifs (proline-directed) and are phosphorylated by Cdk1 *in vitro*. These two phosphosites are necessary for nuclear export of Mastl before NEBD. According to the currently accepted model, phosphorylation by Cdk1 partially activates Mastl by converting the activation loop from DFG-out conformation to DFG-in conformation. Upon partial activation, Mastl phosphorylates itself at its C-terminal tail phosphosite S861, allegedly by both cis-autophosphorylation and trans-autophosphorylation. In most other protein kinases, the phosphorylated C-tail is docked to a basic patch on the N-lobe to provide structural stability and to enhance the enzymatic activity. However, in case of Mastl, the C-tail of the enzyme is short and it can not reach to the basic patch on the N-lobe. For this reason, Mastl allegedly

works as homodimers and heterodimers, with the C-tails of both protein molecules docked to the basic patch on the N-lobe of each other (Blake-Hodek et al., 2012; Labesse et al., 2011).

In the PDB, a single entry (5LOH) is available for Mastl kinase crystal structure with a resolution of 3.1 Å (Ocasio et al., 2016). This crystal structure of human Mastl is incomplete, lacking residues within the activation loop, the glycine-rich loop, and N-terminal and C-terminal ends (Figure 7).

Figure 7. Crystal structure of human Mastl kinase. PDB entry 5LOH.

Structural and catalytic features of Mastl kinase are shown on the model structure of mouse Mastl in Figure 8.
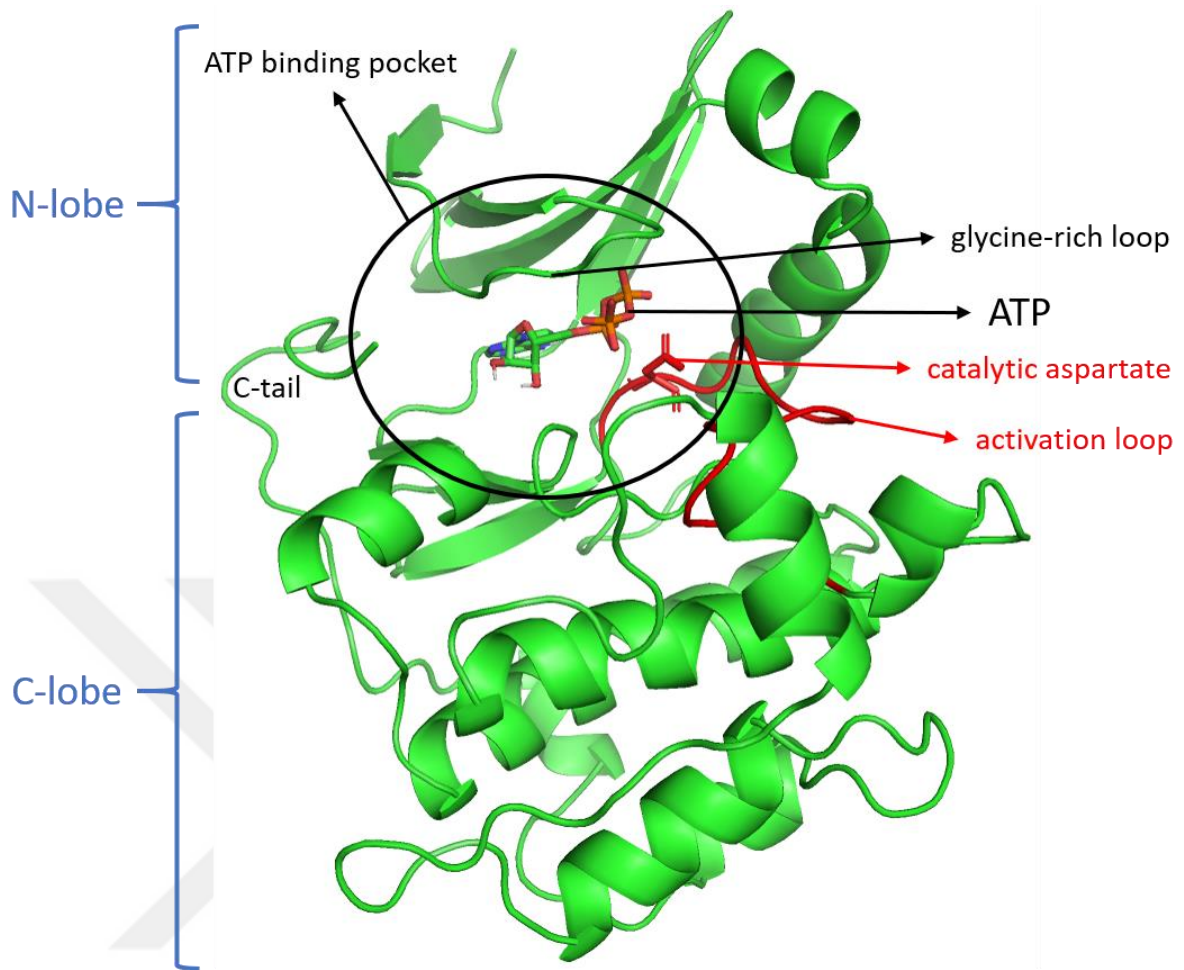
Figure 8. Structural and catalytic features of mouse Mastl. Active site elements such as the catalytic aspartate, activation loop, and glycine-rich loop are located in a cleft between the N-lobe and the C-lobe.

In 2004, Yu *et al.* discovered the importance of Mastl kinase for mitosis in a study in which they were characterizing a loss of function mutation of this gene (Yu et al., 2004). In 2009, Vigneron *et al.* has shown that PP2A, the major antagonist of mitosis, is regulated by Mastl (Vigneron et al., 2009). Mechanism of this regulation was undiscovered at the time. Later it was revealed that Mastl is responsible for the phosphorylation of specific inhibitors of PP2A-B55∂, namely Arpp19 (S62) and Ensa (S67) (Cundell et al., 2013; Gharbi-Ayachi et al., 2010; Okumura et al., 2014). Throughout years, the role of this gene in mitosis was repeatedly demonstrated in independent research articles. Loss of function studies of Mastl have shown phenotypes such as aberrant chromosomal segregation, formation of anaphase bridges, and failure of cytokinesis (Burgess et al., 2010; Galas, Li, Yu, Goldberg, & Zhao, 2006; Krajewska & van Vugt, 2010; Kubiak & Kishimoto, 2016).

In 2016, our work was published offering a possible explanation for the known phenotype (chromosome segregation defects in anaphase) when Mastl kinase is lost (Diril et al., 2016). In this paper, conditional knockout mouse embryonic fibroblasts were subjected to a phosphoproteomic mini-screen, to identify proteins that have an altered phosphorylation status in mitotic Mastl KO cells. Results revealed lowered phosphorylation levels for several proteins, including Mps1, an indispensable mitotic protein kinase that functions in duplication of centrosome and later in SAC signaling as explained in the previous sections. In addition, Mastl deficient cells were found to exit the mitotic state prematurely, supporting the hypothesis that Mastl might play a role in establishment/maintenance of the SAC signaling through phosphorylation of Mps1. However, whether Mastl kinase activity is required only for the initial establishment of SAC or it is also essential for its maintenance could not be addressed by genetic deletion methods. To further elucidate the Mastl kinase functions during different stages of mitosis, a reversible and acute inhibition of its kinase activity would be very useful. Therefore, we decided to utilize chemical genetics and to generate an analogue-sensitive variant of the Mastl kinase.

3. **MATERIALS AND METHODS**

3.1. Materials

Q5 high-fidelity DNA polymerase (M0491S) was purchased from NEB. DreamTaq DNA polymerase (EP0701), Fast Digest BstXI (ER1021), PstI (FD0614), HindIII (FD0504), and EcoRI (FD0274) endonucleases, Fast Alkaline Phosphatase (EF0654), T4 DNA ligase (EL0011), GeneJet PCR purification kit (K0701), PureLink HiPure plasmid miniprep kit (K210002), Lipofectamine 3000 transfection reagent (L3000015), Opti-MEM reduced serum media (11058021), PageRuler Plus prestained protein ladder (26619), 0.45 um PVDF transfer membrane (88518), and dithiothreitol (R0862) were purchased from Thermo Scientific. Skim milk powder (SKI400.250) was purchased from BioShop. Sterile Trypsin-EDTA solution (T4049-100ML), phosphate buffered saline (P4417-100TAB), high-glucose DMEM (D5671-6X500ML), LB Broth (Lennox) (L3022-1KG), Methanol (34860-2.5L-R), isopropanol (34863-2.5L), ethanol (32221-2.5L), glacial acetic acid (695092-2.5L), hydrochloric acid (258148-2.5L), sodium hydroxide (221465-500G), sodium dodecyl sulfate (L3771-500G), triton X-100 ((T8787-100ML), tris base (T1503-1KG), bromophenol blue (114391-5G), potassium acetate (P1190-100G), ethylenediaminetetraaceticacid (EDS-500G), donor goat serum (G6767-500ML), and ammonium persulfate (A3678-100G) were purchased from Sigma (Merck). Fetal bovine serum (16140) was purchased from Gibco. Puromycin (ant-pr-1) was purchased from InvivoGen. Glycerol (TK.070190.01001) and glucose (TK.090271.05004) were purchased from TEKKIM. Cell culture grade DMSO (A3672,0100), N,N,N',N'-Tetramethylethylenediamine (A1148,0025), and agarose (A8963,0250) were purchased from Applichem. Safeview (G108) and 1kb Opti-DNA marker (G106) were purchased from ABM. Enhanced chemiluminescence detection kit (1705061), acrylamide/bisacrylamide 37.5:1 (w/w) 30% solution (1610148), and Bradford protein assay kit 1 (5000001) were purchased from Bio-Rad. Calcium chloride, Coomassie R-250, Mowiol, paraformaldehyde, polybrene, and Tween-20 were obtained from local research laboratories. All reagents were of analytical grade. Microscope slides (1000000) and cover glasses (0111520) were purchased from Marienfeld.

Rabbit anti-Mastl polyclonal antibody was used at 1:5000 dilution for western blot and 1:100 dilution for immunocytochemistry. Rabbit anti-Arpp19 polyclonal antibody was used at 1:1000 dilution for western blot and 1:150 dilution for immunocytochemistry. The Mastl and Arpp19 antibodies are homemade, produced in Kaldis lab (Institute for Molecular and Cell Biology, Agency for Science, Technology and Research, Singapore, Republic of Singapore).

Rat anti-HA tag monoclonal antibody (Roche, clone 3F10, 11867423001) was used at 1:500 dilution, rabbit anti-HA tag monoclonal antibody (Cell Signaling Technology, clone C29F4, 3724) was used at 1:1000 dilution, HRP-linked goat anti-rat IgG (Cell Signaling Technology, 7077P2) was used at 1:1000 dilution, and HRP-linked goat anti-rabbit IgG (Cell Signaling Technology, 7074P2) was used at 1:5000 dilution for Western blot. Mouse anti-HA tag monoclonal antibody (Cell Signaling Technology, clone 6E2, 2367) was used at 1:150 dilution for immunocytochemistry. Mouse anti-HA tag monoclonal antibody (Roche, clone 12CA5, 11583816001) was used at 1:100 dilution for immunocytochemistry. Anti-HA tag primary antibodies and HRP conjugated secondary antibodies were obtained from Kaldis lab. Alexa Fluor 488 goat anti-rabbit secondary antibody (4412), Alexa Fluor 488 goat anti-mouse secondary antibody (4408), Alexa Fluor 594 goat anti-rabbit secondary antibody (8889), and Alexa Fluor 594 goat anti-mouse (8890) secondary antibody were purchased from Cell Signaling Technology, and used at 1:150 dilution for immunocytochemistry. PLAT-E and 293FT packaging cell lines, and immortalized Mastl conditional knockout mouse embryonic fibroblasts were obtained from Kaldis lab.

Primers used in this study are given in Table 1.

Table 1. The list of primers used in this study.

Sequence	Purpose
CTGCAGAACCAGTGTGGTGGATGTACCCATACGATGTT	HA_mmMastl with BstxI site FWD
CTGCAGAACCACTGTGCTGGCTACAGACTAAACCCAGAT	HA_mmMastl with BstxI site REV
GCAACATCTACTTGATAGGGGAGTATCTTATTGGCGGAGA TGTCAAGTCTCTCCTAC	HA_mmMastl M109G FWD
GACATCTCCGCCAATAAGATACTCCCCTATCAAGTAGATG TTGCTTGCTGACTGC	HA_mmMastl M109G REV
GCAACATCTACTTGATAGCGGAGTATCTTATTGGCGGAGA TGTCAAGTCTCTCCTAC	HA_mmMastl M109A FWD
GACATCTCCGCCAATAAGATACTCCGCTATCAAGTAGATG TTGCTTGCTGACTGC	HA_mmMastl M109A REV
TTGCGCATCTCTATTACTCACTGCAGTCAGCAAGCAACATC TACTTGATAGCGGAGTATCTTATTGG	HA_mmMastl V93A/M109A FWD
TCCGCTATCAAGTAGATGTTGCTTGCTGACTGCAGTGAGTA ATAGAGATGCGCAACAAAAGG	HA_mmMastl V93A/M109A REV
TTGCGCATCTCTATTACTCACTGCAGTCAGCAAGCAACATC TACTTGATAGGGGAGTATCTTATTGG	HA_mmMastl V93A/M109G FWD
TCCCCTATCAAGTAGATGTTGCTTGCTGACTGCAGTGAGTA ATAGAGATGCGCAACAAAAGG	HA_mmMastl V93A/M109G REV
CTCAATCCTCCCTTTATCC	pBABEpuro sequencing FWD
CAGGACAAGTCTTATCTCTC	HA_mmMastl sequencing FWD
ATTTCCACTTGGTTGACTC	HA_mmMastl sequencing and colony PCR FWD
CCCTAACTGACACACAT	pBABEpuro sequencing and colony PCR REV
ATGCTCTAGAACCATGTACCCATACGATG	HA_mmMastl with XbaI site FWD
ATGCTCTAGACTACAGACTAAACCCAGATATGG	HA_mmMastl with XbaI site REV
GCCATCCACGCTGTTTTGACCT	pBOBI sequencing and colony PCR FWD
CGGCTCCTTCTGATCTACAGACATAGGAC	HA_mmMastl sequencing and colony PCR reverse
GGCAGGTGGAGGCAAGAGCTCACAGA	mmMastl genotyping primer REV
CATGCCTTCCTTGAAAGAGGTGGAC	mmMastl genotyping primer FWD
GTGGGAGGAATTACAAGAGACAAC	mmMastl genotyping primer REV

Hettich table top centrifuge (Rotanta 460R), Eppendorf table top centrifuge (5810R), Thermo table-top microcentrifuge (Micro CL 17R), Thermo benchtop orbital shaker (MaxQ 4000), Thermo digital shaker drybath (88880028), Thermo compact digital rocker (88880020), Thermo compact digital mini rotator (88880026), Thermo mini centrifuge (mySPIN 6), and Thermo LP vortex mixer (88880018) were used as basic lab equipment.

P330 NanoPhotometer spectrophotometer (Implen) was used for OD600 measurements. SimpliAmp thermal cycler (Applied Biosystems) was used for various applications of polymerase chain reaction. Savant ISS110-230 SpeedVac Concentrator (Thermo) was used for vacuum drying of the DNA preparates. PowerPac Basic and PowerPac Universal (Bio-Rad) power supply systems were used for gel electrophoresis and Western blotting. B Owl™ EasyCast™ B1 and B2 Mini Gel Electrophoresis Systems (Thermo) were used for agarose gel electrophoresis. Mini-PROTEAN Tetra Cell system (Bio-Rad) was used for polyacrylamide gel electrophoresis. AE-6675 semidry transfer system (ATTO) was used for Western blots. DNA concentration measurements were done using Thermo NanoDrop 2000. IX71 microscope (Olympus) with cellSens Entry software was used for acquisition of bright field and fluorescence images. Universal Hood II UV trans illuminator (Bio-Rad) with Image Lab 5.2.1 software was used for acquisition of agarose gel (SafeView), acrylamide gel (Coomassie), and PVDF membrane (Coomassie) stains. When necessary, Image Lab 6.0 software was used for quantitative analysis of the gels and blots. Multiskan GO multiwell plate reader (Thermo Scientific) with SkanIt 3.2 software was used for protein concentration measurements. Chemi-Smart 50001 (Peqlab) with Chemi-Capt software was used for detection of chemiluminescence in Western blot analysis. CLC Main Workbench 7.9.1 software was used for visualization of DNA and protein sequences. PyMOL software was used for molecular visualization. Images were rendered via Adobe Photoshop CS6 software.

3.2. Methods

3.2.1. Computational analysis of the mutations

Webservers, programs, and databases used in this study are listed below:

- RCSB PDB: https://www.rcsb.org/
- UniProt: https://www.uniprot.org/
- Pfam: https://pfam.xfam.org/
- EMBOSS Needle: https://www.ebi.ac.uk/Tools/psa/emboss_needle/

- I-TASSER: https://zhanglab.ccmb.med.umich.edu/I-TASSER/
- ProFit: http://www.bioinf.org.uk/software/profit/
- ConSurf: http://consurf.tau.ac.il/2016/
- TargetATPsite: http://www.csbio.sjtu.edu.cn:8080/TargetATPsite/
- HADDOCK2.2:
  https://milou.science.uu.nl/services/HADDOCK2.2/haddockserver-guru.html
- PLIP: https://projects.biotec.tu-dresden.de/plip-web/plip/

3.2.1.1. Homology modeling

Although crystal structure of the fused kinase domains of Mastl is present (PDB entry 5LOH), ATP or ATP analogue bound crystal structures are not available. To analyze the effects of ATP binding pocket point mutations on the binding affinities of ATP and the ATP analogues, we initially modeled the ATP bound state of mouse Mastl.

The protein sequence of mouse Mastl was downloaded from Uniprot (Uniprot entry GWL_MOUSE Q8C0P0) (Bateman, 2019) and domain annotations were obtained from Pfam (The Protein Family Database) (El-Gebali et al., 2019). Regardless of the protein family and species, ATP bound ten protein kinase crystal structures (PDB entries 1ATP, 3VVH, 4EOQ, 4WB5, 4XBR, 4XX9, 5D9H, 5LPY, 5OBJ, and 5OSP) were downloaded from RCSB PDB (Research Collaboratory for Structural Bioinformatics Protein Data Bank) (Berman et al., 2000).

Sequence homology between the mouse Mastl kinase domains and the sample crystal structures were analyzed via EMBOSS Needle Pairwise Sequence Alignment webserver (Rice, Longden, & Bleasby, 2000; Saul & Christian, 1970). The tool uses the Needleman-Wunsch alignment algorithm to achieve optimum alignment of two protein sequences (Needleman & Wunsch, 1970). The pairwise sequence alignments were created using the default settings of the tool.

I-TASSER (Iterative Threading ASSEmbly Refinement) is an online webserver for prediction of protein structure based on its sequence (Roy, Kucukural, & Zhang, 2010; Yang et al., 2014; Zhang, 2008). This webserver follows a hierarchical approach to prediction of protein structure and function. Utilizing multiple threading approach LOMETS, the program first identifies structural templates from the PDB with full-length atomic models constructed by

iterative template-based fragment assembly simulations. Function insights of the target are then derived by threading the 3D models through protein function database BioLiP. The sequence of mouse Mastl kinase domain and the template crystal structure 1ATP were submitted to I-TASSER. Within the "first option" tab, template was specified without alignment.

3.2.1.2. Analysis of evolutionary conservation of the residues

Wild type mouse Mastl model structure was submitted to ConSurf for estimation of the evolutionary conservation of amino acid positions. Default settings of the server were used and the calculations were done using the Bayesian method. The server generated an MSA (multiple sequence alignment) from an ensemble of 150 homologous protein sequences and calculated the conservation percentage for each amino acid position (Ashkenazy et al., 2016; Ashkenazy, Erez, Martz, Pupko, & Ben-Tal, 2010; Celniker et al., 2013; Glaser et al., 2003; Landau et al., 2005).

3.2.1.3. Prediction of the active site residues

TargetATPsite is a webserver that predicts the ATP binding pocket within a given protein (Yu et al., 2013). To determine the active site residues, model structure of mouse Mastl was submitted to TargetATPsite webserver, using the default settings. After analysis of the trial docking results using this initial set of residues and comparison of the different residue sets obtained by use of different threshold values, we decided to elaborate our active site residue choices. Under the guidance of the initial residue set determined by TargetATPsite, we selected the active site residues empirically.

3.2.1.4. Preparation of the model complexes for HADDOCK refinement

The model structure output files did not contain ligands. The template crystal structure was superimposed to the obtained model structure via the alignment option of PyMOL. The ligand coordinates of the crystal structure were isolated together with the model structure and the desired ATP-bound model structure of mouse Mastl was obtained.

Coordinates of the ATP analogues 1-NA-PP1, 1-NM-PP1, and 3-MB-PP1 were edited based on the ATP coordinates within the model structure of mouse Mastl. Currently, PyMOL lacks small compound-alignment feature. ProFit (Protein Least Squares Fitting) program was used locally for atom-atom alignment of small compounds. A planar alignment of the ligands is aimed in which the weak base group of each molecule is superimposed. Briefly, the coordinates of the ATP analogues were edited via ProFit and the corresponding three atoms of

each ATP analogue were aligned to the C1', N1, and N6 atoms of the ATP from the model structure of mouse Mastl. The ATP analogue-bound model complexes were obtained similarly by isolating the ligand coordinates with the protein moiety of the model structure.

3.2.1.5. HADDOCK refinement

HADDOCK (High Ambiguity Driven protein-protein DOCKing) is a molecular docking program for prediction of the 3D structures of biomolecular complexes (Van Zundert et al., 2016). HADDOCK performs docking by using the three stages explained respectively:

- *it0* (iteration 0): Randomization of orientations and rigid body minimization: In the first stage, intramolecular interaction features such as bond lengths, bond angles, and dihedral angles are fixated and treated as rigid bodies. The partners are randomly rotated around their center of mass. After randomization of starting orientations, rigid body minimization is applied to optimize the interactions.
- *it1* (iteration 1): Semi-flexible simulated annealing in torsion angle space: In the second stage, the interfaces that modeled at the end of *it0* are refined in three steps:
  - *i.* Optimization of orientations of the partners.
  - *ii.* Optimization of interfacial backbone conformations.
  - *iii.* Optimization of interfacial side chain conformations.
- *water*: Refinement with explicit solvent: In the third stage, the interacting partners are immersed in a solvent shell (8 Å for TIP3P model water or 12.5 Å for DMSO). In order to improve the energetics of interactions, short molecular dynamics simulation (at femtosecond timescale) at 300 K is performed on these solvated complexes.

For refinement, HADDOCK 2.2 guru interface was used. To obtain the mutant proteins, side chain information of the residues of interest were erased from the files manually and the name of the residues were changed with respect to the to-be-substituted amino acids. HADDOCK then automatically filled in the new side chain conformations throughout each run. As a control, the triphosphate and ribose groups of the ATP molecule were removed prior to the refinements. Thus, the control results will be directly comparable with the results of ATP analogues which lack triphosphate and ribose groups, and the protein-ligand interface at the site of point mutations will be more focused on for scoring.

A restraint file was prepared to define the atom-atom restraints which will be used during the simulations. Hydrogen bond donor or acceptor candidates from both the protein and the ligand were given priority for preparation of the restraint file. The to-be-substituted residues were avoided when constructing the restraint file. It is a good practice to set the restraints distant to the sites of particular interest, so that these sites will be relatively free throughout the simulation, improving the results. Although all of the three restraints were set on the rigid (planar and non-rotatable) heterobicyclic group, care was taken to select atom pairs distant to the mutation sites just in case. The same set of atoms which utilized for ligand alignment (C1', N1, and N6 atoms) were also used for preparation of the restraint file. Atomic distances were obtained via the measurement option of PyMOL and 0.5 Å error range was defined for each restraint. An example restraint file is given below:

```
assign (resid 79 and name O and segid A)  (resid 1 and name N6 and segid B)  2.9 0.5 0.5
assign (resid 81 and name N and segid A)  (resid 1 and name N1 and segid B)  3.4 0.5 0.5
assign (resid 9 and name C and segid A)  (resid 1 and name C1' and segid B)  4.5 0.5 0.5
```

In order to perform local docking, *it0* stage was skipped by unchecking the "randomize starting orientations", "perform initial rigid body minimization", and "allow translation in rigid body minimization" parameters within the "Advanced sampling parameters" tab in the website.

The final structures were clustered based on their pairwise ligand interface RMSD (Karaca & Bonvin, 2013). After each successfully completed run, a single cluster with an ensemble of 200 water refined complexes was obtained. Van der Waals (kcal/mol), electrostatics (kcal/mol), BSA (Å), and total HADDOCK score values were extracted from the complex with the lowest total HADDOCK score (the highest absolute value). For each run output, these first ranked complexes were submitted to PLIP (Protein-Ligand Interaction Profiler) (Salentin, Schreiber, Haupt, Adasme, & Schroeder, 2015) for physicochemical analysis of the non-covalent protein-ligand interactions.

3.2.2. Preparation of chemically competent cells and DNA transformation

Chemically competent TOP10 strain of *Escherichia coli* cells were prepared according to our modified protocol from Sambrook and Russel, 2013:

- LB media and LB agar plates were prepared according to the common protocols found in the manufacturer's web sites. Briefly, 20 g/L LB broth powder was dissolved in ddH$_2$O for LB media preparation. Additional 15 g/L agar was used for LB-agar plate preparation. Media and agar mixtures were sterilized by autoclave. For antibiotic

selection, ampicillin was added to the media and agar solutions at a working concentration of 100 µg/mL. Sterile 1L LB, 1L 0.1 M CaCl2, and filtered 10 mL 10% glycerol/0.1M CaCl2 solutions were prepared.

- Further steps were carried out under aseptic conditions.

- 1 µL of bacteria from previous competent cell batch (electrocompetent or chemical competent) was added in an LB containing microcentrifuge tube.

- Bacteria were serially diluted in antibiotic free LB media 10^6 folds, in sterile microcentrifuge tubes. 100 µL of the final dilution was seeded to an antibiotic free LB agar plate. The plate was incubated at 37°C overnight.

- A single colony was picked and inoculated in 7.5 mL antibiotic free LB in a 50 mL conical flask. The inoculated media was cultured overnight at 37 degree at 250 rpm.

- 2x 2L conical flasks prefilled with prewarmed 500 mL of antibiotic free LB were inoculated with 2.5 mL of overnight miniculture per conical flask.

- Centrifuge was cooled to 4°C.

- OD600 measurements were initiated after 1 hour, and repeated every 15-20 min. The incubation was immediately terminated by cooling the cultures when the OD600 value reached 0.15-0.3. To do so, cultures were poured in a total of two 500 mL prechilled centrifuge bottles and the centrifuge bottles were placed on ice-water bath.

- Bacteria were spun down at 2750g for 20 minutes.

- Supernatants were discarded. Each pellet was resuspended in 250 mL of ice-cold 0.1 M CaCl$_2$ and held for 1 hour in ice bath.

- Centrifugation step was repeated as before.

- Supernatants were discarded. Each pellet was resuspended in 250 mL of ice-cold 0.1 M CaCl$_2$ and held for 4 hours in ice bath.

- Centrifugation step was repeated as before.

- The supernatants were discarded. Each pellet was resuspended in 4 mL ice-cold 15% glycerol containing 0.1 M CaCl$_2$. Bacterial suspensions were pooled together.

- The total suspension was aliquoted into prechilled 1.5 mL PCR tubes on ice as 100 µL portions. The portions were transferred to a cryobox prechilled at -80°C, in 4°C cold room. Upon completion of the transfer, the cryobox was immediately placed in the -80°C freezer.

- To transform, cells were thawed on ice and at most 5 µL of DNA solution was added. DNA-cell mixtures were mixed 2-3 times with a prechilled 20-200 µL pipette tips.

- The suspensions were left on ice for 30 min. The water bath was heated to 42^0C.

- The suspensions were heat shocked for 50 seconds.

- The suspensions were immediately placed on ice and held on ice for 3 minutes.

- The recovery incubation was initiated by adding 1 mL antibiotic free LB to each suspension. The tubes were incubated at 37^oC for 40 minutes.

- The bacteria were concentrated by centrifugation at 1000xg for 5 minutes using a table top centrifuge. The supernatants were discarded. The pellets were resuspended in the remaining 100-200 µL culture media and seeded to ampicillin containing (100 µg/mL) agar plates. The plates were incubated at 37^oC overnight.

3.2.3. Molecular cloning

3.2.3.1. Site-directed mutagenesis

Full length HA tagged mouse Mastl cDNA inserted in pBABEpuro retroviral expression vector was obtained from Kaldis lab (Institute of Molecular and Cell Biology, Agency for Science, Technology and Research, Singapore, Republic of Singapore). Using site directed mutagenesis approach followed by conventional restriction cloning, substitutions in the ATP binding pocket were performed. Using mutagenesis primers given in Table 1, mutagenesis PCR was performed according to NEB's modified protocols. Principles of the mutagenesis PCR are explained in Figure 9.
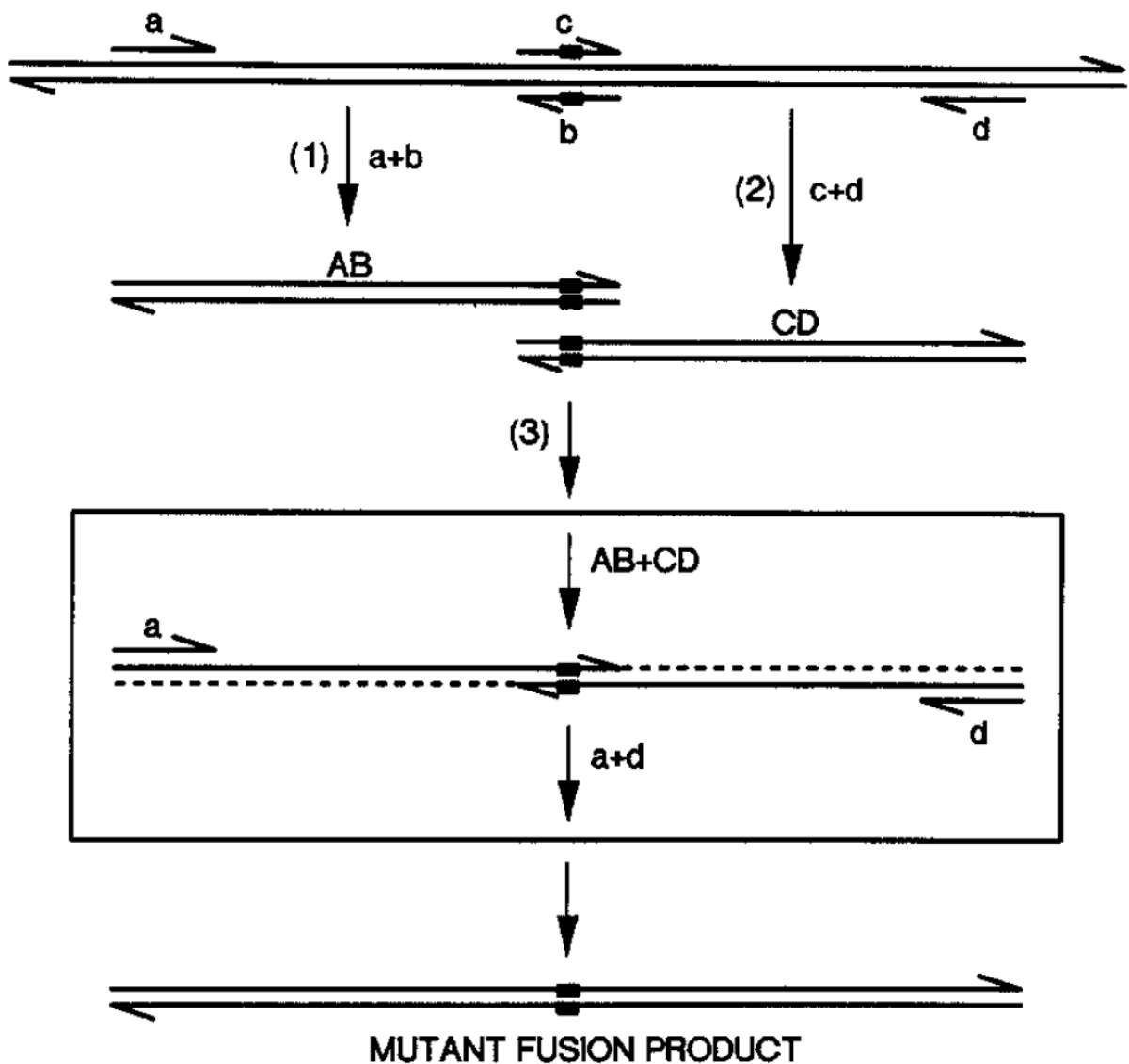
Figure 9. Mechanism of site-directed mutagenesis PCR. The reaction is constituted of two steps. In the first round, the desired point mutation is introduced by the use of overlapping primers (c and b) carrying the intended nucleotide substitutions. The amplification products are established on the mutated primers, as a result, the amplicons carry the mutation. In the second round, the strands of two different fragments (AB and CD) of the complete DNA are annealed by their overlapping region. These annealed fragments prime each other. The full-length DNA fragment (AB+CD) is amplified by the cloning primers "a" and "d" throughout the proceeding cycles (adapted from Ho, Hunt, Horton, Pullen, & Pease, 1989).

Mutagenesis PCR setup and cycling conditions are given in Table 2 and Table 3 respectively.

Table 2. Mutagenesis cloning PCR setup.

Component	Volume (µL)
5x Q5 reaction buffer	10
10 mM dNTPs	1
100 µM FWD primer	0.5
100 µM REV primer	0.5
Template plasmid	10 ng
Q5 high-fidelity polymerase	0.5
ddH$_2$O	to 50 µL

Table 3. Mutagenesis cloning PCR cycling conditions.

Step	Temperature (ºC)	Time
Initial Denaturation	98	30 seconds
First 5 cycles	98	10 seconds
	59	10 seconds
	72	1 minute
Last 20 cycles	98	10 seconds
	72	10 seconds
	72	1 minute
Final extension	72	2 minutes
Hold	10	-

Using GeneJet PCR purification kit (Thermo), spin column purification was performed on cDNA amplicons to get rid of the primers, primer dimers, and small amplicon artefacts coming from the mutagenesis PCR. The kit utilizes a silica-based membrane for adsorption of large DNA fragments under suitable pH condition and buffer composition, so that undesirable

reaction leftovers can be washed away and the purified DNA can be desorbed and eluted at the end of the protocol.

- Equal volume of binding buffer was added and mixed.
- Mixtures were pipetted directly on the column membrane.
- Columns were centrifuged at 14,000xg for 1 minute, the flowthroughs were discarded.
- 700 µL of wash buffer was added to each column.
- Columns were centrifuged at 14,000xg for 1 minute, the flowthroughs were discarded.
- The empty columns were centrifuged at 17000xg for 1 minute.
- Columns were transferred to clean 1.5 mL microcentrifuge tubes and 55 µL hot ddH$_2$O was added.
- Columns were incubated at 70°C for 3 minutes and centrifuged at 17000xg for 1 minute.
- Concentrations were measured using ddH$_2$O as blank and 1.5 µL was used for the blank and each sample on NanoDrop 2000.

The purified cDNA moieties were mixed at equimolar ratios and used as template for fusion PCR. Briefly, mutagenesis PCR conditions were used for fusion PCR, but the cycling stage was carried out as a single stage with a fixed annealing temperature of 72°C. Lentiviral mutant DNA constructs were directly subcloned from the pBABEpuro mutant DNA constructs, without performing additional site directed mutagenesis. The mutant fusion PCR products were subjected to a second round of spin column purification. Downstream processes of molecular cloning experiments require purified, high quality DNA preparates. Because chemical contaminants coming from the preceding experiments (i.e. PCR buffer) may have a negative impact on the subsequent delicate reactions such as restriction, dephosphorylation, and especially ligation.

3.2.3.2. Restriction and ligation

Spin-column purified cDNA preparates were simultaneously digested with DpnI and BstXI (3-6 hours at 37°C). The empty vector was digested with BstXI (3-6 hours at 37°C), purified, and Fast AP treated (1 hour at 37°C) respectively. The reaction setup is given in Table 4.

Table 4. Restriction reaction setup for cloning. Reaction volumes were scaled up with respect to the requirements.

Component	cDNA preparation	Backbone preparation
10x Fast Digest buffer	2 µL	5 µL
DNA	2 µg	5 µg
Dpn1	0.5 µL	-
BstX1	1.5 µL	5 µL
Fast AP	-	5 µL
ddH$_2$O	to 20 µL	to 100 µL

All reaction products were subjected to spin column purification, using GeneJet PCR purification kit (Thermo). The ligation of the purified, cut insert to the purified, cut, and dephosphorylated empty vector was carried out according to the manufacturers modified protocol (Table 5). To achieve the desired insert:vector molar ratio, the calculations were performed using NEBs online "BioCalculator" tool.

Table 5. Ligation reaction setup. Reaction volumes were scaled up with respect to the requirements.

Component	negative control	negative control	ligation
Sample tubes			
Insert DNA	-	3:1 molar ratio	3:1 molar ratio
Linear vector DNA	100 ng	-	100 ng
ddH2O	to 10 µL	to 10 µL	to 10 µL
1X master mix			
10x T4 ligase buffer	2 µL	2 µL	2 µL
T4 ligase	0.2 µL	0.2 µL	0.2 µL
ddH$_2$O	to 10 µL	to 10 µL	to 10 µL

The DNA containing tubes were mixed, heated, and cooled respectively, in order to promote correct ligation. Using the thermal cycler with a cover temperature of 75°C, tubes were incubated at 70°C for 10 minutes. After the incubation step, tubes were cooled to 37°C with a ramp rate of 0.1°C/sec. The heated cover was opened to allow efficient cooling when the samples reached 40-50°C. After completion of the slow cooling step, samples were further cooled to 10°C with a ramp rate of 0.5°C/sec. At the end of the run, DNA containing tubes were transferred to ice. The ligase containing master mix was prepared according to the given reaction setup (Table 5) and the volumes were scaled up with respect to the number of reactions to be set. Ligations were performed at room temperature for at least 10 minutes or overnight.

For cloning of lentiviral mutant DNA constructs, XbaI endonuclease was used for digestion of both the cDNA and the lentiviral vector.

3.2.3.3. Plasmid isolation, colony PCR, and diagnostic restriction

The ligation products were transformed into the chemically competent cells according to the protocol previously described in section 3.2.2. The overgrown colonies were initially screened by colony PCR, using one primer that anneals to the backbone and its partner primer that anneals to the insert. With this approach, a positive result from colony PCR indicates both the presence of the insert in the vector and in which orientation it is inserted. Single colonies

were picked and cultured in 96-well round-bottom plate microculture format. 2 µL of microculture for each colony were directly used as a PCR template, without preprocessing. Colony PCR setup and cycling conditions are given in Table 6 and Table 7 respectively.

Table 6. Colony PCR setup.

Component	Volume (µL)
10x DreamTaq Buffer	2
10 mM dNTP	0.4
100 µM FWD primer	0.2
100 µM REV primer	0.2
Template	2
DreamTaq DNA polymerase	0.2
ddH$_2$O	to 20 µl

Table 7. Colony PCR cycling conditions. 500 bp amplicon indicates positive result.

Step	Temperature (ºC)	Time
Initial Denaturation	95	5 minutes
35 cycles	95	30 seconds
	59	30 seconds
	72	45 seconds
Final extension	72	5 minutes
Hold	10	-

Colonies which gave positive result were cultured and manual plasmid isolation was performed to subject the colonies to further validation via diagnostic restriction, using Pst1 endonuclease (Table 8). Manual plasmid DNA isolation protocol is as described below, modified from Sambrook and Russel, 2013:

- Buffer1: Resuspension buffer. 50 mM glucose, 10 mM EDTA, and 25 mM Tris-Cl, pH 8. RNase was added to ~50 µg/mL if possible. Stored at 4°C.

- Buffer2: Lysis solution. Fresh 1:1 (v/v) mix of buffer 2a&2b of required volume was prepared for each prep session. Buffer2a: 0.4 N NaOH, buffer2b: 2% SDS. Stored at room temperature.

- Buffer3: Neutralization buffer. 3M KOAc (29.4 g potassium acetate), 11.5 mL glacial acetic acid, and water up to 100 mL.

- When required, 0.5-1 mL portion of miniculture was used to establish bacterial clone stocks. Bacterial suspensions were mixed with autoclaved glycerol at 1:5 (v/v) ratio. Glycerol contents were mixed carefully and the clones were stored at -80°C.

- The remaining cells were pelleted at 3900xg for 15 minutes.

- The bacteria were resuspended in 150 µL of buffer1.

- 150 µL of buffer2 was added to each suspension, mixed by inversion a few times, and incubated no longer than 5 minutes.

- 225 µL of buffer3 was added and the samples were mixed by inversion a few times.

- Suspensions were centrifuged at 17000xg in a table top centrifuge for 5 min. After this step, microcentrifuge was cooled to 4°C.

- Supernatants were taken to a new microcentrifuge tube and the pellets were discarded. Supernatants were cooled on ice.

- 650 µL of -20°C 100% isopropanol was added to each sample and vortexed thoroughly.

- Samples were held at -20°C until the cooling of the centrifuge is completed (approximately 20 minutes).

- Samples were centrifuged at max speed at 4°C for 30 minutes.

- Supernatants were discarded.

- 1 mL of -20°C 70% EtOH was added to each white DNA pellet, briefly vortexed, and centrifuged at 17000xg at 4°C for 5 minutes.

- Supernatants were discarded, the tubes were spun down and placed on ice. The residual solvent was discarded using 20-200 µL pipette tips.

- The samples were further dried using vacuum dryer at high rate for 15 min.

- Pellets were dissolved in 50 µL ddH$_2$O by shear vortexing.

Concentrations of manual minipreps were not measured because we did not aim to use them in analytical experiments and due to the dirty content of the preparates.

Table 8. Reaction setup of diagnostic restriction. Reaction volumes were scaled up with respect to the number of colonies to be screened.

Component	cDNA preparation
10x Fast Digest buffer	2 µL
DNA	5 µL
Pst1	0.25 µL
ddH$_2$O	to 20 µL

Restriction mapping of lentiviral vectors were carried out using HindIII and EcoRI endonucleases. Digested plasmid DNAs and colony PCR products were analyzed by agarose gel electrophoresis. 50x TAE buffer is constituted of 242 g/L Tris, 5.7% glacial acetic acid, and 10% 0.5 M pH 8 EDTA-NaOH in ddH$_2$O. 1x TAE running buffer was prepared by diluting the 50x TAE buffer 1:50 in ddH$_2$O. 1% agarose gel containing 1:20000 Safeview was prepared in TAE. Gels were run in TAE buffer at constant 100 V for 1 hour and the gel images were acquired using Bio-Rad Universal Hood II UV transilluminator. "Nucleic acid gel>Ethidium bromide>Intense bands" settings of Image Lab 5.2.1 software were used.

Upon successful colony PCR and restriction mapping verification of clones for each construct, full length cDNAs were sequence verified. Due to the cost and time consumption of sequencing, we avoid using dirty DNA preparates for sequencing reactions. Sequencing-grade plasmid DNA minipreps were prepared from the bacterial clones using GeneJet plasmid miniprep kit (Thermo) according to the manufacturer's protocol. The kit utilizes a silica-based membrane for adsorption of DNA under suitable pH condition and buffer composition, so that undesirable soluble bacterial components that can interfere with the sequencing reaction can be washed away and the purified DNA can be desorbed and eluted at the end of the protocol.

- Minicultures were centrifuged at 3900xg for 10 minutes.
- Clarified culture media were discarded and bacterial pellets were resuspended in 250 µL of resuspension buffer to homogeneity.

- 250 µL of lysis solution was added to each sample and tubes were mixed immediately by inversion. Samples were left 3 minutes for lysis.
- 350 µL of neutralization buffer was added to each sample and the tubes were mixed immediately by inversion.
- The suspension was centrifuged at 17000xg for 5 minutes and the cell debris was discarded.
- The supernatants were pipetted directly on the column membranes.
- Columns were centrifuged at 14,000xg for 1 minute, the flowthroughs were discarded.
- 500 µL of wash buffer was added to each column.
- Columns were centrifuged at 14,000xg for 1 minute, the flowthroughs were discarded.
- The washing step was repeated and a total of two washes were performed.
- The empty columns were centrifuged at 17000xg for 1 minute.
- Columns were transferred to clean 1.5 mL microcentrifuges tube and 55 µL hot ddH$_2$O was added.
- Columns were incubated at 70°C for 3 minutes and centrifuged at 17000xg for 1 minute.
- Concentrations were measured using ddH$_2$O as blank and 1.5 µL was used for the blank and each sample on NanoDrop 2000.

After sequence verification, transfection-grade (endotoxin-free) plasmid DNA minipreps were prepared from the bacterial clones using PureLink HiPure plasmid miniprep kit (Thermo) according to the manufacturer's protocol:

- Minicultures were centrifuged at 3900xg for 10 minutes.
- The columns were equilibrated.
- Clarified culture media were discarded and bacterial pellets were resuspended in 400 µL of resuspension buffer to homogeneity.
- 400 µL of lysis solution was added to each sample and tubes were mixed immediately by inversion. Samples were left 3 minutes for lysis.
- 400 µL of neutralization buffer was added to each sample and the tubes were mixed immediately by inversion.
- The suspension was centrifuged at 17000xg for 5 minutes and the cell debris was discarded.

- Supernatants were applied to the columns and eluted by gravity flow. The flowthroughs were discarded.

- 2.5 mL of wash buffer was applied to each column and eluted by gravity flow 2 times. The flowthroughs were discarded each time.

- 0.9 mL of ddH$_2$O was applied to each column and eluted by gravity flow into sterile 1.5 mL microcentrifuge tubes.

- The DNA eluates were cooled on ice and -20°C 100% isopropanol was added to each DNA eluate and the mixture was thoroughly vortexed.

- The table top microcentrifuge was cooled to 4°C and the alcohol-DNA mixture was incubated for 20 minutes at -20°C.

- The mixtures were centrifuged at 17000xg at 4°C for 30 minutes and supernatants were discarded.

- 1 mL of 70% EtOH was added to each DNA pellet. The samples were briefly vortexed and centrifuged at 17000g at 4°C for 5 minutes.

- The alcohol supernatants were discarded with a pipette and the samples were further dried using vacuum dryer at high rate for 15 minutes.

- Each DNA pellet was dissolved in sterile ddH$_2$O with vigorous vortexing.

- Concentrations were measured using ddH$_2$O as blank and 1.5 µL was used for the blank and each sample on NanoDrop 2000.

3.2.4. Cell culture, transfection, and infection

Cells were cultured in High glucose DMEM (Sigma) containing 10% FBS (Gibco), 1% penicillin-streptomycin (Sigma). Incubation conditions were 37°C, 5% CO$_2$, and 95% humidity. Cells were split at 1:10 ratio upon reaching 90% confluence. Briefly, medium was removed and cells were washed once with phosphate buffered saline (PBS). Cells were trypsinized for 5 minutes in the humid incubator and suspended in culture media. Trypsin containing media was removed by centrifugation at 100xg for 3 minutes. The pellet was diluted in fresh growth media, and required amount of portion from this suspension was seeded in growth medium. The freshly seeded cells were slowly swirled and shaked or mixed by pipetting to achieve uniform distribution of the cells across the growth surface area. Immortalized Mastl cKO-MEFs were obtained from Kaldis lab and cultured in the described growth medium containing 5µg/mL blasticidin. Knockout was induced by adding 20 ng/mL 4-OHT to the culture medium when

required. Serum starvation was performed by culturing the cells in cell culture media containing 0.2% FBS.

PLAT-E (a HEK293 derivative) packaging cell line was obtained from Kaldis lab. PLAT-E cells were cultured in normal growth medium (high glucose DMEM, 10% FBS, 1% penicillin-streptomycin) containing 1 µg/mL puromycin and 10 µg/mL blasticidin. 293FT packaging cell line was obtained from Kaldis lab. The passage protocols are same with that of described for MEFs.

For ecotropic retrovirus packaging, PLAT-E cells were grown under selective pressure until transfection and transfected at 90% confluence in the absence of selective pressure. Cells transfected using Lipofectamine 3000 (Thermo) according to the manufacturers protocol. Transfection for virus production was carried out in 12-well plate format:

- 50 µL Opti-MEM reduced serum media, 1 µg of transfection-grade plasmid DNA, and 2 µL P3000 reagent were added to a sterile microcentrifuge tube respectively, for each plasmid construct to be transfected to PLAT-E cells.

- 1 µl lipofectamine-3000 containing 50 µL Opti-MEM mixture was added to each DNA containing tube. Lipofectamine-3000/Opti-MEM master mix was prepared in a separate sterile microcentrifuge tube and the volume of the master mix was scaled up according to the number of the transfections to be carried out. 1:1 Lipofectamine3000/P3000 ratio was used for transfection of the packaging cells.

- Lipofectamine3000/Opti-MEM master mix was distributed to the DNA containing tubes at 1:1 (v/v) ratio. Tubes were vortexed and incubated at room temperature for 15 minutes.

- The lipid-DNA complexes were briefly vortexed and added dropwise to the packaging cells.

- 2 days post-transfection, viral media were collected and the media were refreshed.

- 3 days post-transfection, viral media were collected again.

- For each viral medium, the cell debris was removed by centrifugation at 300xg for 5 minutes.

- Each clarified viral medium, the viral supernatant was transferred to a new sterile tube. Viral media were stored at 4°C up to a week until infection. Polybrene was added to a final concentration of 8 µg/mL and mixed, immediately before infection.

- MEFs were transduced at 40% confluence. Viral media collected at the second day of transfection was used in the first round of infection for each stable cell line to be established.

- The day after first transduction, viral media was removed and a second round of transduction was carried out using the remaining batch of viral media.

- 8 hours after the second round of transduction, viral media was removed and cells were cultured in normal growth medium overnight for recovery, prior to antibiotic selection.

- Pool stable cell lines were generated under 2 µg/mL puromycin selection. Cells were selected for a week and negative control cells died within the first 2 days of selection.

For lentiviral packaging, 293FT cells were transfected in 24-well plate format. Briefly, the volumes used in the 12-well plate format was halved to adapt the protocol to the 24-well plate format. 230 ng pMDLg/pRRE, 90 ng pRSV-Rev, 125 ng pMD2.G (VSV-G) helper plasmid mix and 315 ng pBOBI expression vector was used for each transfection. The same protocol used for ecotropic retroviral infection was used for lentiviral infection. A portion of each cell line was frozen in normal growth medium containing additional 10% FBS and 10% cell culture grade DMSO.

For single clone isolation, limited dilution technique was used. Briefly, cells were induced and 6 days after induction, cells were subjected to limited dilution. According to the hemocytometer measurements, cells were diluted to achieve 1 cell/well cell concentration in 150 µL culture volume for each well of each 96-well plate. Cavities in between the wells in the 96-well plate were filled with sterile PBS to prevent extended evaporation of the medium throughout the 2-3 weeks of culturing of the clones.

3.2.5. Genotyping

A typical 3 primer system was used for genotyping of the Mastl locus in MEFs (Figure 10). Neomycin cassette has been flrted out, and Mastl gene is floxed but not excised. The uninduced cells are "WT-like". Fourth coding exon of the Mastl gene is floxed, surrounded by loxP recombination sites at its 5' and 3' intronic regions. Genotyping PCR yields a longer band in floxed locus when compared to the WT locus due to the presence of loxP and frt sites in the intronic region. Upon induction of Cre mediated recombination by 4-OHT treatment, the PCR reaction yields 500 bp fragment. Floxed DNA yields 300 bp fragment and WT DNA yields 200 bp fragment.
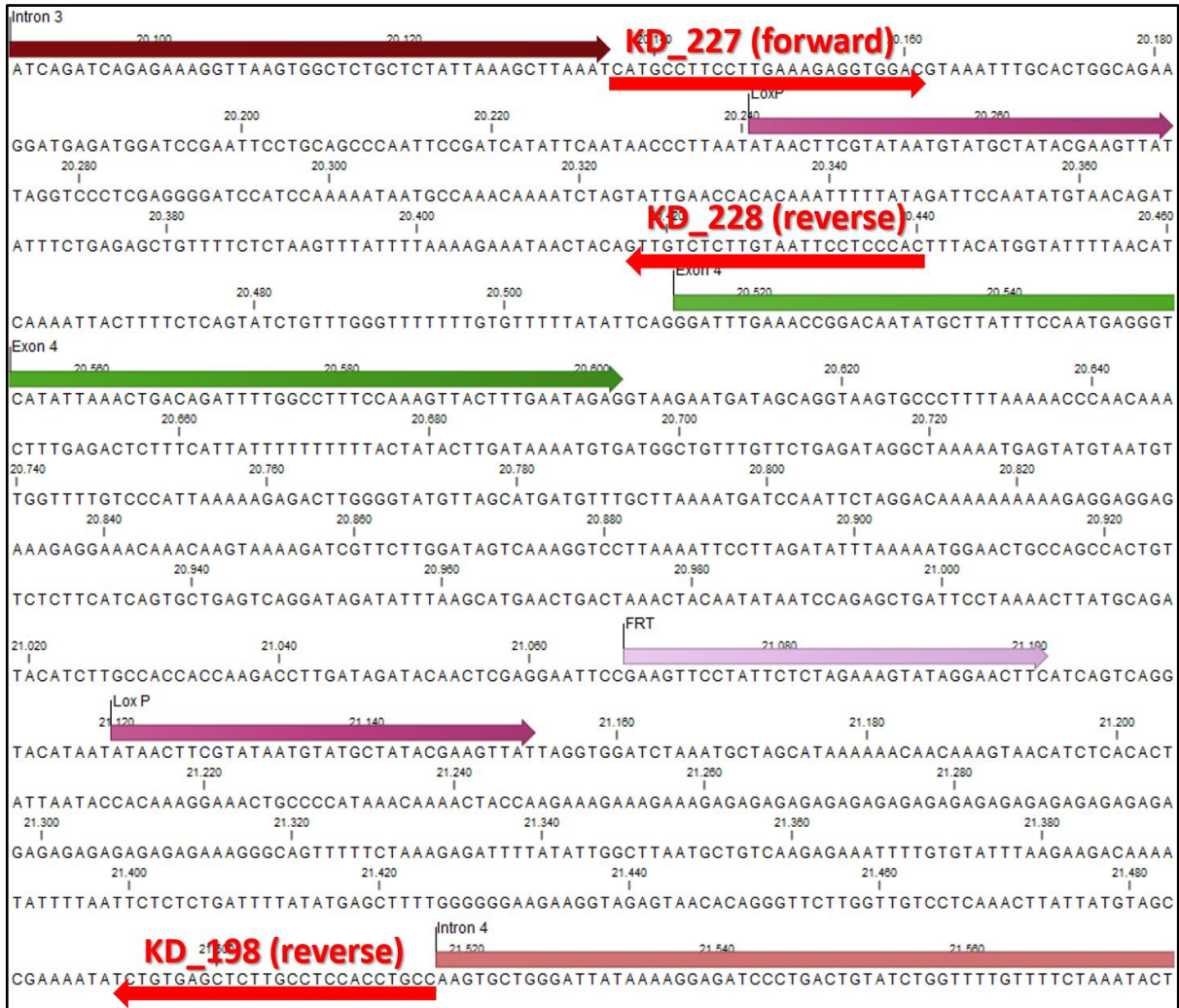
Figure 10. Genomic locus of mouse Mastl. Floxed DNA yields 300 bp fragment amplified by primers KD_227 & 228. Upon recombination, the binding site of KD_228 is excised out and the distance between the binding sites of KD_227 and KD_198 is approximately halved, yielding a 500 bp fragment that indicates a successful knockout.

Samples were harvested from 24-well plates by trypsinization and washed once with PBS. Cells were pelleted and PBS supernatant was discarded. Lysates were prepared from the washed cell pellets by using the HotShot lysis protocol (Montero-Pau & Africa Gómez, 2008). Briefly, 25 µL of lysis solution (25 mM NaOH and 0.2 mM pH 8 EDTA) was added to each sample and the cells were suspended to homogeneity. Cells were vigorously vortexed and incubated at 95ºC for 30 minutes on digital thermal drybath at 900 rpm. Lysates were cooled on ice and 25 µL of neutralization buffer (40 mM pH 5 Tris-HCl) was added and the lysates were mixed by vortexing. Lysates were stored at -20ºC.

42

Genotyping PCR setup and cycling conditions are given in Table 9 and Table 10 respectively.

Table 9. Genotyping PCR setup.

Component	Volume (µL)
10x Buffer	2.5
10 mM dNTP	0.5
100 µM KD_198	0.25
100 µM KD_227	0.25
100 µM KD_228	0.25
Template	2
DreamTaq DNA polymerase	0.125
ddH$_2$O	to 25 µl

Table 10. Genotyping PCR cycling conditions.

Step	Temperature (ºC)	Time
Initial Denaturation	94	3 minutes
40 cycles	94	30 seconds
	67	30 seconds
	72	30 seconds
Final extension	72	2 minutes
Hold	10	-

Genotyping PCR reaction products were analyzed via agarose gel electrophoresis as described in the section 3.2.3.3. Differently, 2% agarose gel was used due to the smaller size of the expected reaction products. Images were acquired via Bio-Rad Universal Hood II UV transilluminator.

3.2.6. Western blot

Reagent recipes used in Western blot are as listed below:

- Lysis buffer: 1% Triton X-100 in 1X PBS. PMSF (1 mM final) and nuclease (5 U/mL final) were freshly added to the required amount of cold lysis buffer before lysis.

- 10x running buffer: 250 mM Tris, 1.9 M glycine, and 1% SDS in ddH$_2$O.

- 1x running buffer: 10x running buffer was diluted 10 times in ddH$_2$O.

- 2x sample buffer: 4% SDS, 50 mM DTT, 0.004% bromophenol blue, 125 mM pH 6.8 Tris-HCl, and 40% glycerol in ddH2O.

- Resolving gel buffer: 1 M pH 8.8 Tris-HCl in ddH$_2$O.

- Stacking gel buffer: 1 M pH 6.8 Tris-HCl in ddH$_2$O.

- 10x transfer buffer: 250 mM Tris, 1.9 M glycine, and 2.5% SDS in ddH2O.

- 1x transfer buffer: 1 volume of 10x transfer buffer was mixed with 7 volumes of ddH$_2$O and 2 volumes of 100% MetOH.

- 80 mM (80x) PMSF stock in isopropanol.

- 10% SDS

- 10% APS

- 30 % acrylamide/bisacrylamide 37.5:1 (w/w)

- 20x TBST: 0.4 M pH 7.5 Tris, 1.5 M NaCl, and 2% Tween-20 in ddH$_2$O.

- 1x TBST: 20x TBST was diluted 20 times in ddH$_2$O.

- Blocking buffer: 5% skim milk powder was heat-dissolved without boiling, in 1x TBST.

- Coomassie staining solution: 0.1% Coomassie Blue R250, 10% glacial acetic acid, 50% MetOH, and 40% ddH$_2$O.

- Coomassie destaining solution: 10% glacial acetic acid, 50% MetOH, and 40% ddH$_2$O.

3.2.6.1. Sample preparation

Cells were harvested by trypsinization. After trypsinization, cells were collected in PBS. The trypsin containing PBS was removed by centrifugation at 500xg for 3 minutes. Cells were washed a second time with PBS and centrifuged again. The PBS supernatant was discarded. The cell pellets were stored at -20ºC until use. The pellets were suspended in lysis buffer and mixed until no clumps were visible. Samples were kept on ice after this step. The table top microcentrifuge was cooled to 4ºC. The suspensions were vigorously vortexed for 10 seconds and left on ice for 10 minutes, 3 times. Cells were centrifuged at 16000xg for 30 minutes at

4°C. The supernatant containing the protein content was taken to a new 1.5 mL microcentrifuge tube.

3.2.6.2. Bradford assay

Bradford assay (Bio-Rad) was used for quantification of protein concentration of the cellular protein extracts. Briefly, one volume of concentrated dye reagent was diluted in eight volumes of ddH$_2$O, achieving a 9x dilution. The diluted reagent was filtered through filter paper. Bio-Rad BSA standard was used at 50-400 µg/mL concentration range with 50 µg/mL concentration increments (Figure 11). Standard measurements were carried out in 5 replicates, blank and sample measurements were carried out in 2 replicates. Preliminary experiments have shown that 1:10 dilution of our samples gave satisfactory results for protein assays. Briefly, in flat bottom 96-well plates, respectively 1 µL of lysis buffer (blank) or sample, 9 µL ddH$_2$O, and 200 µL Bradford dye reagent were added. Plate was shaken at medium speed for 15 seconds in Multiskan GO instrument and the samples were incubated in the instrument for 10 minutes at room temperature in the dark, followed by measurement of absorbance at 595 nm.

y = 0.00118982x + 0.0837671
R^2 = 0.971
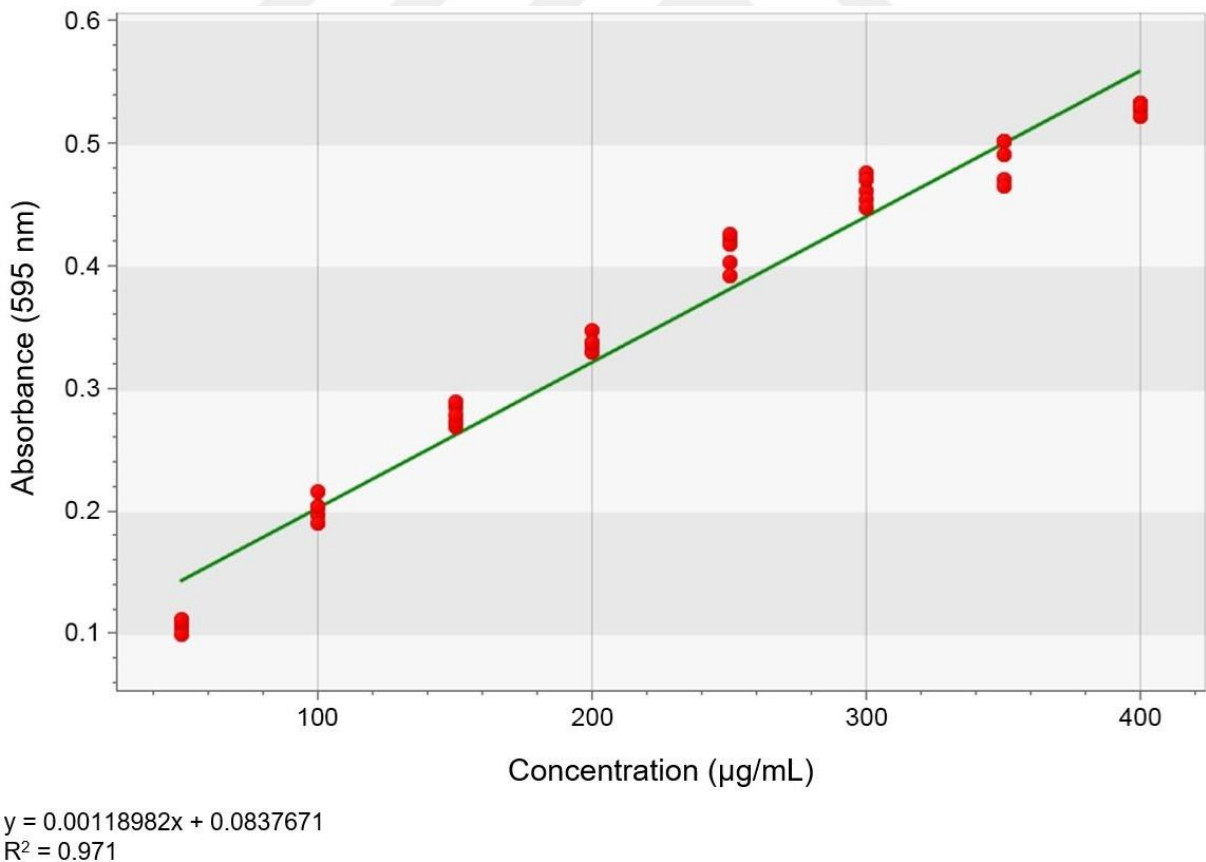
Figure 11. Bradford assay BSA standard curve. BSA concentration range is 50-400 µg/mL.

3.2.6.3. SDS polyacrylamide gel casting

Sodium dodecyl sulfate polyacrylamide gels with 1 mm thickness were cast according to the protocol modified from Bio-Rad (Table 11):

Table 11. SDS-PAGE gel casting setup.

Component	Resolving gel (mL)	Stacking gel (mL)
ddH$_2$O	3.4	3.55
Buffer	3.75	0.625
10% SDS	0.1	0.05
30% 37.5:1 Ac/bis	2.7	0.75
10% APS	0.05	0.025
TEMED	0.005	0.0075
Total volume	~10	~5

Gel components were added in the given order above. The resolving gel was cast first and immediately overlaid with 100% isopropanol layer. 15 minutes later the isopropanol layer was poured off and the polymerized gel was washed 3 times with ddH$_2$O in between the glass plates. The gap between the glass plates were dried with a filter paper without disassembling the glass plates and without disturbing the gel. The stacking gel was cast on top of the resolving gel and the comb was immediately placed. The gel was left to solidify for at least 30 minutes. After pouring each layer of gel, polymerization was ensured before use by observation of solidification of the gel mixture leftovers.

3.2.6.4. Sample preparation, running, and semidry transfer

Previously clarified cell lysates with known protein concentrations were thawed and 2x sample buffer was added to each sample at 1:1 (v/v) ratio. The samples were boiled at 95°C for 5 minutes. The reduced and denatured samples were stored at -20°C. Samples were centrifuged at 17000xg for 1 minute to remove SDS precipitates before loading. When necessary, the loading volumes were normalized according to the protein assay results to load similar amounts of protein for each sample.

The casting apparatus were disassembled and the cores of the tank were assembled with the intact glass plates containing the gel. The cores were placed in the tank and the system was filled with running buffer according to the manufacturer's protocols. The comb was removed and the lanes were filled with running buffer. Samples were loaded and loading dye was added to the empty lanes when necessary to equalize the electrophoretic mobility across the width of the gels. Gels were run at constant 20-25 mA current until the proteins enter the resolving gel. Once the proteins had entered the resolving gel, gels were run at constant 35-50 mA current until the bromophenol blue dye reaches the bottom end of the gel.

PVDF membranes and filter papers were cut as a batch according to the gel size. During running, preparations for semidry transfer was done for each Western blotting session. PVDF membranes were soaked in 100% MetOH for 1 minute, then transferred to transfer buffer without drying and incubated for 15 minutes with agitation. Required amount of filter papers were wetted in transfer buffer. When the running step is finished, the tank cores and the glass plates were carefully disassembled in order not to disrupt the gels. The gels were soaked in 1x transfer buffer immediately before sandwich assembly.

Anode and cathode of the semidry transfer apparatus were wiped with a tissue wetted in transfer buffer. The sandwich assembly was done by overlaying the anode respectively with 14 thin filter papers, PVDF membrane, gel, and 14 more thin filter papers. Air bubbles in the sandwiches were removed by firmly rolling a 25 mL serological pipette on the sandwiches. The apparatus was closed and locked, then the cathode was firmly pressed downwards against the sandwiches before fixing its position. The transfer was done at constant 20-25 V approximately for 40 minutes.

3.2.6.5. Coomassie staining, antibody incubations, and chemiluminescence detection

After the transfer is completed, the sandwiches were disassembled. The PVDF membranes were left to dry on a tissue paper to enhance fixation of the proteins on the membrane. PVDF membranes (after ECL detection) and gels were Coomassie stained to check efficiency of the transfer. Coomassie staining and destaining steps were carried out at room temperature with slow agitation. The stained gel and membrane images were acquired via Bio-Rad Universal Hood II UV transilluminator, using the Protein gel>Coomassie>Intense bands settings.

Dried membranes were wetted in 100% MetOH for 1 minute and then transferred to TBST. PVDF membranes were slowly agitated in TBST for 15 minutes and then blocked in blocking buffer for 1 hour. After blocking, overnight primary antibody incubations of the membranes at 4°C were initiated. The next day, probed membranes were washed with TBST 4 times, 5 minutes for each wash. Membranes were taken to secondary antibody incubation for 1 hour at room temperature, followed by washing with TBST 4 times, 5 minutes for each wash. For each mini gel sized PVDF membrane (~40 cm^2), 1.2 ml of ECL detection reagent was used. Developing solution was constituted of 1:1 (v/v) mixture of the kit components, luminol solution and H$_2$O$_2$ solution. Initially the membranes were auto-exposed. When necessary, membranes were exposed for an additional 30 minutes. Images were acquired using Chemi-Smart 5100 (Peqlab) chemiluminescence detector with Chemi-Capt software.

3.2.7. Microscopy

Reagent recipes used in immunocytochemistry are as listed below:

- 1x PBS: 1 tablet/200 mL ddH$_2$O.
- 4% PFA: PFA was dissolved in 1x PBS by heating up to 60°C and titrated with NaOH until the solution was clarified. The solution was filtered before use.
- Blocking buffer: 10% donor goat serum, 500 mM NaCl, and 0.2% Triton X-100 in 1x PBS.
- Mounting medium: Modified from the manufacturer's protocol, 1.2 g Mowiol was added to 3 g glycerol and vigorously vortexed. 6 mL 0.2 M pH 8.5 Tris-HCl was added and heated to 60°C for 6 hours and vigorously vortexed. Suspension was centrifuged at 5000xg for 15 minutes at room temperature and the clarified supernatant was stored at -20°C.
- DAPI mounting medium: 25 mg/mL DAPI was added to Mowiol at 1:1000 (v/v) ratio to achieve a final working DAPI concentration of 25 µg/mL. The DAPI mounting medium was stored at -20°C.

3.2.7.1. Immunocytochemistry

The cells were seeded on EtOH sterilized and dried 12 mm cover glasses without coating in 24-well plates and grown to be near-confluent before fixation. Growth media was removed and cells were washed 2 times with PBS. Cells were fixed using 4% PFA in PBS for 20 minutes at room temperature. Cells were washed twice with PBS. Cells were stored at 4°C after removal

of the fixative and addition of PBS up to one day when needed. After the second wash, PBS was aspirated and cells were blocked and permeabilized using the blocking buffer for 15 minutes at room temperature. The cavities in between the wells in the plate were filled with ddH$_2$O to provide a humid chamber, thus preventing the coverglasses to get completely dry throughout low-volume antibody incubations. The blocking buffer was aspirated and surroundings of the cover glasses were extensively dried. Cells were incubated in the primary antibodies diluted in blocking buffer for 2 hours, then washed 3 times for 10 minutes with PBS. Cells were incubated in the secondary antibodies diluted in blocking buffer in the dark for 1 hour, then washed 3 times for 10 minutes with PBS. 15 µL of dilute antibody solutions were used for both primary and secondary antibody incubations, for each coverglass. It was ensured that antibody droplets did not leak to the surface of the wells and remained on the cover glasses. Cells were washed 3 times for 10 minutes with PBS. Microscope slides were labeled and 5 µL mowiol droplets were placed on slides for each cover glass. PBS was not completely aspirated from the wells after the last wash to make it easier to take the cover glasses out of the wells, using a twisted injection needle. Cover glasses were mounted and analyzed within 2 days.

3.2.7.2. Microscope settings and use

All micrographs were acquired using Olympus IX71 microscope with cellSens Entry software. Bright field micrographs were acquired at 4x magnification for morphological characterization of the cell populations and for coarse visual demonstration of the difference of proliferation rates among the cell populations. White balance setting was used prior to bright field image acquisition. All bright field images were acquired using 100 milliseconds exposure setting.

For fluorescence microscopy, cells were stained with Alexa Fluor 488, and 594 conjugated secondary antibodies and DAPI. Respectively, 400DF15 excitation light path and 535DF2 emission light path were used for DAPI stain, 490DF20 excitation light path and 535DF25 emission light path were used for Alexa Fluor 488 stain, and 590DF10 excitation light path and 630DF30 emission light path were used for Alexa Fluor 594 stain. Black balance setting was used prior to fluorescence imaging to subtract the background signal. Exposure settings of DAPI, Alexa 488, and Alexa 594 were respectively 50 milliseconds, 2 seconds, and 4 seconds for Mastl and HA-Mastl stains. Exposure settings of DAPI, Alexa 488, and Alexa 594 were respectively 50 milliseconds, 7 seconds, and 7 seconds for Arpp19 and HA-Arpp19 stains.

3.3. Workflow

The project is based on protein engineering and *in vivo* functional analysis of the engineered proteins. To design a chemically switchable protein kinase, we initially tested our mutation-drug combinations *in silico*. Subsequent order of the computational steps is modeling of the protein-ligand complexes, molecular docking, and analysis of the results. Subsequent order of the experimental steps follows a typical pipeline consisting of molecular cloning, cell line engineering, and cell line characterization (Figure 12).
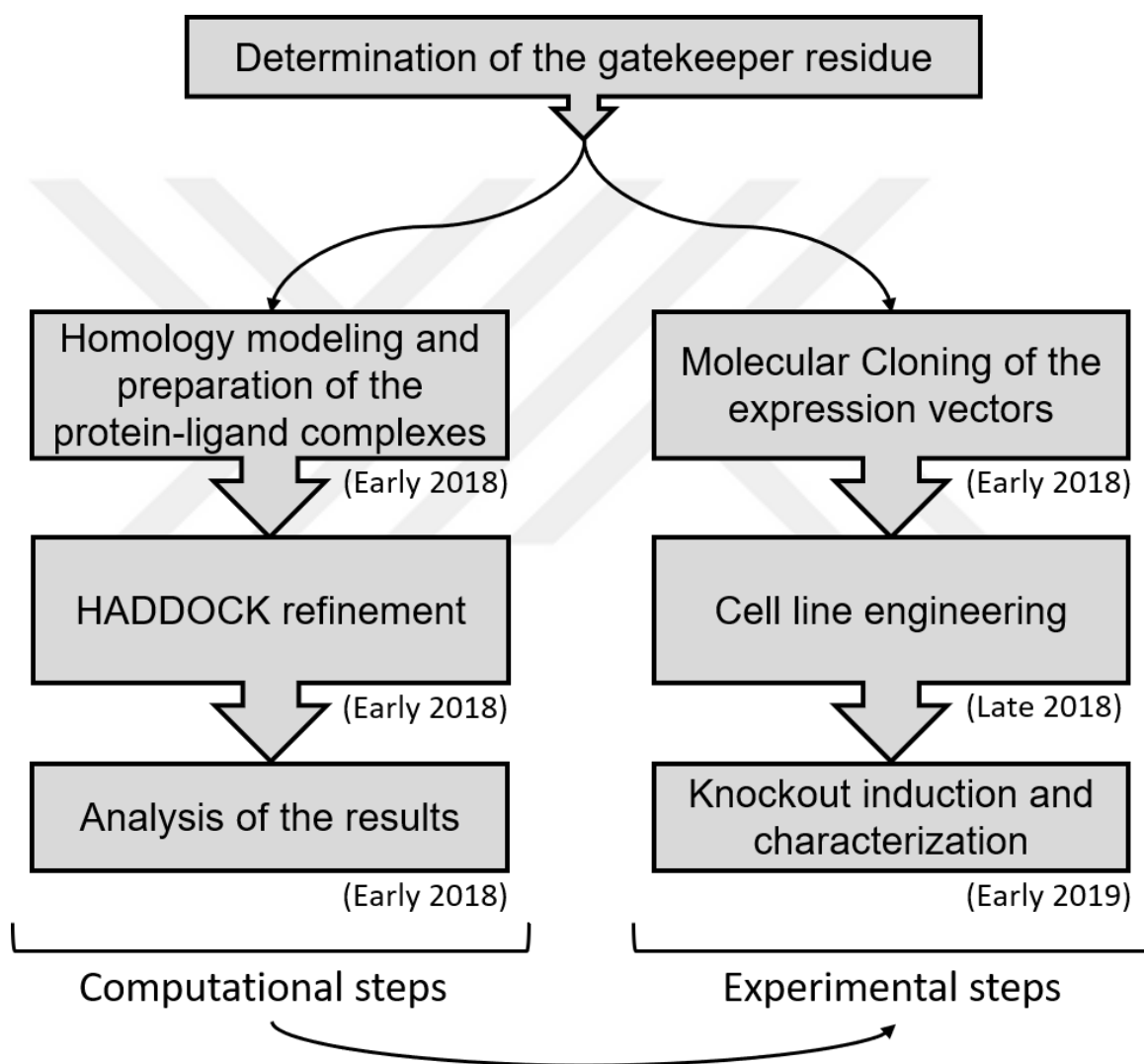
Figure 12. Workflow of the project.

3.4. Possible obstacles

Virtually every step in any given project carries many risk factors. Possible risk factors for this project are listed below regarding each step of the workflow.

- Homology modeling:

We have established ATP bound model structure of mouse Mastl and used the coordinates of the ATP in this model structure for positioning of the ATP analogues. For this purpose, we first set a hypothesis regarding the importance of the nitrogen-rich heterobicyclic group coordinates for correct docking of small compounds in the ATP binding pocket. Adenine ring of ATP and adenine-like rings of the ATP analogues are the highly similar groups within these small molecules. As a result, especially considering the known hydrogen bonds between this nitrogen-rich moiety and the protein, and based on structural alignments given in the results section, we concluded that this group of each ligand has to be superimposed. With this approach, we aimed to obtain near-correct ligand coordinates within the ATP binding pocket, prior to refinements. Currently, crystal structure of gatekeeper-mutant protein kinases in complex with the ATP analogues are not available in the PDB. For this reason, the coordinates we defined for the ATP analogues are relative, based on ATP coordinates.

The structures used during HADDOCK refinements in this study are model structures and the coordinates of ligands were defined based on hypothesis. As a result, coordinates in our structures do not directly originate from an experimental data, which is expected to have a direct impact on the simulation results.

- HADDOCK refinement:

HADDOCK is a very versatile and efficient program for molecular docking. The program offers vast range of parameters and options for integration of various types of experimental data during the docking protocol. In its default settings, the program applies very short, yet relatively accurate simulations on biomolecular complexes.

The biological systems that we used for computational analysis in this study is constituted of protein-small compound pairs. Briefly, we performed molecular docking, specifically local docking, on mouse WT/mutant Mastl variants and ATP/ATP analogues. Throughout *it1* and water refinement stages, interfacial backbone and interfacial residue side chains were flexible and the rest of the protein was kept rigid. With this approach, processing power and time requirements are more reasonable, however, the duration of the simulation is very short and it is active site centric. An unwanted possible biochemical outcome of the point mutations, such as a structural instability, may not be captured with this approach. The

simulation conditions are initially expected to be sufficient for analysis of ATP binding pocket-ligand interactions. Nonetheless, the results also can be suggestive regarding a possible enzyme inactivation.

- Molecular cloning of expression vectors:

Molecular cloning consists of successive multiple steps, respectively, obtaining the insert in the form of an amplicon, digestion of the insert and linearization of the vector, dephosphorylation of the vector, ligation of the insert to the vector, transformation, and colony screening. It is possible to do mistakes or perform wrong applications which were initially assumed to be correct given the multiple steps and inexperience. Failure or success of a molecular cloning experiment can only be detected at the end of the experiment, by screening the colonies, if there any. Given its complicated workflow, molecular cloning experiments are difficult to troubleshoot.

- Cell line engineering:

Stable cell lines used in this study were established by infection of the target cells with ecotropic retrovirus particles. First, the 293 derivative packaging cell line has to be successfully transfected, and then its virus products have to successfully infect the target cells. After infection, successfully infected cells have to be selected via a eukaryotic antibiotic selection marker. In this step of the project, both transfection and transduction efficiency, viral titer, and viability of the target cells in the viral medium can become problematic.

- Induction of knockout in stable cell lines and characterization:

The cell lines established in this study were derived from a conditional knockout mouse embryonic fibroblast (cKO-MEF) parental cell line. Conditional knockout systems are advantageous given their rapid action upon chemical induction. In case of the system used in this study, the cells stably express Cre-ER^{T2} fusion protein. Cre moiety is the recombinase and ER^{T2} moiety is the 4-OHT sensitized triple mutant ligand-binding domain of human estrogen receptor. Upon chemical induction, ER^{T2} binds 4-OHT and this ectopic protein product is imported to the nucleus via estrogen receptor where Cre moiety of the protein can take action to recombine the floxed DNA (Sasson & Notides, 2009; Tymms & Kola, 2003). However, the knockout efficiency is not 100%. This becomes a disadvantage because in the long term, the floxed cells will take over the population and the proportion of the knockout cells which have

a growth disadvantage will gradually decrease. It is especially problematic in our case because the homozygous knockout cells will not be able to proliferate at all.

This is the major obstacle of this research, which can be bypassed with single clone selection from the induced stable cell pools. However, this approach also has disadvantages. The procedure is extremely labor intensive, and the work load exponentially increases when dealing with multiple cell lines. Regardless of the dilution conditions and strict observations of the clones throughout their weeks of growth, chances are high that some colonies may not be monoclonal, again leading to possible contamination of the characterization worthy knockout cells with floxed cells.

The analogue-sensitive knockout cell lines may become unviable due to possible negative impacts of ATP binding pocket point mutations on the enzymatic activity. Another possibility is that the mutation may not render the enzyme analogue-sensitive. In this case, we have multiple mutation-drug combinations to test.

4. RESULTS

4.1. Homology modeling

Due to the lack of an ATP-bound crystal structure of Mastl kinase in literature, we initially modeled this complex with I-TASSER. To determine the homology template to be used for modeling, we performed pairwise sequence alignment between mouse Mastl kinase domains and separately ten ATP bound protein kinase crystal structures. PDB entries of the sample crystal structures are 1ATP, 3VVH, 4EOQ, 4WB5, 4XBR, 4XX9, 5D9H, 5LPY, 5OBJ, and 5OSP. Similarity scores were compared in Figure 13.
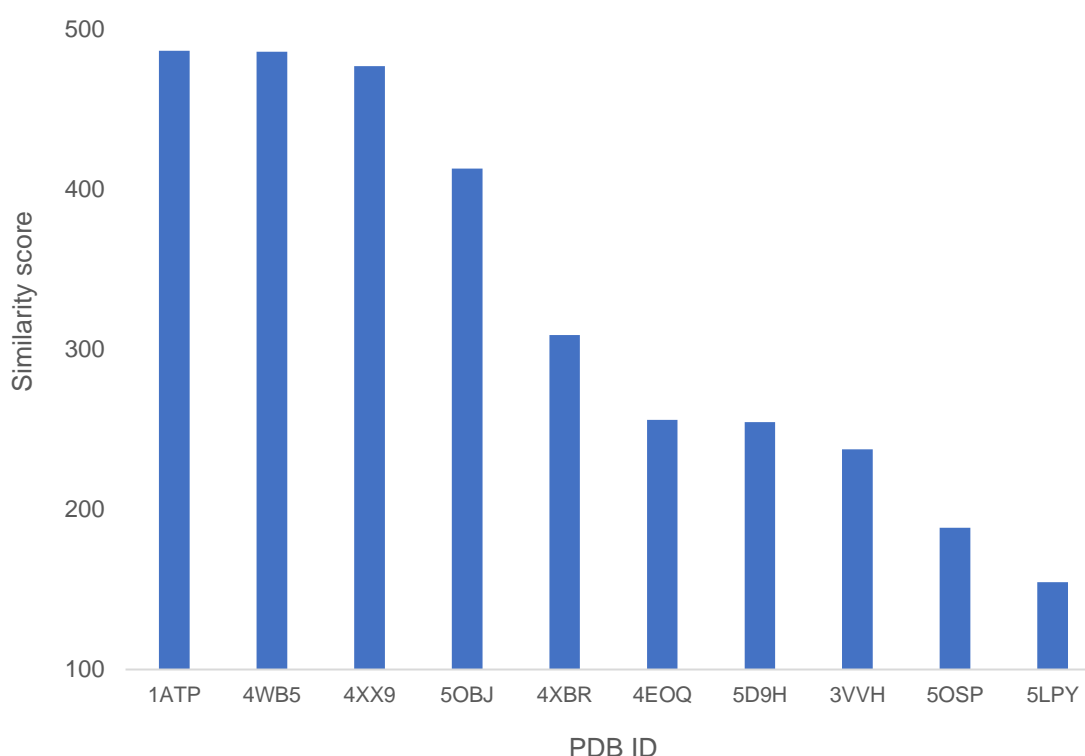
Figure 13. Pairwise sequence alignment similarity scores. Sequence similarity of mouse Mastl kinase domains to the homology template candidate protein kinases. PDB entries 1ATP, 4WB5, 4XX9, 5OBJ, 4XBR, 4EOQ, 5D9H, 3VVH, 5OSP, and 5LYP.

According to the pairwise alignment results, mouse cAMP-dependent protein kinase (PDB entry 1ATP) gave the highest score (486.5) with 29.8% identity and 53.2% similarity. The level of identity is approximate to the required minimum identity threshold (30%) for reliable template-based modeling (Diamond & Zhang, 2018; Fiser, 2010; Xiang, 2006). Therefore, the crystal structure 1ATP was chosen to be used as the template for homology modeling. The model structure of ATP-bound mouse Mastl is given in Figure 14.
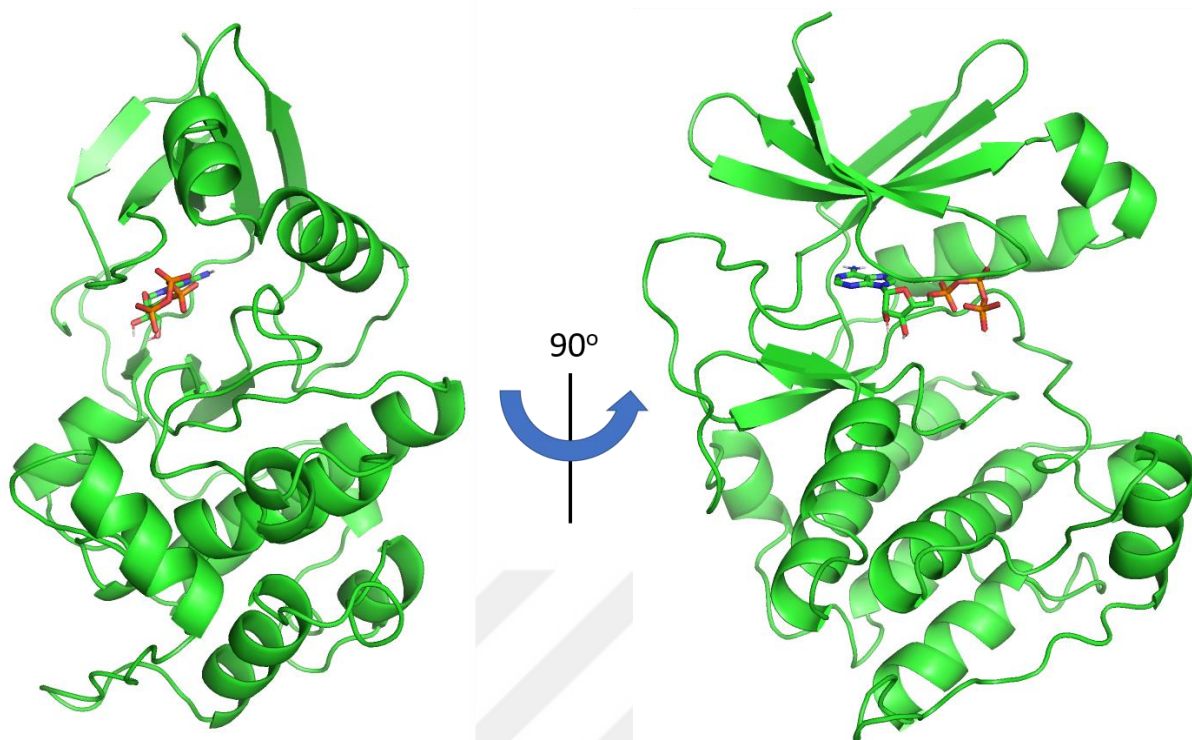
Figure 14. ATP-bound model structure of mouse Mastl.

The NCMR (non-conserved middle region) is excluded from the model structure. The N-terminal (32-179) and the C-terminal (726-849) segments encompassing the complete kinase domains were fused.

4.2. Determination of the active site residues

TargetATPsite webserver was utilized for determination of the ATP binding pocket residues. By synthesizing the result obtained from this webserver and our visual examination of the ATP binding pocket, the active site residues were determined manually (Figure 15).
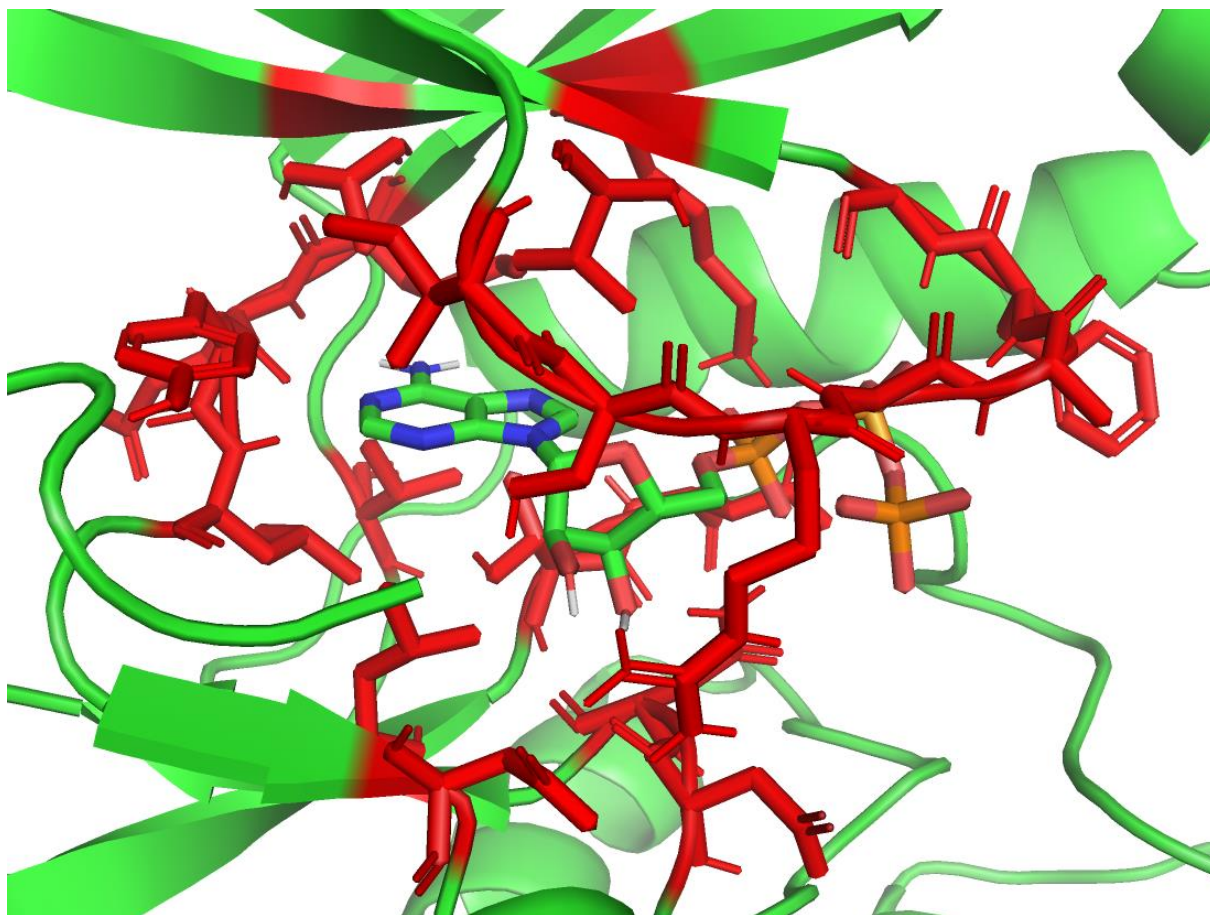
Figure 15. Active site residues of the ATP binding pocket of mouse Mastl. The ligand is in green stick form and the active site residues are indicated as red sticks.

The final form of the active site residue set used in HADDOCK refinement is "9,10,11,12,13,14,15,17,28,30,62,78,79,80,81,85,128,129,131,141,142".

These active site residues and their respective positions within the full-length mouse Mastl protein sequence (Uniprot entry GWL_MOUSE Q8C0P0) are I40, S41, R42, G43, A44, F45, G46, V48, A59, K61, V93, M109, E110, Y111, L112, D116, D159, N160, L162, T172, and D173.

4.3. Determination of the gatekeeper residue, ligand coordinates, and restraints

ATP binding pockets of protein kinases are well-conserved. Although this has been a disadvantage for design of specific inhibitory small compounds, researchers have exploited this similarity to engineer analogue-sensitive mutants of mainly protein kinases and other proteins. The point mutations we chose for this study were based on the previous studies in this research field (Aoi, Kawashima, Simanis, Yamamoto, & Sato, 2014; Bartkowiak, Yan, & Greenleaf, 2015; Bishop, Buzko, & Shokat, 2001; Bishop et al., 2000; Holt et al., 2002; Miadokova et al.,

2011; Sliedrecht et al., 2010). The notion of the "gatekeeper" residue was initially emerged from natural occurrences such as mutations in drug-resistant tumor cells. These key residues were determinants of whether a small compound could efficiently fit in an ATP binding pocket of a protein kinase or not. Due to the high homology of the ATP binding pockets of protein kinases, a strong pattern regarding the alleged place of a gatekeeper residue in a new protein kinase of interest can be captured with simple alignments.

This approach has been accurately and reproducibly utilized throughout the last two decades (Bishop et al., 2000; Gregan et al., 2007; Jones et al., 2005). Following this methodology, we determined the gatekeeper residue of mouse Mastl. A representative of the sequence alignment is given in Figure 16.
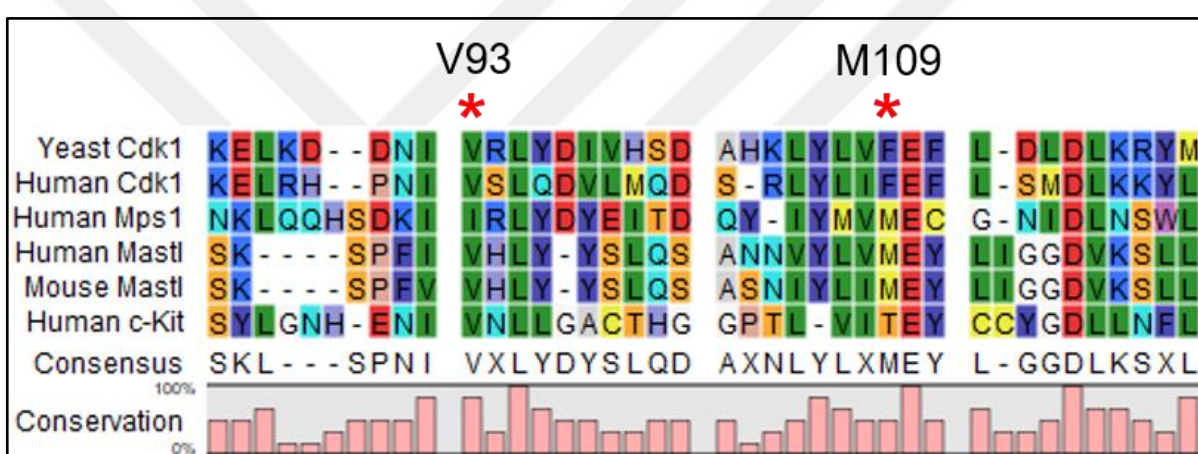
Figure 16. Position of the gatekeeper residue in Cdk1, Mps1, Mastl, and c-Kit. Single red asterisk (V93) indicates our backup choice of gatekeeper residue and double red asterisk (M109) indicates the position of actual gatekeeper residue that has been repeatedly verified in various studies.

The protein kinases used in this alignment have been subjects of chemical genetics studies and their analogue-sensitive mutants were both viable and chemically switchable as desired. Similarly, researchers had used alignments to determine the gatekeeper residues in these studies (Kissova et al., 2016; Miadokova et al., 2011; Sliedrecht et al., 2010). We selected two gatekeeper candidates, V93 and M109, to substitute for smaller hydrophobic amino acids. To increase the probability of obtaining a successful AS Mastl cell line, we aimed to simultaneously screen multiple mutation combinations. Positions of the to-be-substituted residues are indicated in Figure 17-A. The superimposed molecular structures of ATP and the ATP analogues which planned to be used in this study are given in Figure 17-B.
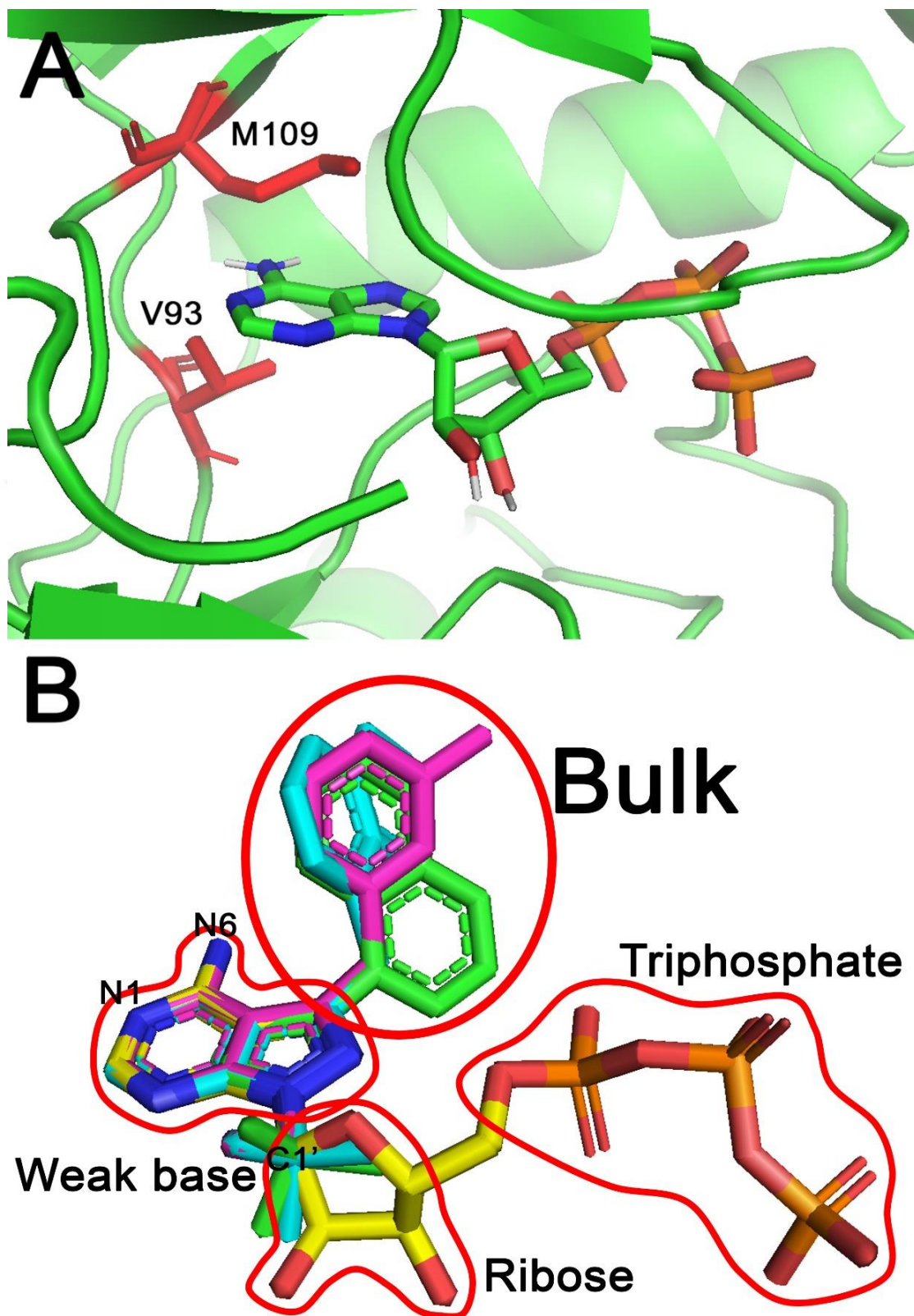
Figure 17. Molecular structures of the ATP binding pocket of Mastl kinase, ATP, and ATP analogues. (A) The to-be-substituted residues within the ATP binding pocket are indicated as red sticks. (B) Superimposed molecular structures of ATP (yellow) and the ATP analogues 1-NA-PP1 (green), 1-NM-PP1 (cyan), and 3-MB-PP1 (magenta).

Four separate mutations that used in this study are listed below:

- M109G: Substitution of 109th methionine with glycine.
- M109A: Substitution of 109th methionine with alanine.
- V93A/M109G: Substitution of 93rd valine with alanine and substitution of 109th methionine with glycine.
- V93A/M109A: Substitution of 93rd valine with alanine and substitution of 109th methionine with alanine.

The van der Waals radius is a determinant of the atomic space occupancy, which defines the distance of closest approach among physically interacting atoms. Due to the vdW repulsion forces, two atoms can not get closer to each other more than their vdW radii allow. This boundary naturally occurs as a result of the balance between the interatomic attractive forces among the opposite charges (nuclei/electron clouds) and interatomic repulsive forces among the same charges (nucleus/nucleus and electron cloud/electron cloud) of the physically encountering atoms. Violation of these boundaries is not possible unless the said atoms are bonded, i.e. covalent bond and hydrogen bond (Rahim & Barman, 1978). Unnatural overlapping of non-bonded atoms cause steric clashes, which is the result of violation of vdW radii *in silico* (Ramachandran, Kota, Ding, & Dokholyan, 2011).

The main gatekeeper residue M109 was also verified by structural alignments. It is a common practice to determine the gatekeeper residue by demonstrating the steric clash between an ATP analogue and the gatekeeper residue candidate. To do so, we initially utilized the same set of proteins with identified gatekeeper residues that we used for sequence alignment (Figure 16). Crystal structures of human WT Cdk1, Mps1, Mastl, c-Kit, (PDB entries 6GU2, 6B4W, 5LOH, and 6GQJ respectively), and model structure of V93A/M109G double mutant mouse Mastl in complex with 1NM-PP1 were superimposed to the model structure of WT mouse Mastl in complex with ATP. According to the hypothesis, it is expected to observe a steric hindrance between the larger gatekeeper residue side chains and the naphthalene (two fused benzene rings) moiety of 1-NM-PP1 ATP analogue (Figure 18).
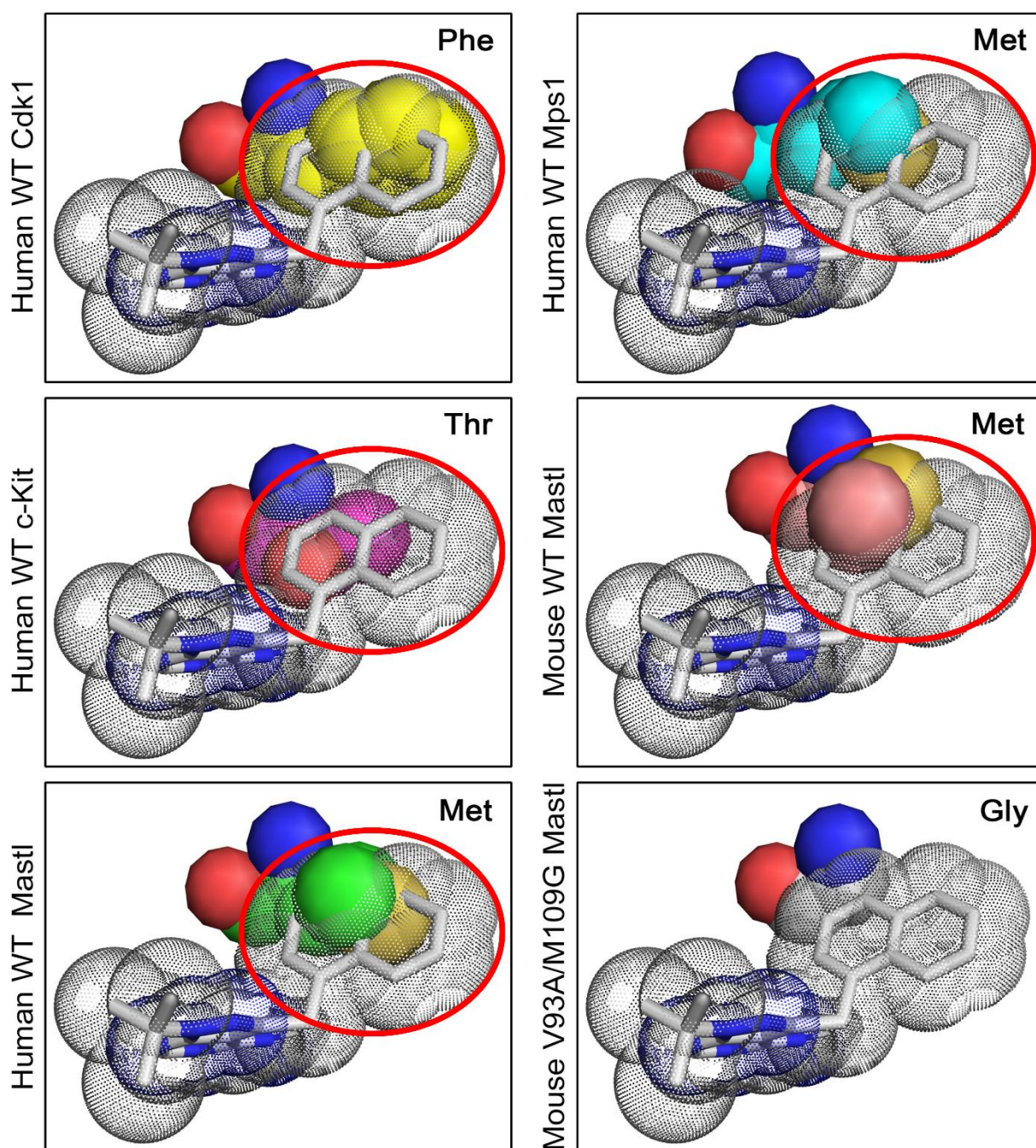
Figure 18. Visual analysis of the interactions between the gatekeeper residues and 1-NM-PP1. The side chains are represented as spheres and the ligand is represented as gray sticks and dots. The steric clashes between the gatekeeper residue side chains and the naphthalene ring of 1-NM-PP1 are indicated in red circles.

Drawing conclusions from this type of structural alignments can be thought as a scientifically unreliable approach. Because the ligand coordinates of one complex is overlaid on the protein coordinates of another complex obtained from a different experimental data or

on a different model structure. This means that the superimposed ligand and protein conformations are not expected to fit each other. We exploited this indirect approach to observe the relatively "free" conformational behavior of the bulky ligand and the gatekeeper residue side chains without one impacting the other. The structures were superimposed and ligands other than 1-NM-PP1 were removed. The steric clashes between the naphthalene group of the ligand and the side chains are clearly visible, which is expectedly not observed in case of the glycine gatekeeper residue in the bottom-right panel of Figure 18. Importantly, within the ATP binding pocket, only the gatekeeper residues specifically contributed to the steric hindrance and other active site residue side chains were relatively distant to the ATP analogue. Furthermore, when we performed HADDOCK refinement on WT and mutant mouse Mastl variants in complex with 1-NM-PP1, only the simulation of the WT complex has repeatedly encountered errors and docking of all mutant complexes were successful (data not shown). These errors are attributed to the insurmountable steric clashes between the restrained ligand and the gatekeeper residue side chain. In the bottom-right panel of Figure 18, glycine substitution at the gatekeeper position expectedly results in a free space between the ligand and the gatekeeper residue, eliminating the said steric hindrance. The threonine gatekeeper of human WT c-Kit shows a relatively weak steric clash unlike the near-completely overlapping atoms observed in other WT structures. In case of c-Kit, the distance between the closest non-hydrogen atoms of the protein and the ligand is 2 Å. Threonine is a relatively small amino acid and chemical genetics engineering of c-Kit involves slight enlargement of this residue by isoleucine substitution. In the study, researchers successfully developed a drug resistant c-Kit (Kissova et al., 2016), which is a reverse approach when compared to our aim of analogue sensitization on Mastl kinase and the aims of other researchers on Cdk1 (Miadokova et al., 2011) and Mps1 (Jones et al., 2005; Sliedrecht et al., 2010) kinases. This is consistent with the hypothesis that substitution of the gatekeeper residue alters the substrate specificity. A larger mutated gatekeeper residue confers drug resistance as in the case of c-Kit, while a smaller mutated gatekeeper residue confers analogue sensitization as in the case of Cdk1 and Mps1. In both sequence and structure alignments, the positions of the gatekeeper residues are overlapping for each protein kinase (Figure 16, 18). Taken together, these results consistently suggest that the gatekeeper position of mouse Mastl is the M109 residue.

Another evidence regarding the location of the gatekeeper residue is captured by alignment of sequences and crystal structures of PP1 analogue-kinase complexes. In human

WT c-Kit, threonine is present at the gatekeeper position (Figure 16, 18) and this residue was mutated to a larger amino acid- isoleucine, to achieve drug resistance against imatinib. Acinetobacter WT APH(3')-Ia also possess a threonine and protozoan WT CaMK1 kinases from different species possess a glycine at their gatekeeper position (Figure 19, 20).
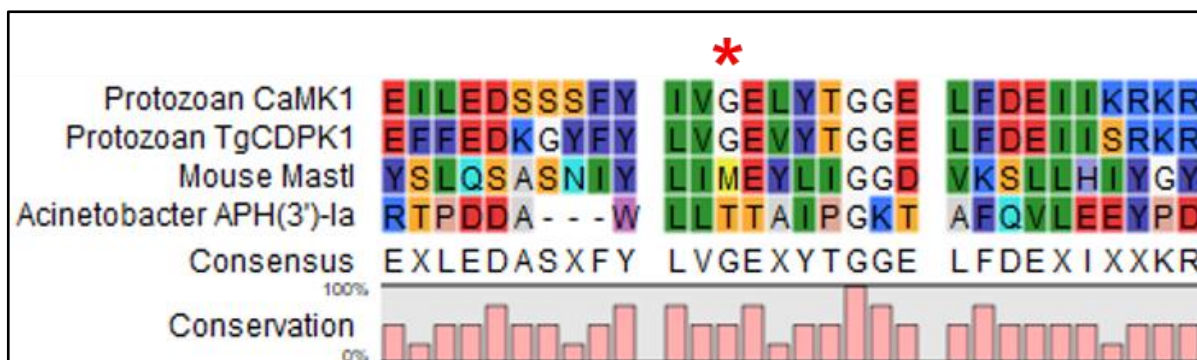
Figure 19. Sequence alignment of CaMK1, TgCDPK1, APH(3')-Ia, and mouse Mastl. Position of the gatekeeper residue is indicated with a red asterisk.

The crystal structures in complex with PP1 analogues are examined and it is seen that, the bulky rings of the ligands are solvent exposed in Acinetobacter APH(3')-Ia (PDB entries 4FEV, 4GKH, and 4GKI), whereas they are buried in protozoan CaMK family kinases (PDB entries 2WEI, 3I7B, and 3NCG) (Figure 20). According to the data, threonine confers drug sensitivity in case of c-Kit/imatinib complex but allegedly confers drug resistance in case of APH(3')-Ia/PP1 analogue complexes. This contrast of outcomes can be attributed to the different physicochemical characteristics of imatinib and PP1/ATP analogues, affecting their accommodation in the ATP binding pocket.
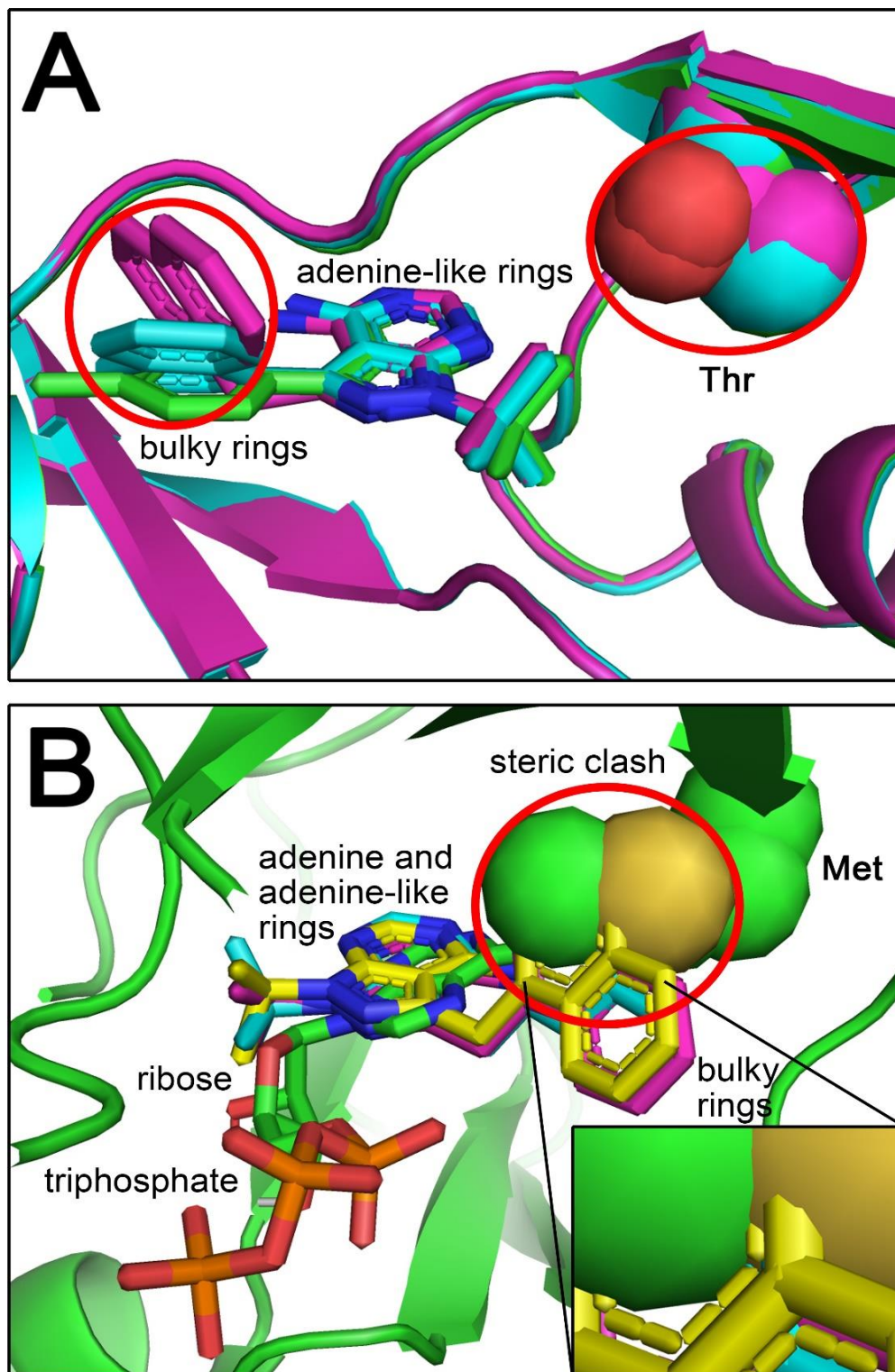
Figure 20. Structural alignments of PP1 analogue-protein kinase complex crystal structures and model structure of ATP bound mouse WT Mastl. (A) Bulky rings of the ATP analogues are solvent exposed in the presence of threonine gatekeeper residue. (B) The steric clashes between the bulky rings of crystal structure ATP analogue compounds and the model structure methionine side chain is indicated by the red circle. The steric clashes are shown in detail in the zoomed section of the picture given in the bottom-right panel.

In superimposed crystal structures of Acinetobacter APH(3')-Ia in complex with ATP analogues that planned to be used in this study, the position of adenine-like moiety is conserved while the complete ligand structure is coordinated in an inverted position, exposing the bulky rings of the ligands out of the ATP binding pocket (Figure 20-A). This can be attributed to the presence of threonine at the gatekeeper position, not allowing accommodation of the bulky rings of ATP analogues. Because when the superimposed crystal structure complexes of protozoan WT CaMK kinases and ATP analogues are examined, the bulky rings of ligands face the small gatekeeper residue glycine. These data are consistent with the relative sizes of the gatekeeper residues, threonine and glycine. In Figure 20-B, these CaMK family of kinases are superimposed to our model structure of mouse WT Mastl in complex with ATP. While the bulky rings of ligands are relatively free in these complexes because of the small glycine gatekeeper residue, especially the epsilon-carbon (green) and the sulfur (yellow) atoms of the methionine gatekeeper residue of our model structure shows steric clash with these rings. Considering that both protein side chain and ligand non-polar hydrogen atoms are hidden in all of the structural alignments, steric clashes demonstrated in Figure 18 and Figure 20-B are remarkable.

In the structure alignments, it is seen that the heterobicyclic moiety and an extending additional carbon atom (namely C1' atom in ATP) are homologous among ATP and the ATP analogues. Consistently, these common groups of ATP and ATP analogues are coordinated similarly in superimposed complex structures. This information is valuable considering that PyMOL perform structural alignments by considering only the protein residues. As a result, alignment option of PyMOL did not align the ligands, but coordinates of the ligands were modified only with respect to the changing protein coordinates throughout the alignment process. Based on this finding, the weak base moiety of ATP and each ATP analogue were preferred for atom-atom alignment to set the coordinates of the drugs in the mouse Mastl model structure, as explained in the computational methods section.

We initially determined the position of the gatekeeper residue by sequence alignment. We then demonstrated this structurally, showing the hypothetical steric clashes between an ATP analogue and the gatekeeper residues by superimposing the WT protein kinase crystal structures to the mutant mouse Mastl/1-NM-PP1 complex model structure. Using HADDOCK simulations, we proved the incompatibility of an ATP analogue example- 1-NM-PP1, with a WT protein kinase, Mastl. Lastly, we sampled the available crystal structures of kinase/ATP

analogue complexes to use them in sequence and structure alignments, further verifying the position of the gatekeeper residue. Moreover, we observed that the positions of heterobicyclic moieties of ATP and ATP analogues are well-conserved among the crystal structures and our model structures, meaning that the coordinates that we defined for the ATP analogues in our model structures and the atom-atom restraints that we defined for molecular docking are unbiased.

4.4. Analysis of the evolutionary conservation of the mutation sites

Evolutionary conservation of the residues of wild type mouse Mastl was analyzed via ConSurf webserver. The server generated an MSA from an ensemble of 150 homologous protein sequences. A representative of the MSA is given in Figure 21.
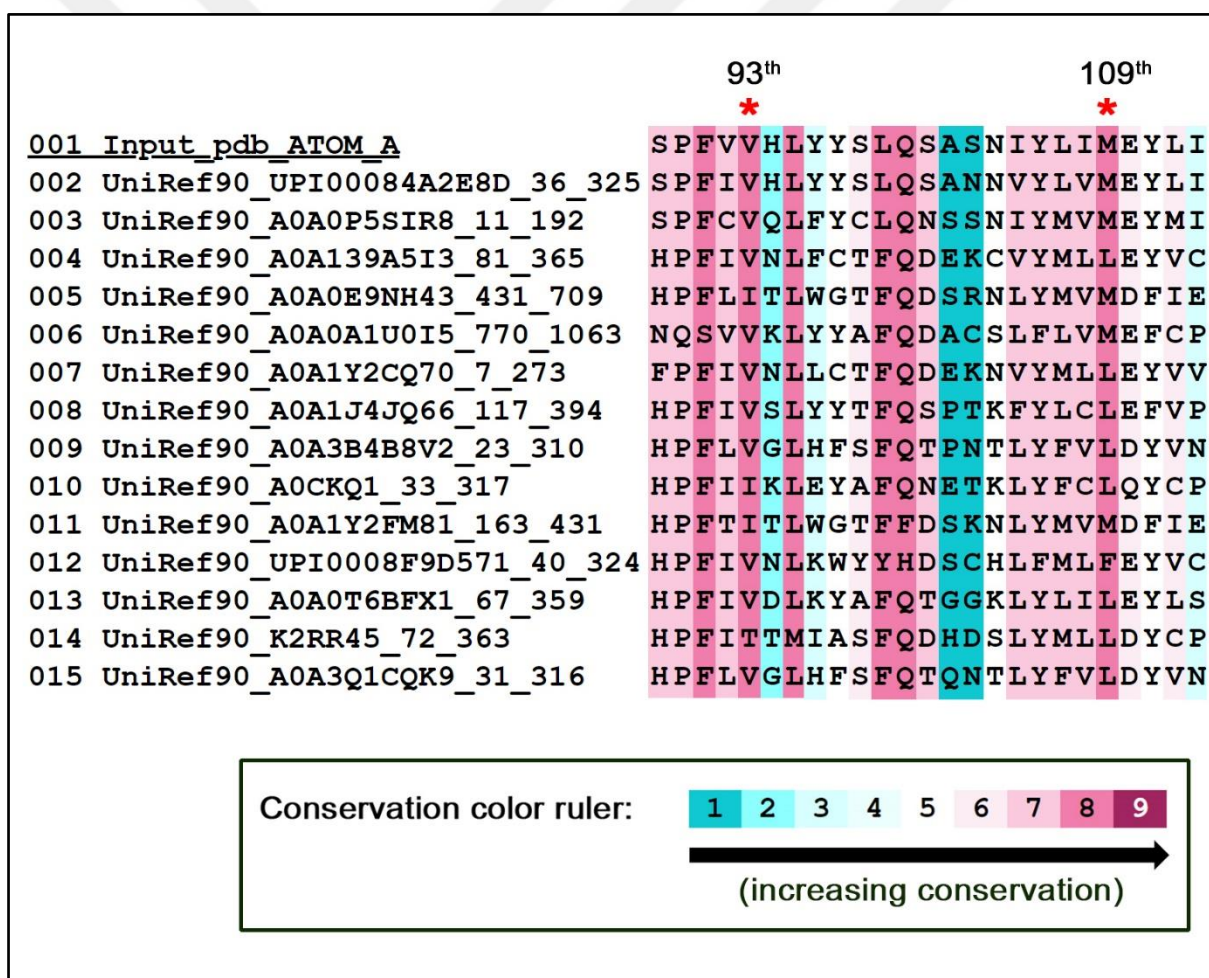

Figure 21. Analysis of the evolutionary conservation of the mouse Mastl residues by ConSurf. Representatively first 15 sequences of the MSA is given in the figure. The UniProt reference cluster IDs of the sequences (left) and the sequence stretches which encompass the to-be-substituted residues are shown (right). Conservation levels were semi-quantified with a

color ruler with dark-cyan representing the weakest level of conservation and dark-magenta representing the strongest level of conservation.

Residues were numbered with respect to their positions in mouse Mastl protein sequence. At the position 93, approximately 64% of the sequences have a valine. At the position 109, approximately 50% of the sequences have a methionine. Both 93th and 109th positions of mouse Mastl are remarkably conserved.

4.5. HADDOCK refinement and analysis of the computational results

Using the atom-atom restraints and empirically determined active site residues, HADDOCK refinement was applied on the prepared model complexes. According to the results, all of the mutations yielded an increase in the electrostatic interactions but a decrease in non-polar interactions (Figure 22).
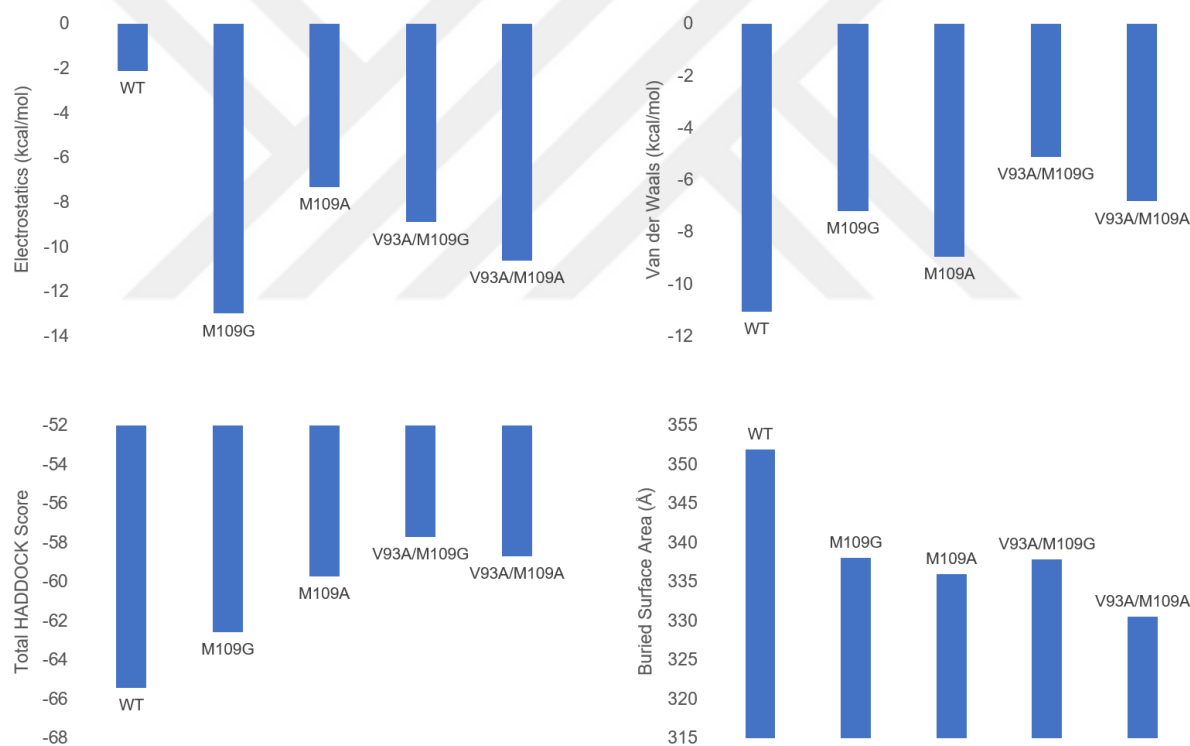
Figure 22. HADDOCK scores. HADDOCK refinement scores (electrostatics, van der Waals, BSA, and total score) of the WT, M109G, M109A, V93A/M109G, and V93A/M109A mutant mouse Mastl-ATP complexes. Lower values indicate stronger interaction for electrostatics, vdW, and total score. Higher values indicate stronger interaction for BSA.

Increase in the electrostatics is attributed to the possible decrease of distance between a hydrogen bond donor from the protein and a hydrogen bond acceptor from the ligand. It is possible that with the loss of a large aliphatic side chain, the adenine ring can get closer to the

backbone of the protein, thus increasing the probability of establishment of a new hydrogen bond between the ligand and the peptide bond.

Model complexes with the complete ATP molecule, 1-NA-PP1, 1-NM-PP1, and 3-MB-PP1 were also simulated (data not shown). All complexes possessing the complete ATP molecule have generally shown the strongest interactions when compared to the other complexes. In case of electrostatics, the difference is dramatic. Fold change of electrostatics score fluctuated approximately within a range of 10 to 140 folds, which is expected due to the presence of a triphosphate group in the complete ATP molecule. When the truncated ATP molecule (adenine) complexes were compared to the ATP analogue complexes, the electrostatics score difference was insignificant among mutant complexes. Mouse Mastl V93A-M109A double mutant/1-NA-PP1 complex yielded the lowest electrostatics score (-17.92 kcal/mol) and the strongest electrostatic interactions. The ATP analogue complexes yielded vdW scores approximately in a range of 2 to 5 folds that of adenine complexes, with mouse Mastl V93A-M109A double mutant/1-NM-PP1 complex showing the lowest vdW score (27.09 kcal/mol) and the strongest vdW interactions. BSA scores of the ATP analogue complexes were approximately two times that of the adenine complexes, with mouse Mastl V93A-M109G double mutant/1-NM-PP1 complex yielding the highest BSA score (633.6 Å) and the strongest hydrophobic interactions. Total HADDOCK scores of the ATP analogue complexes were approximately 1.3 folds that of adenine complexes, with Mouse Mastl M108G mutant/1-NM-PP1 complex showing the lowest total HADDOCK score (-84.6) and the strongest interactions. For each type of score, the score difference among the subsequently ranked complexes were generally insignificant.

PLIP detects hydrophobic interactions, hydrogen bonds, water bridges, parallel π-stacking, perpendicular π-stacking, π-cation interactions, halogen bonds, salt bridges, and metal complexation among a given protein-ligand pair. We checked the selected HADDOCK output complexes on PLIP to set a mechanistic hypothesis regarding the HADDOCK scores. In the HADDOCK refined complexes, using PLIP, the only detectable interaction type was hydrogen bond. In contrast to our comments on the raw HADDOCK scores, the results of PLIP indicated loss of one hydrogen bond in the presence of any mutation (Figure 23).
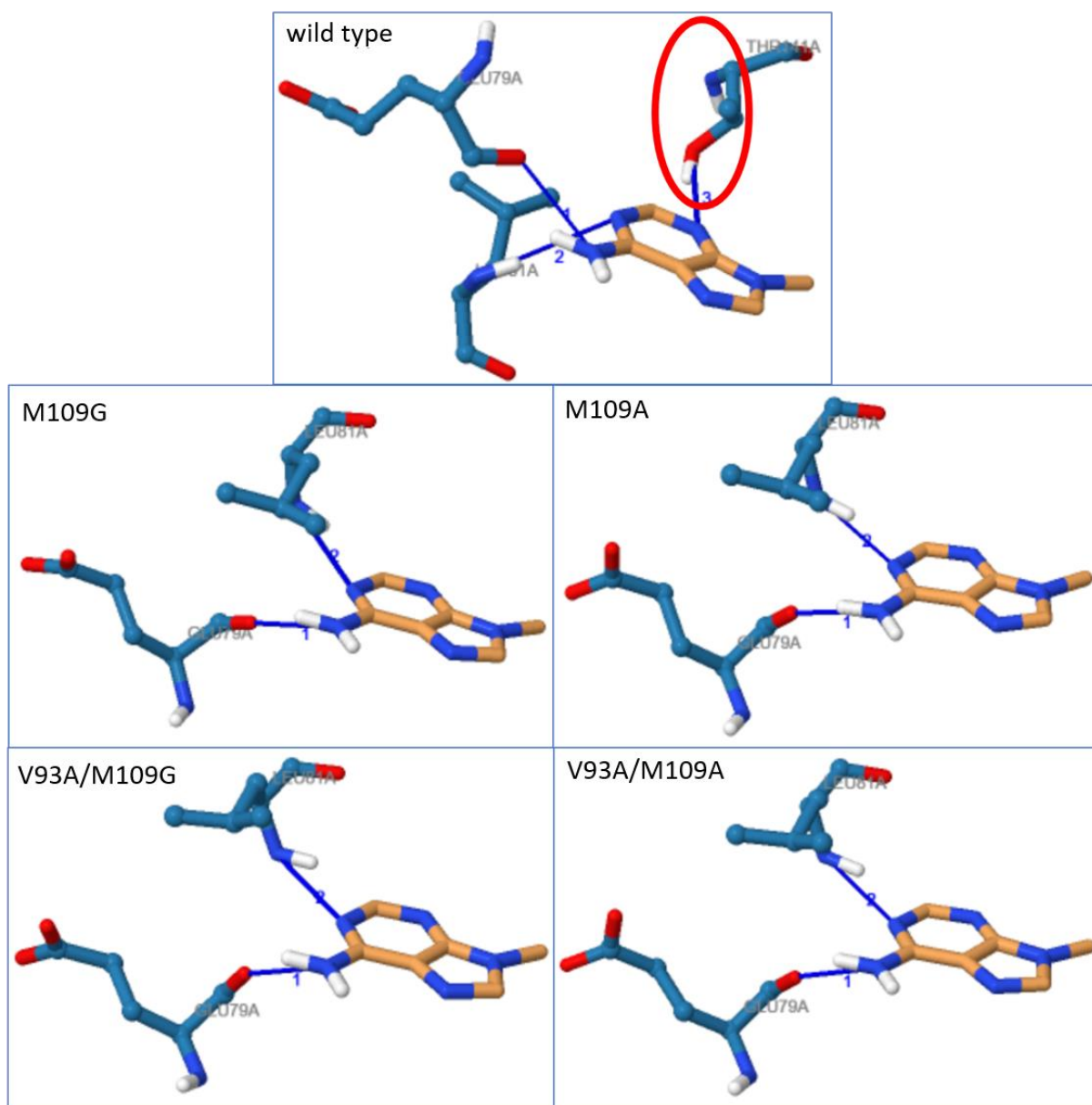
Figure 23. Protein-ligand interactions of the HADDOCK refined complexes. HADDOCK output complexes were submitted to PLIP webserver for characterization of the protein-ligand interactions. When compared to the mutant complexes, the wild type complex possesses an extra hydrogen bond. The different residue (threonine) that contributes to this extra hydrogen bond as a donor is indicated by the red circle.

In the sequence order of mouse Mastl model structure, residues which contribute to hydrogen bond formation are E79, L81, and T141. While the glutamate backbone carboxyl and the leucine backbone amino groups are conserved among all complexes as the H-bond acceptor and donor respectively, only in the case of WT complex, the side chain hydroxyl of the threonine is present as an extra H-bond donor.

Both approaches are in agreement that the overall interaction is weakened in mutant proteins although the loss of interaction is attributed to the different aspects of physical properties.

4.6. Molecular cloning

An HA tagged full-length mouse Mastl cDNA in pBABEpuro retroviral expression vector was used as a template for the mutagenesis PCR and subcloning of the mutant Mastl cDNAs. The mutant cDNAs were successfully subcloned into the empty vector and verified by colony PCR, restriction mapping, and Sanger sequencing subsequently.

Using PstI or HindIII and EcoRI endonucleases for restriction analysis, colony PCR-verified clones for each DNA construct gave the correct pattern (Figure 24).
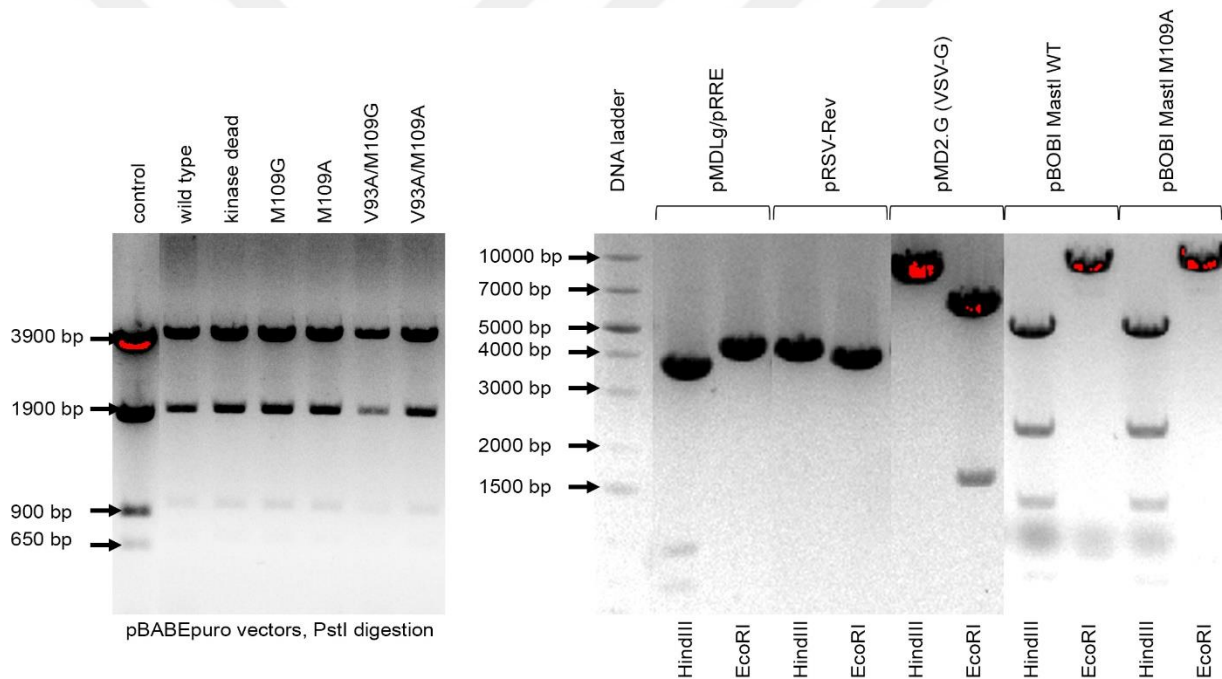
Figure 24. Restriction analysis of the plasmid DNA constructs used in this project. pBABEpuro DNA constructs were digested using PstI. Lentiviral vectors were digested using HindIII and EcoRI.

Selected pBABEpuro mutant Mastl clones were further subjected to sequence verification. A representative of the Sanger sequencing results is given in Figure 25.
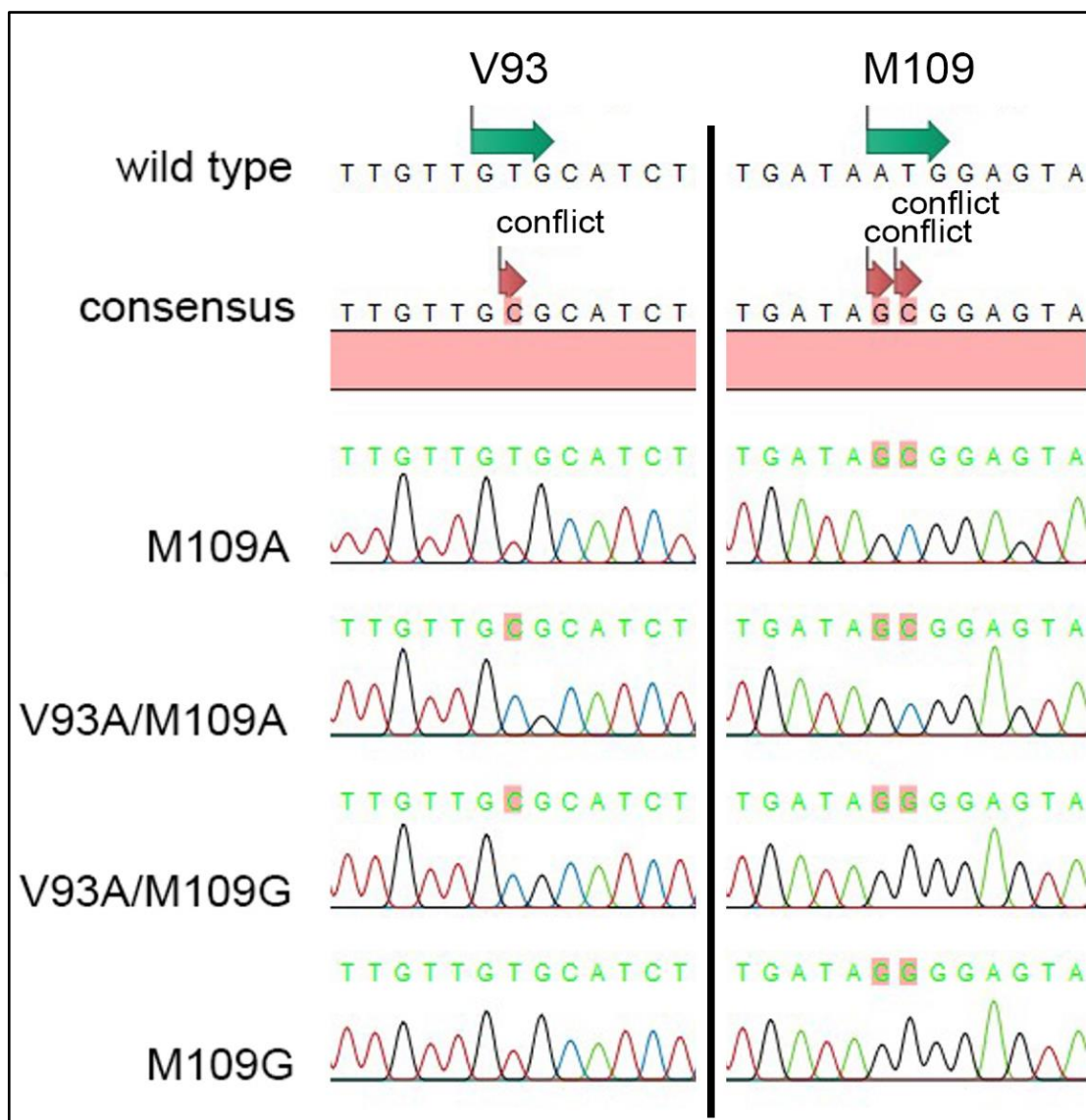
Figure 25. Sanger sequencing results of pBABEpuro mouse HA-Mastl DNA constructs. The codons encoding the gatekeeper residues were successfully changed. The codon encoding the 93th position in the protein sequence was mutated from GTG to G**C**G for substitution of valine for alanine. The codon encoding the 109th position in the protein sequence was mutated from ATG to **GG**G for substitution of methionine for glycine or to **GC**G for substitution of methionine for valine.

The verified bacterial clones were stored frozen as glycerol stocks. Transfection grade plasmids were prepared from these bacterial clones and each new preparate was verified again by restriction mapping.

4.7. Cell line engineering

The efficiency of Mastl gene knockout by the tamoxifen-inducible Cre-ER[T2] system was verified at the protein level by Western blot and immunocytochemistry (Figure 26).
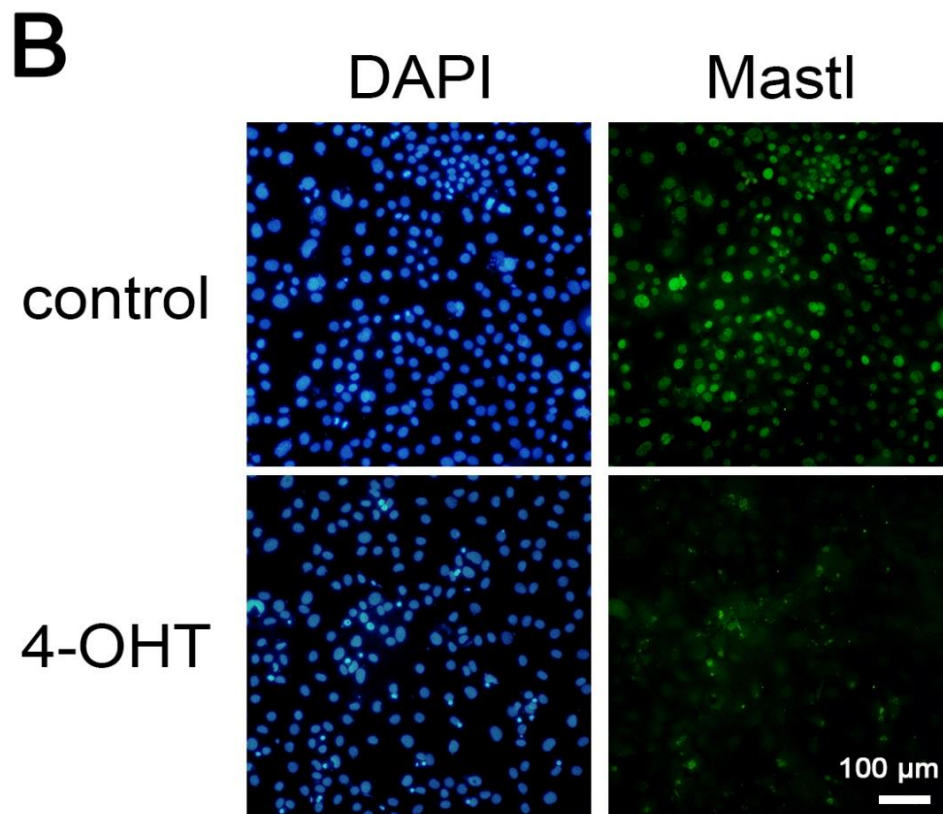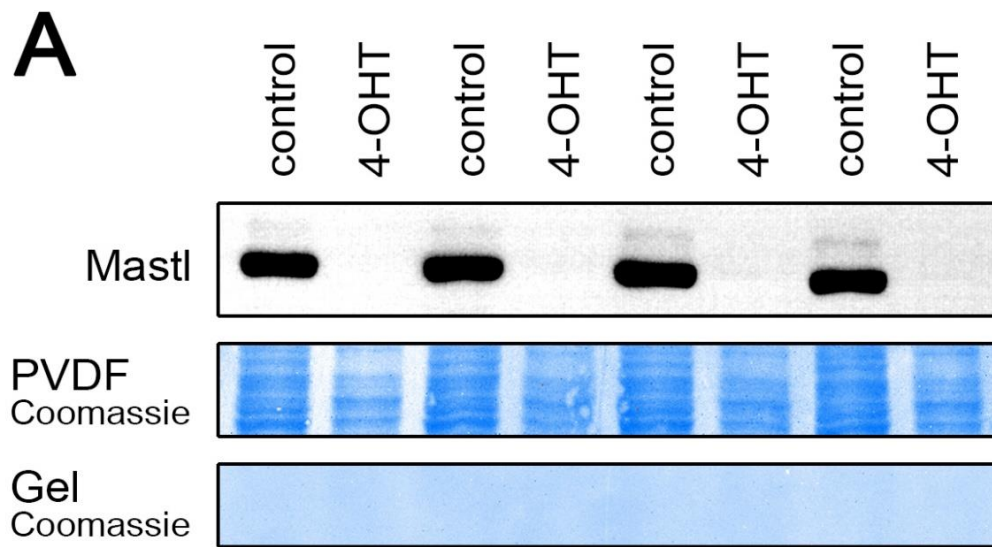
Figure 26. Analysis of the efficiency of tamoxifen-inducible Cre-ER^{T2} system. Knockout was induced when cells were confluent and under contact inhibition. 20 ng/mL 4-OHT containing starvation medium was added to the confluent cells and cells were analyzed three days post-induction. (A) Approximately 30 µg/lane protein was loaded for Western blot analysis of Mastl expression. (B) Immunocytochemical analysis of the Mastl stained (green) uninduced and induced cells. Scale bar 100 µm.

Three days post-induction, Mastl protein levels were analyzed by both Western blotting and immunocytochemistry and the protein levels were below detectable levels using both techniques. For Western blots, even when the exposure was increased, Mastl could not be detected in 4-OHT treated cells. During interphase, Mastl is localized to the nucleus. In immunocytochemistry experiments, increasing the exposure levels pre-acquisition or post-acquisition did not show a specific nuclear signal.

The control group used in the Western blot experiment was an asynchronous MEF population, as a result, the population contained a low proportion of mitotic cells at the time of harvest. Mastl is hyperphosphorylated in the mitotic cells. The faint band above the intense Mastl band is the slower migrating phosphorylated form of Mastl kinase. In immunocytochemistry results, specific Mastl stain was not observed in 4-OHT treated cells. Mainly background signal and autofluorescent particles were detected. In summary, the comparative Western blot and immunocytochemistry results of uninduced and induced cells showed that the Cre-ER^{T2} system works efficiently.

Next, protein expression from the pBABEpuro DNA constructs was tested by Western blot analysis of the transiently transfected 293FT cells (Figure 27).
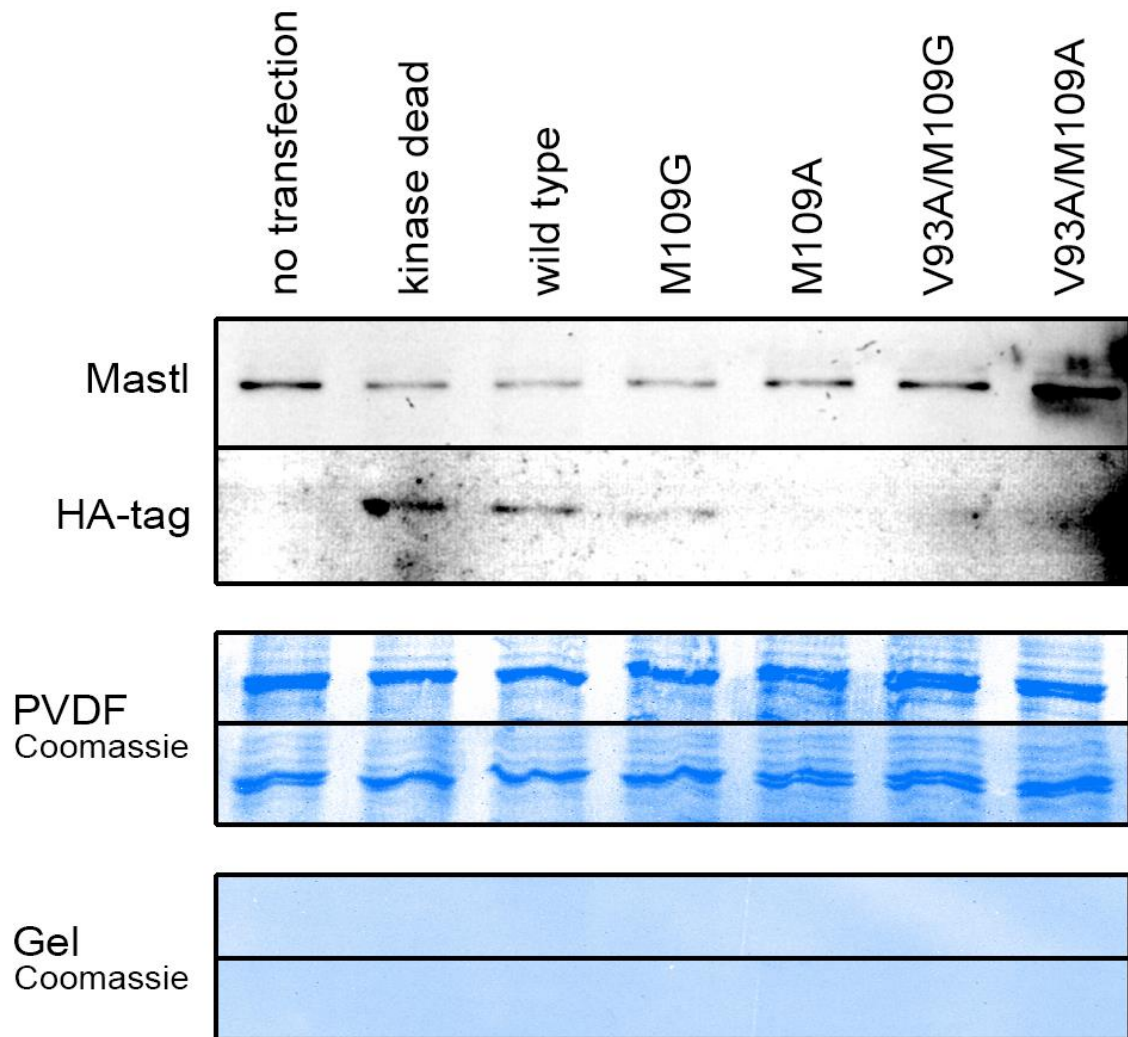
Figure 27. Western blot analysis of protein expression using the pBABEpuro DNA constructs. 293FT cells were transfected with the indicated Mastl DNA constructs. Cells were harvested two days post-transfection and approximately 10 μg/lane protein was loaded. Utilizing anti-Mastl and anti-HA tag antibodies, total Mastl and transfected Mastl (HA tag) expression levels were analyzed by Western blot.

Using the pBABEpuro DNA constructs, exogenous protein expression levels were found to be very low. Mastl signal intensity was similar between cells transfected with the empty vector versus Mastl coding vectors. Using anti-HA antibodies, transfected Mastl could be barely detected. Given that we performed transient transfection and analyzed the protein levels when the expression levels are expected to be at peak, the exogenous protein expression was several folds below the expected levels.

pBABEpuro Mastl vectors were used to prepare retrovirus particles as described in the Materials and Methods section. Conditional knockout cells were infected by retrovirus particles and selected using the puromycin antibiotic resistance marker for longer than one week. Selected cells were analyzed by immunocytochemistry (Figure 28).
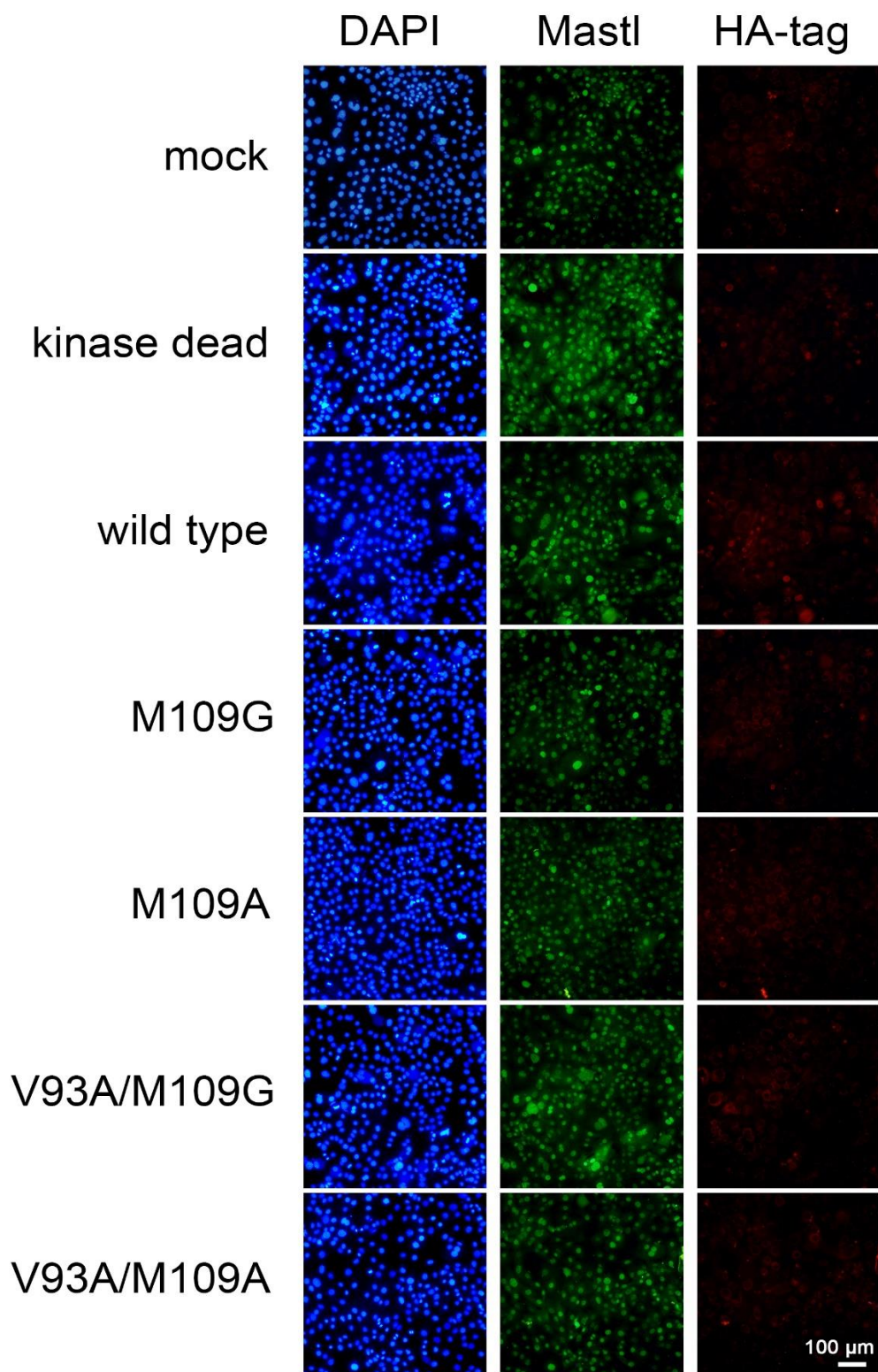
Figure 28. Immunocytochemical analysis of Mastl expression in the stable cell lines. Rabbit anti-Mastl primary antibody and goat anti-rabbit Alexa 488 secondary antibody (green) were used for total Mastl staining. Mouse anti-HA tag primary antibody and goat anti-mouse Alexa 594 secondary antibody (red) were used for HA tag staining. Scale bar 100 μm.

In interphase, Mastl is localized to the nucleus. Asynchronous populations are >95% constituted of interphase cells for these cell lines, as a result, the Mastl stain and the HA tag stain are expected to be localized to the nuclei in majority of the cells. We did not observe a significant increase in Mastl expression levels in virally transduced cell populations.

4.8. Genotyping

Knockout was induced in the stable cell lines with 4-OHT (dissolved in DMSO) treatment. Control groups were treated with an equal volume of DMSO without 4-OHT. Briefly, for each cell line, samples were taken at day 0, 3, and 14 post-induction to verify the success of knockout by genotyping PCR (Figure 29).
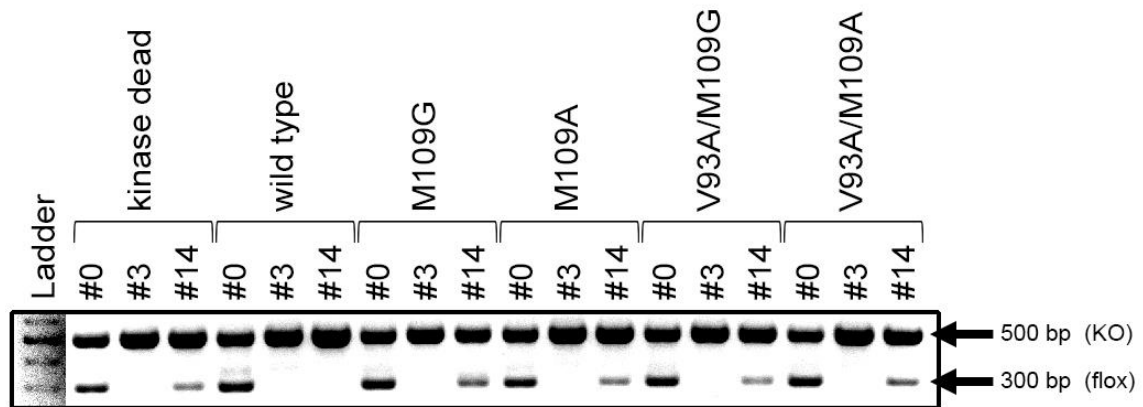
Figure 29. Genotyping PCR results of the knockout induced stable cell lines. Samples were collected from the induced cell pools for genotyping, at day 0, 3, and 14. 500 bp band indicates knockout and 300 bp band indicates the presence of the floxed DNA.

Due to the nature of the inducible Cre systems, each cell line has a basal level of knockout cells as a result of spontaneous Cre leakage into the nucleus, in this case even without 4-OHT induction (Hans et al., 2011; Zhong et al., 2015). Three days post-induction, practically complete knockout of each cell population was observed. However, initially undetectable numbers of floxed cells (both homozygous and heterozygous) have proliferated and dominated the population within two weeks in all cell lines, except for the ectopic WT HA-Mastl expressing cell line (Figure 29). Cells escaping knockout is a known disadvantage of the inducible Cre systems (Bao, Ma, Schuster, Lin, & Yan, 2013; Song & Palmiter, 2018).

Considering these facts and the essentiality of Mastl for proliferation, we decided to use these technical obstacles as a means to determine whether the mutant Mastl variants can rescue the loss of function phenotype or not. Briefly, exogenous KD HA-Mastl expressing induced stable cell line was used as a negative control, and exogenous WT HA-Mastl expressing induced stable cell line was used as a positive control. Even after two weeks of culturing, there was not detectable amount of floxed cells in the exogenous WT HA-Mastl expressing population, but exogenous KD HA-Mastl expressing population has shown floxed genotype (Figure 29). This result verified the notion that exogenous WT HA-Mastl expression rescued Mastl knockout, therefore cells which might have escaped knockout induction could not take over the population. Furthermore, single clones were isolated and genotyped from knockout induced exogenous KD HA-Mastl expressing cell line and knockout induced exogenous WT HA-Mastl expressing cell line. A total of eight clones were genotyped from both of these cell populations (Figure 30).
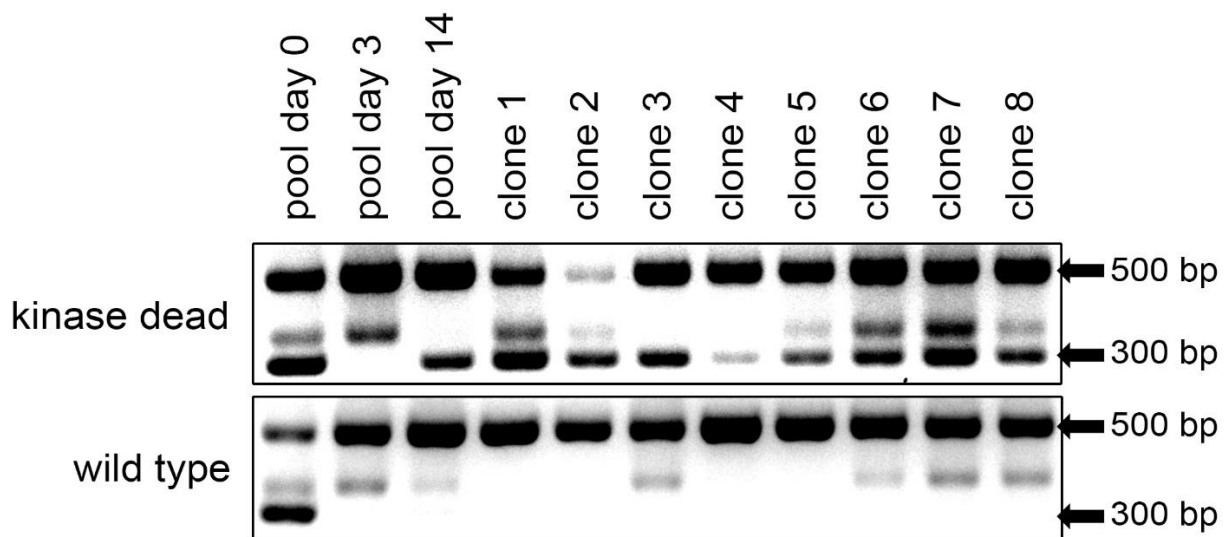
Figure 30. PCR genotypes of single clones isolated from the knockout induced stable cell lines. KD or WT HA-Mastl expressing cKO-MEFs were induced and single clones were isolated from the cell pools 6 days post-induction. For both cell lines, eight grown clones were selected, expanded, and PCR genotyped.

All of the clones derived from exogenous KD HA-Mastl expressing cell line were floxed and all of the clones derived from exogenous WT HA-Mastl expressing cell line were homozygous knockout (Figure 31).
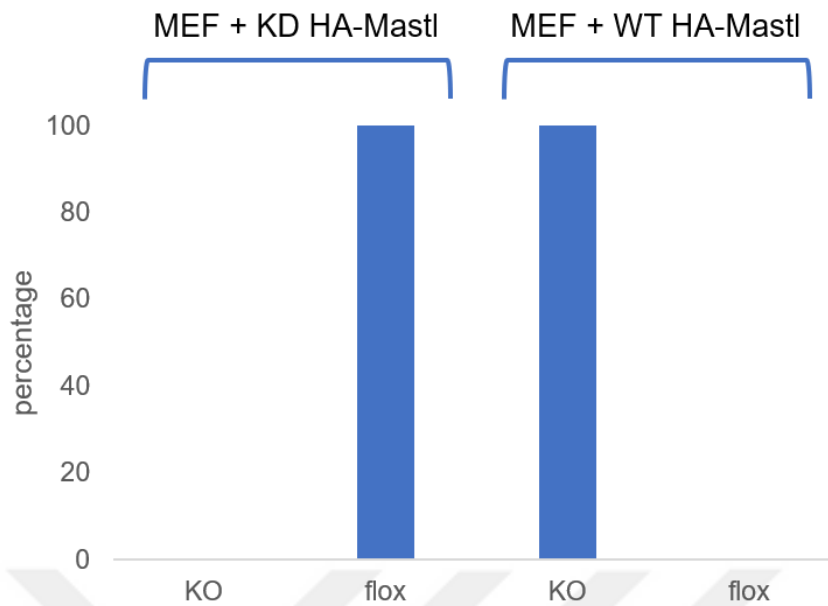
Figure 31. KO and flox genotype percentage of single clones isolated from induced stable cell lines.

Our experimental approach works from a proof of principle perspective. Nevertheless, according to our results, it is clear that none of the engineered mutants can rescue the loss of endogenous Mastl.

4.9. Bright field microscopy

Conditional knockout cells were engineered and selected to stably express exogenous Mastl mutants. Knockout was induced by 4-OHT treatment and micrographs were taken at day 0, 3, and 14. Phenotypic features of Mastl-null cells were explained in previous sections. Mastl is essential for cell cycle. As a result, Mastl-null cells show significant visual phenotypes, i.e. senescence, enlarged cell size, and multilobular nuclei. This is an advantage in terms of ease of analysis, because abnormalities can be detected without the need of delicate techniques. Proliferation and morphological features of the knockout induced and control group cell lines were initially analyzed by bright field microscopy (Figure 32).
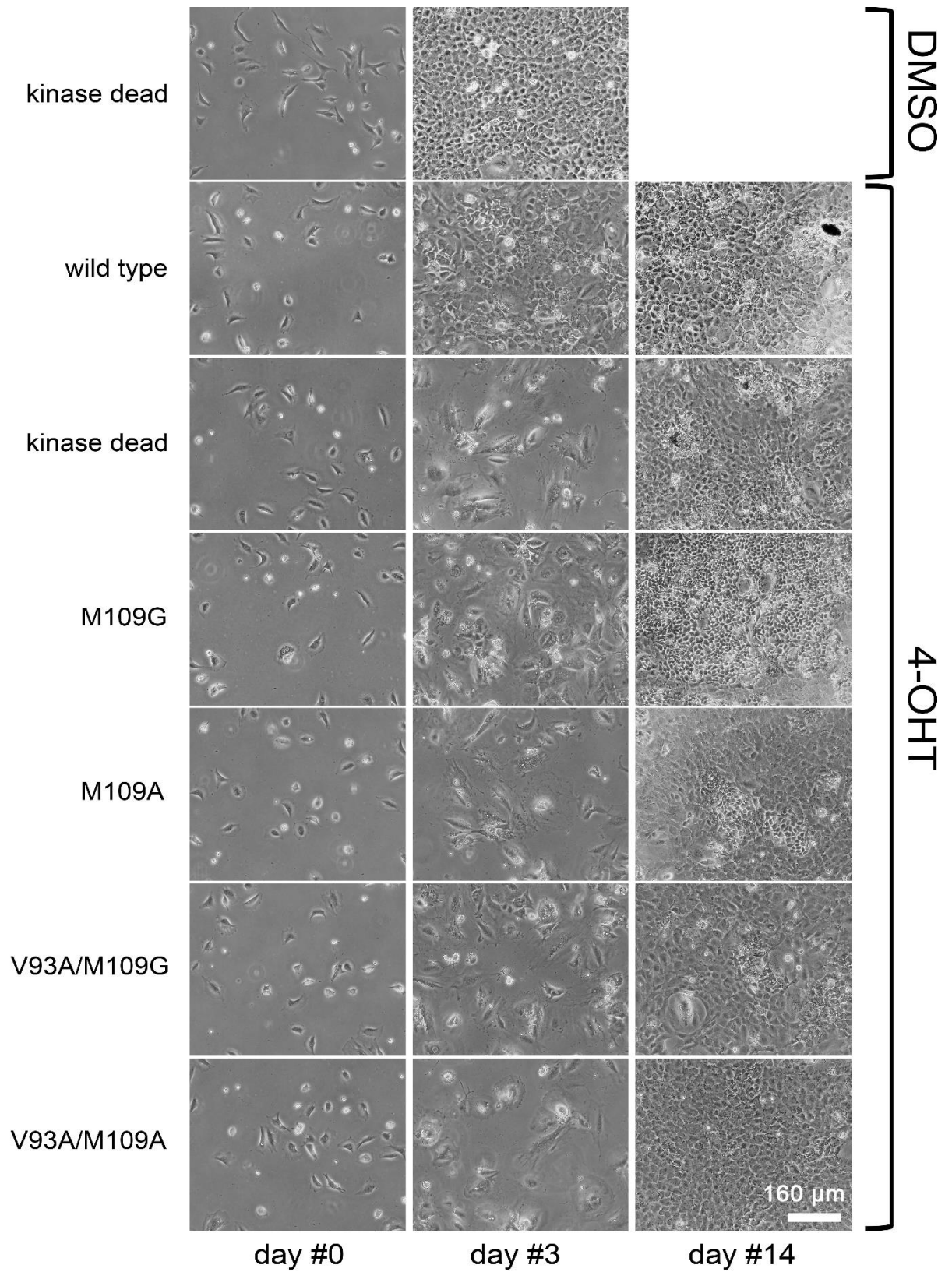
Figure 32. Bright field micrographs of DMSO or 4-OHT treated stable cell lines. Micrographs were taken at day 0, 3, and 14 post-induction. Scale bar 160 μm.

Stable cells were seeded at low density and similar amounts before induction. At day three, it is visible that only the exogenous WT HA-Mastl expression could rescue the loss of endogenous Mastl. However, we concluded that expression levels may not be sufficient because we have repeatedly observed that DMSO treated control cell line proliferated at a visibly faster rate than 4-OHT treated exogenous WT HA-Mastl expressing cell line.

Cell lines which failed to rescue the loss of endogenous Mastl have undergone senescence as observed in the micrographs taken at day three. Cells were analyzed periodically until day fourteen and we observed that the proportion of morphologically abnormal cells decreased and morphologically normal cells gradually dominated the population, consistent with the genotyping results.

4.10.   Use of lentiviral vectors for ectopic Mastl expression

Ectopic expression levels of the transduced and selected stable cell lines were insufficient. To achieve higher expression levels, in our final attempt, we switched from ecotropic retroviral expression system to lentiviral expression system. According to our previous observations, lentiviral expression systems have shown higher transduction efficiency and yielded higher expression levels. The reason we initially used an ecotropic retroviral expression vector- pBABEpuro, is that, it includes a eukaryotic antibiotic selection marker-puromycin, that allows the enrichment of the successfully transduced cells. However, our lentiviral expression system does not possess such a selection feature or a fluorescent marker to use for FACS (fluorescence-activated cell sorting).

To test this alternative with a fast trial, we initially subcloned one of the mutants to the empty lentiviral vector pBOBI and used it in parallel with the preexistent pBOBi mouse WT HA-Mastl construct. After the last round of infection, cells were seeded on coverglasses and analyzed by immunocytochemistry. Total Mastl expression and exogenous Mastl expression were shown in Figure 33.
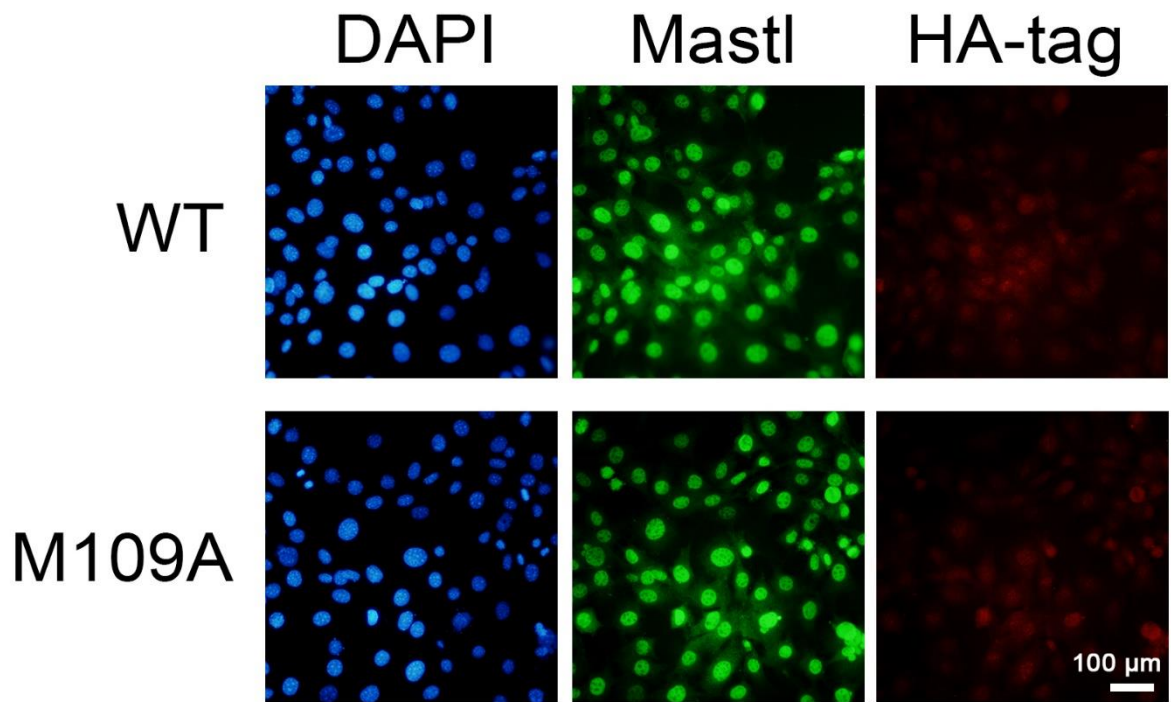
Figure 33. Immunocytochemical analysis of lentiviral mouse HA-Mastl expression in MEFs. Immunocytochemical analysis of MEFs were infected with WT HA-Mastl and M109A HA-Mastl lentivirus particles. Using HA tag staining, presence of the exogenous Mastl was shown by immunocytochemistry. Rabbit anti-Mastl primary antibody and goat anti-rabbit Alexa 488 secondary antibody (green) was used for total Mastl staining. Mouse anti-HA tag primary antibody and goat anti-mouse Alexa 594 secondary antibody (red) were used for HA tag staining. Scale bar 100 μm.

Next, total Mastl expression levels from the ecotropic retroviral transduction and lentiviral transduction were compared by immunocytochemistry. The visibly highest expressing single cells were sampled from the micrographs for both techniques (Figure 34).
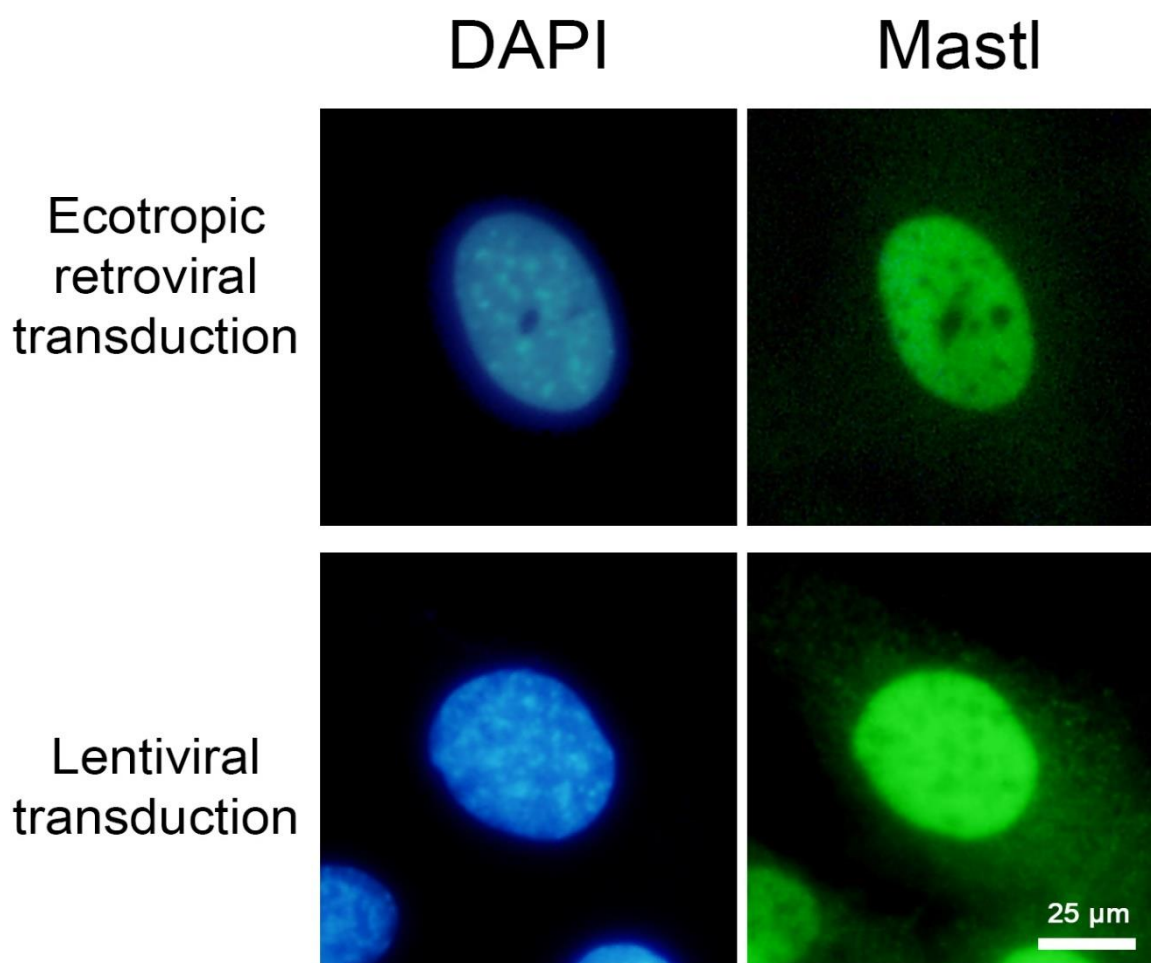
Figure 34. Immunocytochemical comparison of total Mastl expression levels using ecotropic retroviral transduction and lentiviral transduction techniques. Total Mastl expression levels are shown in Mastl stained (green) ecotropic retroviral and lentiviral transduced MEFs. Scale bar 25 µm.

Immunocytochemical comparison of two different transduction approaches have shown that lentiviral transduction yielded visibly higher expression levels. The majority (>95%) of ecotropic retroviral transduced cells lacked exogenous expression and the majority (>95%) of lentiviral transduced cells showed exogenous expression (data not shown).

In our laboratory, lentiviral overexpression system has been used previously in other projects. We have used pBOBI vector for expression of Arpp19 protein. pBOBI HA-Arpp19 expression vector was transiently transfected into HEK293T cells. Expression levels of total Arpp19 and HA tag was analyzed by Western blot two days post-transfection (Figure 35-A). Lentivirus particles were produced for overexpression of WT HA-Arpp19 and S62A HA-

Arpp19, and cKO-MEFs were infected. Overexpressing single clones were isolated from the transduced cell pools and their expression levels were analyzed by Western blot (Figure 35-B).
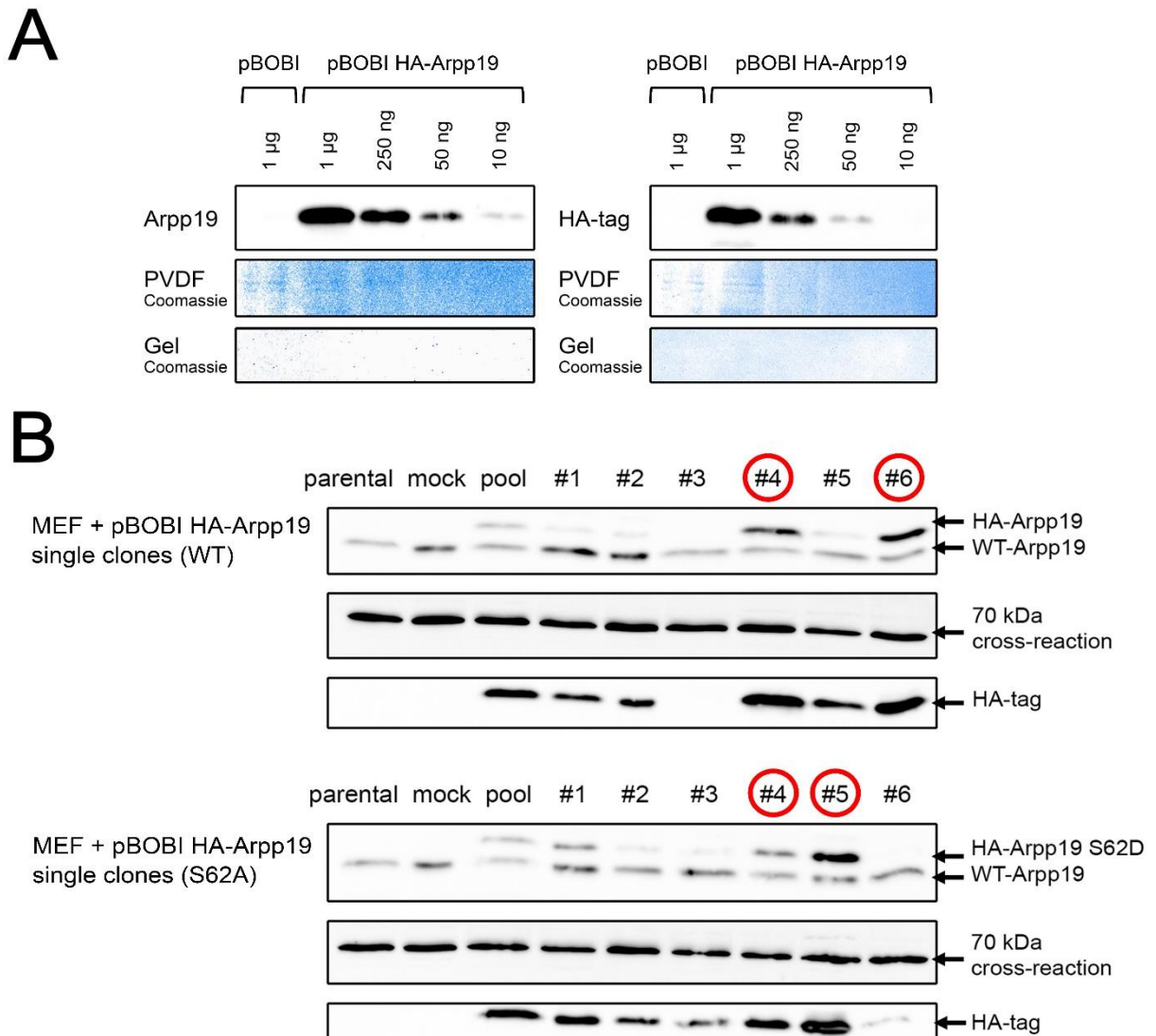
Figure 35. Western blot analysis of protein expression using the pBOBI DNA constructs. Arpp19 and HA tag primary antibodies were used at 1:1000 dilution. (A) The expression vector is transiently transfected to HEK293T cells and expression levels were analyzed by Western blot 2 days post-transfection by loading the indicated amounts of protein. (B) Lentiviral overexpression of WT HA-Arpp19 and S62A HA-Arpp19. Expression levels of the single clones were screened by Western blot. 10 μg/lane protein was loaded.

Expression levels of the selected overexpressing clones were verified by immunocytochemical analysis (Figure 36).
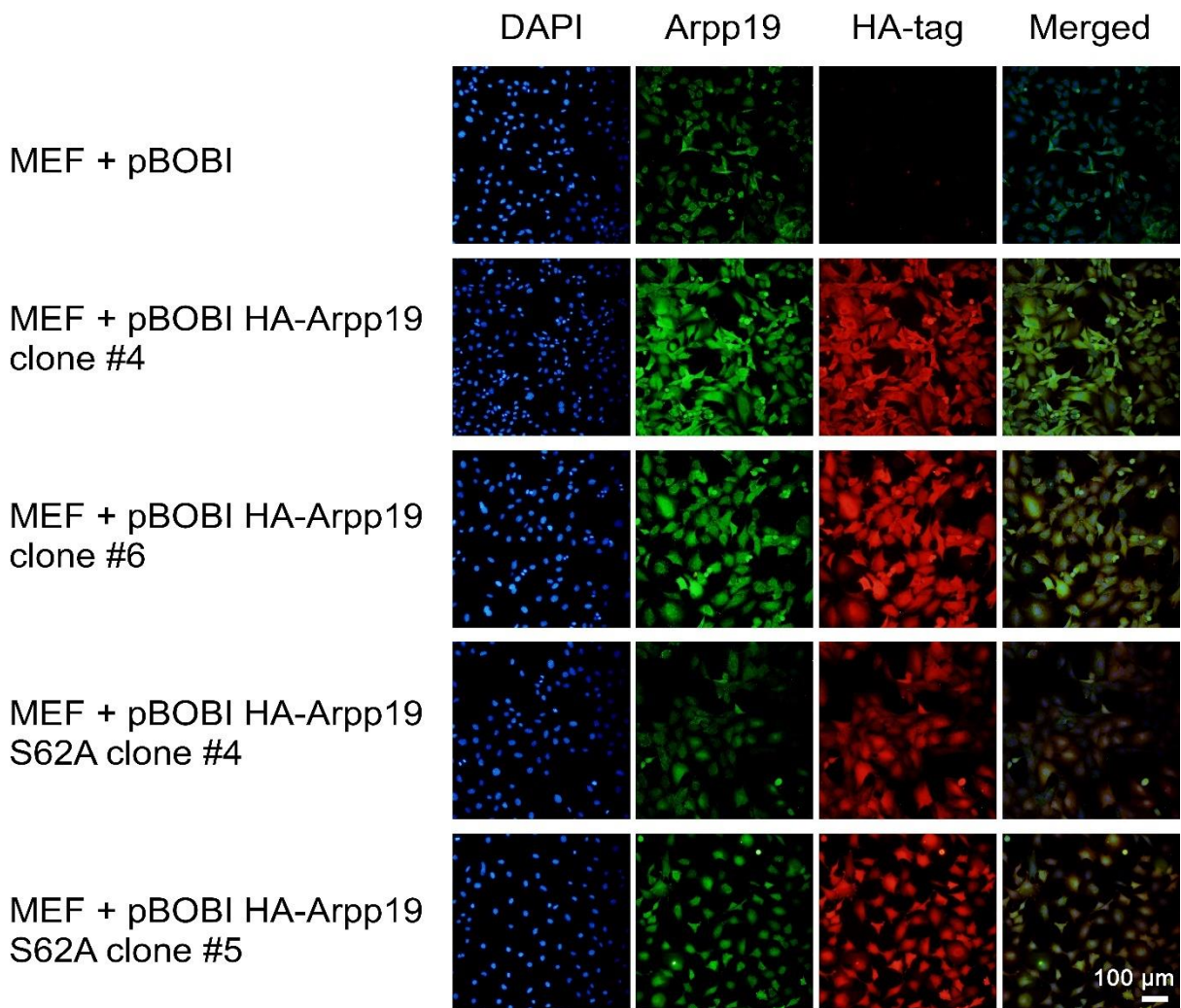
Figure 36. Immunocytochemical analysis of protein expression using the pBOBI DNA constructs. Rabbit anti-Arpp19 primary antibody and goat anti-rabbit Alexa 488 secondary antibody (green) was used for total Arpp19 staining. Mouse anti-HA tag primary antibody and goat anti-mouse Alexa 594 secondary antibody (red) was used for HA tag staining. Scale bar 100 μm.

Using pBOBI lentiviral protein expression vector, approximately up to 4 folds of overexpression was achieved at the protein level.

Among the factors that may affect expression levels are the protein to be expressed and length of the insert in between the LTR sequences. For this reason, lentiviral overexpression data given in Figure 35 and Figure 36 are not directly comparable to the overexpression attempt of Mastl cDNAs. However, our trial data of Mastl overexpression (Figure 33, 34) and the data

of Arpp19 overexpression (Figure 35, 36) are together promising for the capabilities of pBOBI lentiviral protein expression vector.

Ecotropic retroviruses can only infect rodents while pseudotyped pantropic lentiviruses can infect also many other species (Cronin, Zhang, & Reiser, 2005; Gladow, Becker, Blankenstein, & Uckert, 2000). In this study, we used ecotropic retrovirus to transduce murine cells. Both the retroviral and lentiviral vectors we used in this study utilize a CMV promoter. CMV promoters are strong promoters and they are known to achieve high transgene expression levels (Benabdallah, Rousseau, Bouchentouf, & Tremblay, 2005; Qin et al., 2010).

It is known that lentiviral transduction achieves higher transgene expression levels when compared to retroviral transduction (Abdellatif et al., 2006). When other distinguishing features of retroviruses and lentiviruses are compared, the higher expression levels achieved by lentiviral transduction is understandable. The retroviral transgene integration pattern is more focused on transcriptionally active sites while the lentiviral transgene integration pattern shows a more random distribution across the genome (Šenigl, Miklík, Auxt, & Hejnar, 2017). Retroviral transgene integration requires that the target cells are actively proliferating, because genome integration is limited to the S phase and the retroviral elements can not penetrate the nuclear envelope (Swanstrom & Vogt, 1990). Lentiviruses can achieve genome integration in both proliferating and non-proliferating cells, because genome integration is not limited to the S phase and the lentiviral elements can penetrate the intact nuclear envelope (Mühlebach et al., 2005).

Viral particles are active supramolecular complexes with limited lifespan, during which they have the potential to successfully infect the host cells. Throughout the procedure of infection, the host cells are exposed to the viral media for up to approximately 24 hours. Within this period of time, the host cells are incubated at 37°C, which is not a favorable condition for the lifespan of viral particles (Beer, Meyer, Müller, & Wirth, 2003). We performed infections on asynchronous cell populations. Retroviral elements can reach the host DNA only in the portion of cells undergoing mitosis. Mitosis is the shortest phase (~1 hour) of mammalian cell cycle and as a result, the proportion of mitotic cells in an asynchronous cell population is low. Upon reconstitution of nuclear envelope, the local retroviral elements can not efficiently perform the genome integration until the newly generated host cells enter the next S phase. The duration of the S phase takes approximately one fifth of the mammalian cell cycle (Anglana,

Apiou, Bensimon, & Debatisse, 2003). This means that even after successful penetration of the cell membrane, genome integration may not occur throughout the following several hours, thus some viral particles may lose activity. But in case of lentivirus, virtually every viable cell in the culture is available for genome integration in any given time period.

Briefly, it can be stated that, when compared to retroviruses, lentiviruses can achieve higher amounts of successful genomic integration. As explained, lentiviruses target a broader range of sites across the genome throughout a broader range of time period during the cell cycle progression of the host cells. Based on this, it can be expected for lentiviral transduction to be more efficient, because probabilistically, higher copy numbers of transgene can be successfully integrated into the genome.

5. <u>DISCUSSION</u>

In this study we aimed to develop ATP analogue-sensitive Mastl mutant cell lines in order to be able to further probe the functions of the enzyme via spatio-temporal techniques. Our initial approach was to edit the endogenous loci utilizing the CRISPR-Cas9 system. After a year of failed attempts, we switched to readily available Mastl conditional knockout cells. With this approach, we first had to exogenously express the mutant Mastl variants, and then induce knockout.

Exogenous Mastl expressing stable cell lines were established and exogenous Mastl levels were analyzed by immunocytochemistry. Although the cells were subjected to antibiotic selection post-transduction, the expression levels did not significantly increase for each cell line or expression levels were below detectable levels for the majority of the cells within the populations (Figure 28). This result is consistent with the protein analysis result of the transient transfection experiment (Figure 27), which showed near-undetectable expression levels when compared to our other Western blot results (Figure 35) of another project using a different overexpression vector. However, according to the initial trials, exogenous HA tagged wild type Mastl expression could rescue the Mastl knockout phenotype but kinase dead Mastl expression could not. Although the ectopic protein levels in the stable cell lines are below detectable levels, it is clear that our system works in principle. Reliability of our system was repeatedly verified by genotyping and periodical visual analysis of the 4-OHT treated pool cell populations (Figure 29, 32 respectively) and genotyping of the isolated single clones (Figure 30, 31). Based on these results, we can conclude that our allegedly analogue sensitizing mutations inactivate the kinase. However, we can not rule out the fact that a successful overexpression of these mutant proteins can rescue the knockout by compensating for the possible partial inactivation of the mutant enzyme. Because even low-level expression of the ectopic wild type Mastl efficiently rescued the knockout phenotype.

Regarding the inactivation of the enzyme by mutations, several possible explanations can be made by checking the evolutionary conservation of the residues of interest (Figure 21), positions (Figure 17-A) and characteristics of the mutations, and visual examination of the protein-ligand interface (Figure 18, 20).

Although the to-be-substituted residues are not located in a catalytically known motif, their relatively high conservation levels (64% for the valine at 93th position and 50% for the

methionine at 109th position) may designate an unknown biochemical importance for the protein structure and function.

At first glance, valine (93th) to alanine substitutions may not be in a critical position to present a danger in terms of enzymatic activity. It is uncharged and located in the middle of a loop between conserved secondary structures. Valine and alanine side chains possess similar characteristics, thus substitution of one for another is not expected to cause a direct structural instability or loss of a key protein-ligand interaction. On the other hand, methionine (109th) to glycine or methionine (109th) to alanine substitutions are arguably more dramatic. This residue takes place at the end of a β-strand within the anti-parallel β-sheet moiety of ATP binding pocket (Figure 17-A). In this case, especially methionine to glycine substitution can be expected to cause a structural instability due to the truncation of the secondary structure. Methionine has a large aliphatic side chain, also including a large sulfur atom. Although methionine, alanine, and glycine are similar in terms of polarity, these substitutions can cause a formidable difference in intramolecular and intermolecular non-polar interactions as a result of the remarkable decrease in the space occupancy.

The computational data we obtained in this study can not be directly correlated with an experimental result. Due to the technical shortages, we could not perform in vitro kinase activity assays on purified WT and mutant mouse Mastl variants. Our data is qualitative, showing whether a mutant exogenous protein can rescue the loss of endogenous Mastl or not. Regardless of that, we performed the simulations to aid our choice of optimal mutation-drug combinations and to understand the effect of point mutations on the ATP and drug binding energetics.

In previous studies carried out in this research field, using yeast as a model organism, partial inactivation has been observed in analogue-sensitive mutant enzymes. The reasons behind that are possibly similar to those explained in this section. In our case, aside from the chemical aspect, practically total unviability of our mutant cell lines can be attributed to the low expression levels and the fact that we are working on a more delicate biological system. Under circumstances in which the exogenous protein can be expressed at higher folds, partial loss of activity as a result of the mutation can be rescued by excess quantities of the protein.

6. <u>CONCLUSION AND RECOMMENDATIONS</u>

In this work, we have aimed to engineer mammalian cell lines expressing analogue-sensitive mutants of Mastl kinase. Our initial approaches of editing the Mastl loci in human cell lines using CRISPR/Cas9 system and homology directed repair were not successful (data not shown). As a result of these earlier efforts, we decided to utilize the Mastl conditional knockout mammalian cell line that was obtained from Kaldis lab (IMCB A*STAR, Singapore), to test the analogue-sensitive kinase variants. In these cells, the Mastl locus can be easily deleted with the addition of 4-OHT to the culture medium. We aimed to express the mutant cDNAs by transduction of retroviral constructs and delete the endogenous loci by 4-OHT addition respectively. Although the system worked well from a proof of principle perspective, as exogenous HA tagged wild type Mastl expression could rescue the deletion of endogenous Mastl, none of the mutant constructs were able to rescue the knockout. In conclusion, the mutant kinase variants we have engineered are either producing inactive enzymes or enzymes with reduced activity due to possible conformational changes of the ATP binding pocket or loss of key protein-ligand interactions, such as a hydrogen bond (Figure 23). Reduction of the enzymatic activity may result in a kinase dead phenotype as the expression of the exogenous Mastl was found to be at low levels when we utilized the pBABEpuro system.

In the future follow up studies, we aim to express the exogenous Mastl, using a lentiviral vector- pBOBI, which can overexpress ectopic proteins in higher quantities according to our previous observations from another project. These studies have already been initiated and currently underway.

Alternatively, as a parallel backup approach, we aim to express exogenous Mastl constructs in common human cell lines (i.e. HEK293, HeLa) and silence/knockout the endogenous Mastl using shRNAs or CRISPR/Cas9 system, respectively. Briefly, both for overexpression and silencing, we aim to generate stably transfected cells from transiently transfected cell populations by use of eukaryotic antibiotic selection post-transfection. These studies are also currently underway.

According to the computational results, no single mutation-drug combination stood out as an optimal choice. Because ranking of the complexes varied among different type of scores. As a result, we again decided to simultaneously use more than one mutant construct throughout the alternative experimental approaches, lentiviral transduction and stable transfection.

7. <u>REFERENCES</u>

Abdellatif, A. A., Pelt, J. L., Benton, R. L., Howard, R. M., Tsoulfas, P., Ping, P., … Whittemore, S. R. (2006). Gene delivery to the spinal cord: Comparison between lentiviral, adenoviral, and retroviral vector delivery systems. *Journal of Neuroscience Research*, *84*(3), 553–567. https://doi.org/10.1002/jnr.20968

Adams, J. A. (2001). Kinetic and catalytic mechanisms of protein kinases. *Chemical Reviews*, *101*(8), 2271–2290. https://doi.org/10.1021/cr000230w

Alberts, B., Johnson, A., Lewis, J., Morgan, D., Raff, M., Roberts, K., & Walter, P. (2015). Molecular Biology of the Cell. *Ch 17: Cell Cycle*. (Sixth Edit). *Garland Science*. ISBN 978-0-8153-4432-2

Álvarez-Fernández, M., & Malumbres, M. (2014). Preparing a cell for nuclear envelope breakdown: Spatio-temporal control of phosphorylation during mitotic entry. *BioEssays*, *36*(8), 757–765. https://doi.org/10.1002/bies.201400040

Anglana, M., Apiou, F., Bensimon, A., & Debatisse, M. (2003). Dynamics of DNA replication in mammalian somatic cells: Nucleotide pool modulates origin choice and interorigin spacing. *Cell*, *114*(3), 385–394. https://doi.org/10.1016/S0092-8674(03)00569-5

Ashkenazy, H., Abadi, S., Martz, E., Chay, O., Mayrose, I., Pupko, T., & Ben-tal, N. (2016). ConSurf 2016 : an improved methodology to estimate and visualize evolutionary conservation in macromolecules, *Nucleic Acids Research*, *44*, 344–350. https://doi.org/10.1093/nar/gkw408

Ashkenazy, H., Erez, E., Martz, E., Pupko, T., & Ben-Tal, N. (2010). ConSurf 2010: Calculating evolutionary conservation in sequence and structure of proteins and nucleic acids. *Nucleic Acids Research*, *38*(2), 529–533. https://doi.org/10.1093/nar/gkq399

Bao, J., Ma, H. Y., Schuster, A., Lin, Y. M., & Yan, W. (2013). Incomplete cre-mediated excision leads to phenotypic differences between *Stra8-iCre*; *Mov10l1$^{lox/lox}$* and *Stra8-iCre*; *Mov10l1$^{lox/\Delta}$* mice. *Genesis*, *51*(7), 481–490. https://doi.org/10.1002/dvg.22389

Barouch-Bentov, R., & Sauer, K. (2011). Mechanisms of drug resistance in kinases. *Expert

Opinion on Investigational Drugs, *20*(2), 153–208.
https://doi.org/10.1517/13543784.2011.546344

Bateman, A. (2019). UniProt: A worldwide hub of protein knowledge. *Nucleic Acids Research*, *47*(1), 506–515. https://doi.org/10.1093/nar/gky1049

Beer, C., Meyer, A., Müller, K., & Wirth, M. (2003). The temperature stability of mouse retroviruses depends on the cholesterol levels of viral lipid shell and cellular plasma membrane. *Virology*, *308*(1), 137–146. https://doi.org/10.1016/S0042-6822(02)00087-9

Benabdallah, B. F., Rousseau, J., Bouchentouf, M., & Tremblay, J. P. (2005). PGK and CMV Promoters Exert the Strongest Activity in Lentiviral Gene Transduction of Myeloid Cells Including Mature Neutrophils. *Molecular Therapy*, *11*(1), 42. https://doi.org/10.1016/j.ymthe.2005.06.109

Berman, H. M., Westbrook, J., Feng, Z., Gilliland, G., Bhat, T. N., Weissig, H., … Bourne, P. E. (2000). The Protein Data Bank. *Nucleic Acids Research*, *28*(1), 235–242. https://doi.org/10.1093/nar/28.1.235

Bishop, A. C., Ubersax, J. A., Petsch, D. T., Matheos, D. P., Grayk, N. S., Blethrow, J., … Shokat, K. M. (2000). A chemical switch for inhibitor-sensitive alleles of any protein kinase. *Cell*, (407), 395–401. https://doi.org/10.1038/35030148

Blake-Hodek, K. A., Williams, B. C., Zhao, Y., Castilho, P. V., Chen, W., Mao, Y., … Goldberg, M. L. (2012). Determinants for Activation of the Atypical AGC Kinase Greatwall during M Phase Entry. *Molecular and Cellular Biology*, *32*(8), 1337–1353. https://doi.org/10.1128/MCB.06525-11

Burgess, A., Vigneron, S., Brioudes, E., Labbé, J., Lorca, T., & Castro, A. (2010). Loss of human Greatwall results in G2 arrest and multiple mitotic defects due to deregulation of the cyclin B-Cdc2 / PP2A balance. *Proceedings of the National Academy of Sciences*, *107*(28), 12564–12569. https://doi.org/10.1073/pnas.0914191107

Celniker, G., Nimrod, G., Ashkenazy, H., Glaser, F., Martz, E., Mayrose, I., … Ben-Tal, N. (2013). ConSurf: Using evolutionary data to raise testable hypotheses about protein function. *Israel Journal of Chemistry*, *53*(3–4), 199–206. https://doi.org/10.1002/ijch.201200096

Chen, J., & Liu, J. (2015). Erroneous Silencing of the Mitotic Checkpoint by Aberrant Spindle Pole-Kinetochore Coordination. *Biophysical Journal*, *109*(11), 2418–2435. https://doi.org/10.1016/j.bpj.2015.10.024

Ciliberto, A., & Shah, J. V. (2009). A quantitative systems view of the spindle assembly checkpoint. *EMBO Journal*, *28*(15), 2162–2173. https://doi.org/10.1038/emboj.2009.186

Cronin, J., Zhang, X.-Y., & Reiser, J. (2005). Altering the Tropism of Lentiviral Vectors through Pseudotyping. *Current Gene Therapy*, *5*(4), 387–398. https://doi.org/10.2174/1566523054546224

Cundell, M. J., Bastos, R. N., Zhang, T., Holder, J., Gruneberg, U., Novak, B., & Barr, F. A. (2013). The BEG (PP2A-B55/ENSA/Greatwall) Pathway Ensures Cytokinesis follows Chromosome Separation. *Molecular Cell*, *52*(3), 393–405. https://doi.org/10.1016/j.molcel.2013.09.005

Diamond, J. S., & Zhang, Y. (2018). THE-DB: A threading model database for comparative protein structure analysis of the E. coli K12 and human proteomes. *Database*, *2018*, bay090. https://doi.org/10.1093/database/bay090

Diril, M. K., Bisteau, X., Kitagawa, M., Caldez, M. J., Wee, S., Gunaratne, J., … Kaldis, P. (2016). Loss of the Greatwall Kinase Weakens the Spindle Assembly Checkpoint. *PLoS Genetics*, *12*(9), 1–26. https://doi.org/10.1371/journal.pgen.1006310

Diril, M. K., Ratnacaram, C. K., Padmakumar, V. C., Du, T., Wasser, M., Coppola, V., … Kaldis, P. (2012). Cyclin-dependent kinase 1 (Cdk1) is essential for cell division and suppression of DNA re-replication but not for liver regeneration. *Proceedings of the National Academy of Sciences*, *109*(10), 3826–3831. https://doi.org/10.1073/pnas.1115201109

El-Gebali, S., Mistry, J., Bateman, A., Eddy, S. R., Luciani, A., Potter, S. C., … Finn, R. D. (2019). The Pfam protein families database in 2019. *Nucleic Acids Research*, *47*(1), 427–432. https://doi.org/10.1093/nar/gky995

Fiser, A. (2010). Template-Based Protein Structure Modeling. *Methods in Molecular Biology*, *2010*(673), 73–94. https://doi.org/10.1007/978-1-60761-842-3_6

Foley, E. A., & Kapoor, T. M. (2013). Microtubule attachment and spindle assembly

checkpoint signalling at the kinetochore. *Nature Reviews Molecular Cell Biology*, *14*(1), 25–37. https://doi.org/10.1038/nrm3494

Galas, S., Li, Z., Yu, J., Goldberg, M. L., & Zhao, Y. (2006). Greatwall Kinase Participates in the Cdc2 Autoregulatory Loop in Xenopus Egg Extracts. *Molecular Cell*, *22*(1), 83–91. https://doi.org/10.1016/j.molcel.2006.02.022

Gharbi-Ayachi, A., Labbé, J. C., Burgess, A., Vigneron, S., Strub, J. M., Brioudes, E., … Lorca, T. (2010). The substrate of Greatwall kinase, Arpp19, controls mitosis by inhibiting protein phosphatase 2A. *Science*, *330*(6011), 1673–1677. https://doi.org/10.1126/science.1197048

Gladow, M., Becker, C., Blankenstein, T., & Uckert, W. (2000). MLV-10A1 retrovirus pseudotype efficiently transduces primary human CD4+ T lymphocytes. *Journal of Gene Medicine*, *2*(6), 409–415. https://doi.org/10.1002/1521-2254(200011/12)2:6<409::AID-JGM144>3.0.CO;2-K

Glaser, F., Pupko, T., Paz, I., Bell, R. E., Bechor-Shental, D., Martz, E., & Ben-Tal, N. (2003). ConSurf: Identification of functional regions in proteins by surface-mapping of phylogenetic information. *Bioinformatics*, *19*(1), 163–164. https://doi.org/10.1093/bioinformatics/19.1.163

Glover, D. M. (2012). The overlooked greatwall: A new perspective on mitotic control. *Open Biology*, *2*(3). https://doi.org/10.1098/rsob.120023

Gregan, J., Zhang, C., Rumpf, C., Cipak, L., Li, Z., Uluocak, P., … Shokat, K. M. (2007). Construction of conditional analog-sensitive kinase alleles in the fission yeast schizosaccharomyces pombe. *Nature Protocols*, *2*, 2996-3000. https://doi.org/10.1038/nprot.2007.447

Hans, S., Freudenreich, D., Geffarth, M., Kaslin, J., Machate, A., & Brand, M. (2011). Generation of a non-leaky heat shock-inducible Cre line for conditional Cre/lox strategies in zebrafish. *Developmental Dynamics*, *240*(1), 108–115. https://doi.org/10.1002/dvdy.22497

Ho, S. N., Hunt, H. D., Horton, R. M., Pullen, J. K., & Pease, L. R. (1989). Site-directed mutagenesis by overlap extension using the polymerase chain reaction. *Gene*, *77*(1), 51–

59. https://doi.org/10.1016/0378-1119(89)90358-2

Horiuchi, D., Zhang, C., E. Huskey, N., Merrick, K. A., Wohlbold, L., Kusdra, L., … Fisher, R. P. (2012). Chemical-genetic analysis of cyclin dependent kinase 2 function reveals an important role in cellular transformation by multiple oncogenic pathways. *Proceedings of the National Academy of Sciences*, *109*(17), 1019–1027. https://doi.org/10.1073/pnas.1111317109

Huse, M., & Kuriyan, J. (2002). The conformational plasticity of protein kinases. *Cell*, *109*(3), 275–282. https://doi.org/10.1016/S0092-8674(02)00741-9

Izawa, D., & Pines, J. (2015). The mitotic checkpoint complex binds a second CDC20 to inhibit active APC/C. *Nature*, *517*(7536), 631–634. https://doi.org/10.1038/nature13911

Jia, L., Li, B., & Yu, H. (2016). The Bub1-Plk1 kinase complex promotes spindle checkpoint signalling through Cdc20 phosphorylation. *Nature Communications*, *7*, 1–14. https://doi.org/10.1038/ncomms10818

Jones, M. H., Huneycutt, B. J., Pearson, C. G., Zhang, C., Morgan, G., Shokat, K., … Winey, M. (2005). Chemical genetics reveals a role for Mps1 kinase in kinetochore attachment during mitosis. *Current Biology*, *15*(2),160–165. https://doi.org/10.1016/j.cub.2005.01.010

Kaisari, S., Sitry-Shevah, D., Miniowitz-Shemtov, S., & Hershko, A. (2016). Intermediates in the assembly of mitotic checkpoint complexes and their role in the regulation of the anaphase-promoting complex. *Proceedings of the National Academy of Sciences*, *113*(4), 966–971. https://doi.org/10.1073/pnas.1524551113

Karaca, E., & Bonvin, A. M. J. J. (2013). Advances in integrative modeling of biomolecular complexes. *Methods*, *59*(3), 372–381. https://doi.org/10.1016/j.ymeth.2012.12.004

Kelly, A. E., & Funabiki, H. (2009). Correcting aberrant kinetochore microtubule attachments: an Aurora B-centric view. *Current Opinion in Cell Biology*, *21*(1), 51–58. https://doi.org/10.1016/j.ceb.2009.01.004

Kim, H., Fernandes, G., & Lee, C. (2016). Protein Phosphatases Involved in Regulating Mitosis: Facts and Hypotheses. *Molecules and Cells*, *39*(9), 654–662. https://doi.org/10.14348/molcells.2016.0214

Kim, M. Y., Bucciarelli, E., Morton, D. G., Williams, B. C., Blake-Hodek, K., Pellacani, C., … Goldberg, M. L. (2012). Bypassing the Greatwall-Endosulfine pathway: Plasticity of a pivotal cell-cycle regulatory module in Drosophila melanogaster and caenorhabditis elegans. *Genetics*, *191*(4), 1181–1197. https://doi.org/10.1534/genetics.112.140574

Kishimoto, T. (2015). Entry into mitosis: a solution to the decades-long enigma of MPF. *Chromosoma*, *124*(4), 417–428. https://doi.org/10.1007/s00412-015-0508-y

Kissova, M., Maga, G., & Crespan, E. (2016). The human tyrosine kinase Kit and its gatekeeper mutant T670I, show different kinetic properties: Implications for drug design. *Bioorganic and Medicinal Chemistry*, *24*(19), 4555–4562. https://doi.org/10.1016/j.bmc.2016.07.059

Kops, G. J. P. L., Kim, Y., Weaver, B. A. A., Mao, Y., McLeod, I., Yates, J. R., … Cleveland, D. W. (2005). ZW10 links mitotic checkpoint signaling to the structural kinetochore. *Journal of Cell Biology*, *169*(1), 49–60. https://doi.org/10.1083/jcb.200411118

Kornev, A. P., & Taylor, S. S. (2015). Dynamics-Driven Allostery in Protein Kinases. *Trends in Biochemical Sciences*, *40*(11), 628–647. https://doi.org/10.1016/j.tibs.2015.09.002

Krajewska, M., & van Vugt, M. A. T. M. (2010). Building a great wall around mitosis: Evolutionary conserved roles for the Greatwall/MASTL kinases in securing chromosome stability. *Cell Cycle*, *9*(19), 3842–3847. https://doi.org/10.4161/cc.9.19.13282

Kubiak, J. Z., & Kishimoto, T. (2016). MPF , starfish oocyte and cell-free extract in the background - an interview with Takeo Kishimoto. *The International Journal of Developmental Biology*, *60*, 193–200. https://doi.org/10.1387/ijdb.160348jk

Labesse, G., Monsarrat, B., Lorca, T., Labbe, J.-C., Gharbi-Ayachi, A., Castro, A., … Vigneron, S. (2011). Characterization of the Mechanisms Controlling Greatwall Activity. *Molecular and Cellular Biology*, *31*(11), 2262–2275. https://doi.org/10.1128/mcb.00753-10

Lampson, M. A., & Kapoor, T. M. (2005). The human mitotic checkpoint protein BubR1 regulates chromosome-spindle attachments. *Nature Cell Biology*, *7*(1), 93–98. https://doi.org/10.1038/ncb1208

Landau, M., Mayrose, I., Rosenberg, Y., Glaser, F., Martz, E., Pupko, T., & Ben-Tal, N.

(2005). ConSurf 2005: The projection of evolutionary conservation scores of residues on protein structures. *Nucleic Acids Research*, *33*(2), 299–302. https://doi.org/10.1093/nar/gki370

Lera, R. F., & Burkard, M. E. (2012). The final link: Tapping the power of chemical genetics to connect the molecular and biologic functions of mitotic protein kinases. *Molecules*, *17*(10), 12172–12186. https://doi.org/10.3390/molecules171012172

Lodish, H., Berk, A., Kaiser, C. A., Krieger, M., Bretscher, A., Ploegh, H., … Martin, K. C. (2016). Molecular Cell Biology. *Ch 19: The Eukaryotic Cell Cycle*. (Eighth Edit). *Macmillan Learning*. ISBN: 9781319117191

LoGrasso, P. V., Frantz, B., Rolando, A. M., O'Keefe, S. J., Hermes, J. D., & O'Neill, E. A. (1997). Kinetic mechanism for p38 MAP kinase. *Biochemistry*, *36*(34), 10422–10427. https://doi.org/10.1021/bi9706778

Maheshwari, S., Miller, M. S., O'Meally, R., Cole, R. N., Amzel, L. M., & Gabelli, S. B. (2017). Kinetic and structural analyses reveal residues in phosphoinositide 3-kinase α that are critical for catalysis and substrate recognition. *Journal of Biological Chemistry*, *292*(33), 13541–13550. https://doi.org/10.1074/jbc.M116.772426

Miadokova, E., Cipak, L., Kovacikova, I., Zhang, C., Rumpf, C., Gregan, J., & Shokat, K. M. (2011). Generation of a set of conditional analog-sensitive alleles of essential protein kinases in the fission yeast Schizosaccharomyces pombe. *Cell Cycle*, *10*(20), 3527–3532. https://doi.org/10.4161/cc.10.20.17792

Mochida, S., & Hunt, T. (2012). Protein phosphatases and their regulation in the control of mitosis. *EMBO Reports*, *13*(3), 197–203. https://doi.org/10.1038/embor.2011.263

Mochida, S., Maslen, S. L., Skehel, M., & Hunt, T. (2010). Greatwall phosphorylates an inhibitor of protein phosphatase 2A that is essential for mitosis. *Science*, *330*(6011), 1670–1673. https://doi.org/10.1126/science.1195689

Montero-Pau, J., & Africa Gómez, and J. M. (2008). Application of an inexpensive and high-throughput genomic DNA extraction method for the molecular ecology of zooplanktonic diapausing eggs. *Limnology and Oceanography: Methods*, *6*(6), 218–222. https://doi.org/10.4319/lom.2008.6.218

Mühlebach, M. D., Wolfrum, N., Schüle, S., Tschulena, U., Sanzenbacher, R., Flory, E., … Schweizer, M. (2005). Stable transduction of primary human monocytes by simian lentiviral vector PBj. *Molecular Therapy*, *12*(6), 1206–1216. https://doi.org/10.1016/j.ymthe.2005.06.483

Needleman, S. B., & Wunsch, C. D. (1970). A general method applicable to the search for similarities in the amino acid sequence of two proteins. *Journal of Molecular Biology*, *48*(3), 443–453. https://doi.org/10.1016/0022-2836(70)90057-4

Ocasio, C. A., Rajasekaran, M. B., Walker, S., Le Grand, D., Spencer, J., Pearl, F. M. G., … Oliver, A. W. (2016). A first generation inhibitor of human Greatwall kinase, enabled by structural and functional characterisation of a minimal kinase domain construct. *Oncotarget*, *7*(44), 71182–71197. https://doi.org/10.18632/oncotarget.11511

Okumura, E., Morita, A., Wakai, M., Mochida, S., Hara, M., & Kishimoto, T. (2014). Cyclin B-Cdk1 inhibits protein phosphatase PP2A-B55 via a greatwall kinase-independent mechanism. *Journal of Cell Biology*, *204*(6), 881–889. https://doi.org/10.1083/jcb.201307160

Qin, J. Y., Zhang, L., Clift, K. L., Hulur, I., Xiang, A. P., Ren, B. Z., & Lahn, B. T. (2010). Systematic comparison of constitutive promoters and the doxycycline-inducible promoter. *PLoS ONE*, *5*(5), 3–6. https://doi.org/10.1371/journal.pone.0010611

Rahim, Z., & Barman, B. N. (1978). The van der Waals criterion for hydrogen bonding. *Acta Crystallographica Section A*, *34*, 761–764. https://doi.org/10.1107/s0567739478001576

Ramachandran, S., Kota, P., Ding, F., & Dokholyan, N. V. (2011). Automated minimization of steric clashes in protein structures. *Proteins: Structure, Function and Bioinformatics*, *79*(1), 261–270. https://doi.org/10.1002/prot.22879

Rice, P., Longden, L., & Bleasby, A. (2000). EMBOSS: The European Molecular Biology Open Software Suite. *Trends in Genetics*, *16*(6), 276–277. https://doi.org/10.1016/S0168-9525(00)02024-2

Roy, A., Kucukural, A., & Zhang, Y. (2010). I-TASSER: A unified platform for automated protein structure and function prediction. *Nature Protocols*, *5*(4), 725–738. https://doi.org/10.1038/nprot.2010.5

Salentin, S., Schreiber, S., Haupt, V. J., Adasme, M. F., & Schroeder, M. (2015). PLIP: Fully automated protein-ligand interaction profiler. *Nucleic Acids Research*, *43*(1), 443–447. https://doi.org/10.1093/nar/gkv315

Sambrook, J., & Russel, D. W. (2001). Molecular Cloning. *Ch 1: Plasmids and Their Usefulness in Molecular Cloning*. (Third Edit). *Cold Spring Harbor Laboratory Press*, *1*. ISBN 0-87969-576-5

Santamaría, D., Barrière, C., Cerqueira, A., Hunt, S., Tardy, C., Newton, K., … Barbacid, M. (2007). Cdk1 is sufficient to drive the mammalian cell cycle. *Nature*, *448*(7155), 811–815. https://doi.org/10.1038/nature06046

Sasson, S., & Notides, A. C. (2009). Mechanism of the Estrogen Receptor Interaction with 4-Hydroxytamoxifen. *Molecular Endocrinology*, *2*(4), 307–312. https://doi.org/10.1210/mend-2-4-307

Saul, N. B., & Christian, W. (1970). A General Method Applicable To Search for Similarities in Amino Acid Sequence of two Proteins. *Journal of Molecular Biology*, *48*(3), 443–453. https://doi.org/10.1016/0022-2836(70)90057-4

Šenigl, F., Miklík, D., Auxt, M., & Hejnar, J. (2017). Accumulation of long-term transcriptionally active integrated retroviral vectors in active promoters and enhancers. *Nucleic Acids Research*, *45*(22), 12752–12765. https://doi.org/10.1093/nar/gkx889

Shindo, N., Kumada, K., & Hirota, T. (2012). Separase Sensor Reveals Dual Roles for Separase Coordinating Cohesin Cleavage and Cdk1 Inhibition. *Developmental Cell*, *23*(1), 112–123. https://doi.org/10.1016/j.devcel.2012.06.015

Sliedrecht, T., Zhang, C., Shokat, K. M., & Kops, G. J. P. L. (2010). Chemical Genetic Inhibition of Mps1 in Stable Human Cell Lines Reveals Novel Aspects of Mps1 Function in Mitosis. *PLoS ONE*, *5*(4), 1–12. https://doi.org/10.1371/journal.pone.0010251

Slupe, A. M., Merrill, R. A., & Strack, S. (2011). Determinants for substrate specificity of protein phosphatase 2A. *Enzyme Research*, *2011*(1). https://doi.org/10.4061/2011/398751

Song, A. J., & Palmiter, R. D. (2018). Detecting and Avoiding Problems When Using the

Cre–lox System. *Trends in Genetics*, *34*(5), 333–340.
https://doi.org/10.1016/j.tig.2017.12.008

Sudakin, V., Chan, G. K. T., & Yen, T. J. (2001). Checkpoint inhibition of the APC/C in
HeLa cells is mediated by a complex of BUBR1, BUB3, CDC20, and MAD2. *Journal of
Cell Biology*, *154*(5), 925–936. https://doi.org/10.1083/jcb.200102093

Swanstrom, R., & Vogt, P. K. (1990). Retroviruses: Strategies of Replication. *Ch 2:
Integration of Retroviral DNA*. (First Edit). *Springer*, *Current Topics in Microbiology
and Immunology*, *157*, 34–35. ISBN 978-3-642-75218-6

Szafranska, A. E., & Dalby, K. N. (2005). Kinetic mechanism for p38 MAP kinase α: A
partial rapid-equilibrium random-order ternary-complex mechanism for the
phosphorylation of a protein substrate. *FEBS Journal*, *272*(18), 4631–4645.
https://doi.org/10.1111/j.1742-4658.2005.04827.x

Tang, Z., Bharadwaj, R., Li, B., & Yu, H. (2001). Mad2-Independent Inhibition of
APCCdc20 by the Mitotic Checkpoint Protein BubR1. *Developmental Cell*, *1*(2), 227–
237. https://doi.org/10.1016/S1534-5807(01)00019-3

Tang, Z., Shu, H., Oncel, D., Chen, S., & Yu, H. (2004). Phosphorylation of Cdc20 by Bub1
provides a catalytic mechanism for APC/C inhibition by the spindle checkpoint.
Molecular Cell, *16*(3), 387–397. https://doi.org/10.1016/j.molcel.2004.09.031

Tauchman, E. C., Boehm, F. J., & DeLuca, J. G. (2015). Stable kinetochore-microtubule
attachment is sufficient to silence the spindle assembly checkpoint in human cells.
Nature Communications, *6*, 1–9. https://doi.org/10.1038/ncomms10036

Tymms, M. J., & Kola, I. (2003). Gene Knockout Protocols. *Methods in Molecular Biology*,
530, 343–363. https://doi.org/10.1385/1592592201

Van Zundert, G. C. P., Rodrigues, J. P. G. L. M., Trellet, M., Schmitz, C., Kastritis, P. L.,
Karaca, E., … Bonvin, A. M. J. J. (2016). The HADDOCK2.2 Web Server: User-
Friendly Integrative Modeling of Biomolecular Complexes. *Journal of Molecular
Biology*, *428*(4), 720–725. https://doi.org/10.1016/j.jmb.2015.09.014

Vigneron, S., Brioudes, E., Burgess, A., Labbé, J. C., Lorca, T., & Castro, A. (2009).
Greatwall maintains mitosis through regulation of PP2A. *EMBO Journal*, *28*(18), 2786–

2793. https://doi.org/10.1038/emboj.2009.228

Vleugel, M., Hoogendoorn, E., Snel, B., & Kops, G. J. P. L. (2012). Evolution and Function of the Mitotic Checkpoint. *Developmental Cell*, *23*(2), 239–250. https://doi.org/10.1016/j.devcel.2012.06.013

Weber, T. J. (2010). Protein Kinases. (Second Edit). *Elsevier*, *Comprehensive Toxicology*, *2*, 473–493. http://dx.doi.org/10.1016/B978-0-08-046884-6.00225-6

Weber, T. J., Qian, W., & States, U. (2018). Protein Kinases. (Third Edit). *Elsevier*, *Comprehensive Toxicology*, *8*, 264–285. https://doi.org/10.1016/B978-0-12-801238-3.01925-5

Westhorpe, F. G., Tighe, A., Lara-Gonzalez, P., & Taylor, S. S. (2011). p31comet-mediated extraction of Mad2 from the MCC promotes efficient mitotic exit. *Journal of Cell Science*, *124*(22), 3905–3916. https://doi.org/10.1242/jcs.093286

Xiang, Z. (2006). Advances in Homology Protein Structure Modeling. *Current Protein & Peptide Science*, *7*(3), 217–227. https://doi.org/10.2174/138920306777452312

Yang, J., Yan, R., Roy, A., Xu, D., Poisson, J., & Zhang, Y. (2014). The I-TASSER suite: Protein structure and function prediction. *Nature Methods*, *12*(1), 7–8. https://doi.org/10.1038/nmeth.3213

Yu, D. J., Hu, J., Huang, Y., Shen, H. Bin, Qi, Y., Tang, Z. M., & Yang, J. Y. (2013). TargetATPsite: A template-free method for ATP-binding sites prediction with residue evolution image sparse representation and classifier ensemble. *Journal of Computational Chemistry*, *34*(11), 974–985. https://doi.org/10.1002/jcc.23219

Yu, J., Fleming, S. L., Williams, B., Williams, E. V., Li, Z. X., Somma, P., … Goldberg, M. L. (2004). Greatwall kinase: A nuclear protein required for proper chromosome condensation and mitotic progression in Drosophila. *Journal of Cell Biology*, *164*(4), 487–492. https://doi.org/10.1083/jcb.200310059

Yu, J., Zhao, Y., Li, Z., Galas, S., & Goldberg, M. L. (2006). Greatwall Kinase Participates in the Cdc2 Autoregulatory Loop in Xenopus Egg Extracts. *Molecular Cell*, *22*(1), 83–91. https://doi.org/10.1016/j.molcel.2006.02.022

Zhang, Y. (2008). I-TASSER server for protein 3D structure prediction. *BMC Bioinformatics*, *9*, 40. https://doi.org/10.1186/1471-2105-9-40

Zhong, Z. A., Sun, W., Chen, H., Zhang, H., Lay, Y. A. E., Lane, N. E., & Yao, W. (2015). Optimizing tamoxifen-inducible Cre/loxp system to reduce tamoxifen effect on bone turnover in long bones of young mice. *Bone*, *81*, 614–619. https://doi.org/10.1016/j.bone.2015.07.034

Zuccotto, F., Ardini, E., Casale, E., & Angiolini, M. (2010). Through the "gatekeeper door": Exploiting the active kinase conformation. *Journal of Medicinal Chemistry*, *53*(7), 2681–2694. https://doi.org/10.1021/jm901443h

8. APPENDIX

8.1. Curriculum Vitae

Mehmet Ergüven

Year of Birth	1994
Address:	İzmir Uluslararası Biyotıp ve Genom Enstitüsü (iBG-izmir) Dokuz Eylül Üniversitesi Sağlık Yerleşkesi Balçova 35340 İzmir
Mobile:	+90 541 410 8294
Fax:	
e-mail:	erguven.mhmt@gmail.com

EDUCATION

Country Code	Unviersity	Faculty/Institute	Field	Degree	Year of Graduation
TR	Dokuz Eylul University	Izmir International Biomedicine and Genome Institute	Molecular Biology and Genetics	M.Sc.	2019
TR	Ege University	Faculty of Science	Biochemistry	B.Sc.	2016

RESEARCH FIELDS

Life sciences

ACADEMIC EXPERIENCES

Ege University ARGEFAR – Intern

PUBLICATIONS

Kocadag Kocazorbaz, E., Erguven, M., Memecan S. S., Menfaatli, E., Yıldırım, H., & Zihnioglu, F. (2017). Purification and characterization of chymotrypsin-like serine protease from *Euphorbia rigida* latex. *Current Topics in Peptide & Protein Research*, 18, 35-40.

Konu: Karar hk.
Sayı : 128

12.02.2016

Sayın Yard.Doç.Dr.Kasım DİRİL,

Kurulumuz tarafından 11.02.2016 tarih ve 2437-GOA protokol numaralı 2016/04-31 karar numarası ile görüşülen "**Mitotik Kinaz Fonksiyonlarının Kimyasal Genetik Yöntemlerle Analizi**"" konulu araştırmanıza ilişkin Kurulumuz kararı ekte sunulmuştur.

Bilgilerinizi ve gereğini rica ederim.

Prof.Dr.Banu ÖNVURAL
Başkan

Ek: Etik Kurul Kararı

103

DOKUZ EYLÜL ÜNİVERSİTESİ
GİRİŞİMSEL OLMAYAN ARAŞTIRMALAR ETİK KURUL KARARI

ETİK KOMİSYONUN ADI	DOKUZ EYLÜL ÜNİVERSİTESİ GİRİŞİMSEL OLMAYAN ARAŞTIRMALAR ETİK KURULU
AÇIK ADRES	Dokuz Eylül Üniversitesi Tıp Fakültesi Dekanlığı 2. Kat İnciraltı-İZMİR
TELEFON	0 232 412 22 54-0 232 412 22 58
FAKS	0 232 412 22 43
E-POSTA	etikkurul@deu.edu.tr

<table>
<tr><td rowspan="9">BAŞVURU BİLGİLERİ</td><td>DOSYA NO:</td><td colspan="2">2437-GOA</td></tr>
<tr><td>ARAŞTIRMA</td><td>UZMANLIK TEZİ ☐</td><td>AKADEMİK AMAÇLI ☐</td></tr>
<tr><td>ARAŞTIRMANIN AÇIK ADI</td><td colspan="2">Mitotik Kinaz Fonksiyonlarının Kimyasal Genetik Yöntemlerle Analizi</td></tr>
<tr><td>ARAŞTIRMA PROTOKOL KODU</td><td colspan="2"></td></tr>
<tr><td>SORUMLU ARAŞTIRMACI ÜNVANI/ADI/SOYADI ve UZMANLIK ALANI</td><td colspan="2">Yard.Doç.Dr.Kasım Diril
İzmir Biyotıp ve Genom Merkezi</td></tr>
<tr><td>DESTEKLEYİCİ VE AÇIK ADRESİ</td><td colspan="2">-</td></tr>
<tr><td>DESTEKLEYİCİNİN YASAL TEMSİLCİSİ VE ADRESİ</td><td colspan="2">-</td></tr>
<tr><td>ARAŞTIRMAYA KATILAN MERKEZLER</td><td>TEK MERKEZ ☒</td><td>ÇOK MERKEZLİ ☐</td></tr>
</table>

<table>
<tr><td rowspan="5">DEĞERLENDİRİLEN BELGELER</td><td>Belge Adı</td><td>Tarihi</td><td>Versiyon Numarası</td><td colspan="3">Dili</td></tr>
<tr><td>ARAŞTIRMA PROTOKOLÜ</td><td>Mevcut</td><td></td><td>Türkçe ☒</td><td>İngilizce ☐</td><td>Diğer ☐</td></tr>
<tr><td>ARAŞTIRMA İLE İLGİLİ LİTERATÜR</td><td>Mevcut</td><td></td><td>Türkçe ☐</td><td>İngilizce ☒</td><td>Diğer ☐</td></tr>
<tr><td>BİLGİLENDİRİLMİŞ GÖNÜLLÜ OLUR FORMU</td><td>Mevcut</td><td></td><td>Türkçe ☒</td><td>İngilizce ☐</td><td>Diğer ☐</td></tr>
<tr><td>OLGU RAPOR FORMU</td><td>Mevcut</td><td></td><td>Türkçe ☒</td><td>İngilizce ☐</td><td>Diğer ☐</td></tr>
</table>

	Karar No:2016/04-31	Tarih:11.02.2016
KARAR BİLGİLERİ	Yard.Doç.Dr.Kasım Diril'in sorumlusu olduğu **"Mitotik Kinaz Fonksiyonlarının Kimyasal Genetik Yöntemlerle Analizi"** isimli klinik araştırmaya ait başvuru dosyası ve ilgili belgeler araştırmanın gerekçe, amaç, yaklaşım ve yöntemleri dikkate alınarak incelenmiş, etik açıdan çalışmanın gerçekleştirilmesinin uygun olduğuna oy birliği ile karar verilmiştir.	

ETİK KURUL BİLGİLERİ	
ÇALIŞMA ESASI	Dokuz Eylül Üniversitesi Girişimsel Olmayan Araştırmalar Etik Kurulu İşleyiş Yönergesi İyi Klinik Uygulamaları Kılavuzu

ETİK KURUL ÜYELERİ

Unvanı/Adı/Soyadı	Uzmanlık Alanı	Kurumu	Cinsiyet	Araştırma ile İlişkili mi?		İmza
Prof.Dr.Banu ÖNVURAL (Başkan)	Tıbbi Biyokimya	DEU Tıp Fakültesi Tıbbi Biyokimya Anabilim Dalı	Kadın	E ☐	H ☒	
Prof.Dr.Ş.Reyhan UÇKU (Başkan Yardımcısı)	Halk Sağlığı	DEU Tıp Fakültesi Halk Sağlığı A.D.	Kadın	E ☐	H ☒	katılmadı
Prof.Dr.Nejat SARIOSMANOĞLU	Kalp Damar Cerrahisi	DEU Tıp Fakültesi Kalp Damar Cerrahisi Anabilim Dalı	Erkek	E ☐	H ☒	
Prof.Dr.Ece BÖBER	Pediatrik Endokrinoloji	DEU Tıp Fakültesi Çocuk Sağlığı ve Hastalıkları Anabilim Dalı	Kadın	E ☐	H ☒	
Prof.Dr.Vesile ÖZTÜRK	Nöroloji	DEU Tıp Fakültesi Nöroloji Anabilim Dalı	Kadın	E ☐	H ☒	
Prof.Dr.Sevinç ERASLAN	Endokrinoloji	DEU Tıp Fakültesi İç Hastalıkları Anabilim Dalı	Kadın	E ☐	H ☒	katılmadı
Prof.Dr.Mukaddes GÜMÜŞTEKİN	Tıbbi Farmakoloji	DEU Tıp Fakültesi Tıbbi Farmakoloji Anabilim Dalı	Kadın	E ☐	H ☒	katılmadı
Prof.Dr.Ayşe Aydan ÖZKÜTÜK	Tıbbi Mikrobiyoloji	DEU Tıp Fakültesi Tıbbi Mikrobiyoloji Anabilim Dalı	Kadın	E ☐	H ☒	
Prof.Dr.Nihal GELECEK	Fizik Tedavi ve Rehabilitasyon	DEU Fizik Tedavi ve Rehabilitasyon Yüksek Okulu	Kadın	E ☐	H ☒	
Prof.Dr.Müge KİRAY	Fizyoloji	DEU Tıp Fakültesi Fizyoloji Anabilim Dalı	Kadın	E ☐	H ☒	
Doç.Dr.Şeyda SEREN İNTEPELER	Hemşirelik Yönetimi	DEU Hemşirelik Fakültesi Hemşirelik Yönetimi A.D	Kadın	E ☐	H ☒	
Doç.Dr.Sefa KIZILDAĞ	Tıbbi Biyoloji ve Genetik	DEU Tıp Fakültesi Tıbbi Biyoloji ve Genetik A.D	Erkek	E ☐	H ☒	
Prof.Dr.Sevda ÖZKARDEŞLER	Anesteziyoloji	DEÜ Tıp Fakültesi Anesteziyoloji ve Reanimasyon A.D.	Kadın	E ☐	H ☒	
Uzm.Dr.Ahmet Can BİLGİN	Hukuk	DEU Tıp Tarihi ve Etik A.D	Erkek	E ☐	H ☒	katılmadı
Mehmet Erhan ÖZKUL	Sağlık mensubu olmayan üye	D.E.U Tıp Fakültesi İdari Mali İşler	Erkek	E ☐	H ☒	

Dokuz Eylül Üniversitesi Girişimsel Olmayan Araştırmalar Etik Kurulu Karar Formu